Joona Jäntti

Spectrum Sensing and Waveform Classification Using Cepstral Analysis

School of Electrical Engineering

Thesis submitted for examination for the degree of
Master of Science in Technology.
Espoo 26.6.2014

Thesis supervisor:

Prof. Visa Koivunen

Thesis advisor:

D.Sc. (Tech.) Sachin Chaudhari

Aalto University
School of Electrical
Engineering

AALTO UNIVERSITY
SCHOOL OF ELECTRICAL ENGINEERING

ABSTRACT OF THE
MASTER'S THESIS

Author: Joona Jäntti

Title: Spectrum Sensing and Waveform Classification Using Cepstral Analysis

Date: 26.6.2014 Language: English Number of pages: 10+80

Department of Signal Processing and Acoustics

Professorship: Signal Processing Code: S-88

Supervisor: Prof. Visa Koivunen

Advisor: D.Sc. (Tech.) Sachin Chaudhari

Current usable radio frequency spectrum is beginning to be heavily crowded due to the inefficient use of the licensed spectrum bands along with the rapid growth of wireless technologies. Cognitive radios are developed to overcome this underutilization problem by allowing secondary users to use licensed spectrum bands in an agile manner as long as they do not harm the primary receivers. In order to access unoccupied licensed spectrum bands effectively and to achieve awareness of the radio environment, opportunistic secondary users must perform spectrum sensing.

This thesis is focused on spectrum sensing techniques that utilize cepstral analysis. The scope is on sensing multi-carrier primary signals that utilize orthogonal frequency division multiplexing (OFDM) modulation. OFDM a key modulation method in current as well as future wireless transmission systems.

In this thesis, the distributions of the cepstral coefficients of OFDM signals in additive white Gaussian noise (AWGN) channel are derived analytically. The problem of finding idle spectrum is modeled as a statistical hypothesis testing problem. For solving such problem, two local detection algorithms based on cepstral analysis for detecting OFDM signals are proposed. Furthermore, cepstrum-based algorithms for estimating the data length and the cyclic prefix (CP) length of an OFDM symbol are proposed. Finally, all proposed single-user detection and parameter estimation algorithms are extended to a cooperative scenario where multiple distributed sensors operate simultaneously. Distributed sensing is implemented for achieving better decision reliability especially in challenging radio environments. The performances of the proposed algorithms as well as the results obtained from theoretical analysis are justified through extensive simulations.

Keywords: Cepstrum analysis, classification, cognitive radios, detection, spectrum sensing

AALTO-YLIOPISTO
SÄHKÖTEKNIIKAN KORKEAKOULU

DIPLOMITYÖN
TIIVISTELMÄ

Tekijä: Joona Jäntti

Työn nimi: Spektrin aistinta ja aaltomuotojen luokittelu kepstrianalyysia käyttäen

Päivämäärä: 26.6.2014 Kieli: Englanti Sivumäärä: 10+80

Signaalinkäsittelyn ja akustiikan laitos

Professuuri: Signaalinkäsittely Koodi: S-88

Valvoja: Prof. Visa Koivunen

Ohjaaja: TkT Sachin Chaudhari

Lisensoitujen taajuskaistojen tehoton käyttö sekä langattoman tiedonsiirron nopea kasvu on ruuhkauttanut nykyisen käytettävissä olevan radiospektrin. Radiospektrin tehokkaammaksi ja joustavammaksi hyödyntämiseksi on kehitetty kognitiivisia radiojärjestelmiä, jotka antavat toissijaisille käyttäjille luvan käyttää lisensoituja taajuuskaistoja, kunhan käytöstä ei aiheudu haittaa ensisijaisille käyttäjille. Jotta toissijaiset käyttäjät voisivat hyödyntää vapaita taajuuskaistoja tehokkaasti, tulisi niiden pystyä keräämään informaatiota ja muodostaa tilannetietoisuutta radioympäristöstä aistimalla spetriä.

Tämä diplomityö keskittyy spektrin aistintamenetelmiin, jotka pohjautuvat kepstrianalyysiin. Menetelmät soveltuvat monikantoaaltoteknologiaan perustuvien ortogonaalista taajuusjako-multipleksausta (OFDM) käyttävien signaalien aistimiseen. OFDM on merkittävin nykyisten ja tulevaisuuden langattomien tiedonsiirtojärjestelmien käyttämä modulaatiomenetelmä.

Työssä johdetaan analyyttiset jakaumat kohinaisessa kanavassa olevan OFDM-signaalin kepstrikertoimille. Vapaan spektrin löytäminen mallinnetaan tilastollisena hypoteesin testausongelmana, jonka ratkaisemiseksi esitetään kaksi kepstrianalyysiin pohjautuvaa OFDM-signaalin ilmaisumenetelmää. Lisäksi työssä esitetään menetelmät sekä OFDM-symbolin datapituuden että syklisen etuliitteen pituuden estimoimiseksi. Lopulta kaikki ehdotetut yhden aistijan menetelmät laajennetaan hajautettuun monen sensorin aistimisongelmaan. Monen sensorin käytöllä pyritään parantamaan päättelyn luotettavuutta vaativissa radioympäristöissä. Esitettyjen algoritmien suorituskykyä sekä teoreettisten analyysien tuloksia tarkastellaan kattavien simulaatioiden avulla.

Avainsanat: Ilmaisu, kepstrianalyysi, kognitiivinen radio, luokittelu, spektrin aistinta

Aknowledgements

First of all, I would like to address my sincere thanks to Professor Visa Koivunen for giving me the opportunity to work in this research group and for supervising this thesis. In addition, I want to express my deepest gratitude to Dr. Sachin Chaudhari who has instructed me. I am extremely humbled by the amount of care you have taken in guiding me in various aspects during my research career.

Many thanks to all my friends and fellow students. Especially I would like to thank Mr. Juhani Koo for intriguing and mind-opening discussions and all members of Retuperän WBK for helping me to fulfill my artistic dreams.

Finally, I would like to thank my family for all of the support and encouragement that I have got throughout my life. Many thanks to my beloved fiancée Marjo for her love, support and patience.

Otaniemi, June 26, 2014

Joona Jäntti

List of Abbreviations

ACF	autocorrelation function
ALRT	average likelihood ratio test
AMC	automatic modulation classification
ASK	amplitude shift keying
AWGN	additive white Gaussian noise
CLT	central limit theorem
CP	cyclic prefix
CR	cognitive radio
DFT	discrete Fourier transform
DTFT	discrete-time Fourier transform
DSA	dynamic spectrum access
DSL	digital subscriber line
DVB	digital video broadcasting
ED	energy detection
ECG	electrocardiogram
ECMA	European Association for Standardizing Information and Communication Systems
ETSI	European Telecommunications Standards Institute
FC	fusion center
FCC	Federal Communications Committee
FFT	fast Fourier transform
FICORA	Finnish Communications Regulatory Authority
FSK	frequency shift keying
GLRT	generalized likelihood ratio test
HLRT	hybrid likelihood ratio test
IDFT	inverse discrete Fourier transform
IEEE	Institute of Electrical and Electronics Engineers
IFFT	inverse fast Fourier transform
ITU	International Telecommunication Union
i.i.d.	independent and identically distributed
LF	likelihood function
LRT	likelihood ratio test
LTE	Long Term Evolution
MFCC	mel-frequency cepstral coefficient
MLE	maximum likelihood estimate

MSE	mean squared error
NP	Neyman-Pearson criterion
OFDM	orthogonal frequency division multiplexing
PDF	probability density function
PSK	phase shift keying
PU	primary user
QAM	quadrature amplitude modulation
QoS	quality of service
RF	radio frequency
SNR	signal-to-noise ratio
SU	secondary user
WiMAX	Worldwide interoperability for Microwave Access
WLAN	wireless local area network
WMAN	wireless metropolitan area network
WPAN	wireless personal area network
WRAN	wireless regional area network

List of Symbols

$\hat{a}$	estimate of a scalar a
a^*	conjugate of a scalar a
$\|a\|$	modulus of a scalar a
$\| \mathbf{A} \|_F^2$	Frobenius-norm of a matrix $\mathbf{A}$
$\mathbf{A}^{\mathrm{T}}$	transpose of a matrix $\mathbf{A}$
$\arg[\cdot]$	argument operator
$\mathcal{A}$	set of allowed values
B	number of symbols in an OFDM signal
$c(n)$	(real) cepstrum
$c_a(n)$	phase cepstrum
$c_c(n)$	complex cepstrum
$c_p(n)$	power cepstrum
$\mathbb{E}[\cdot]$	expectation operator
erf	error function
erfc	complementary error function
erfc^{-1}	inverse of the complementary error function
$f(x)$	probability density function
$F(x)$	cumulative distribution function
$\mathcal{F}\{\cdot\}$	discrete Fourier transform operator
$\mathcal{F}^{-1}\{\cdot\}$	inverse discrete Fourier transform operator
H_0	null hypothesis
H_1	alternative hypothesis
$I_0(\cdot)$	zeroth order Bessel function
$\mathcal{I}\{x\}$	imaginary part of a complex value x
j	unit imaginary number
k	discrete frequency index
log	natural logarithm
$\mathrm{Log}\{\cdot\}$	complex logarithm operator
M	total number of received samples
$\mathrm{Md}(\cdot)$	median operator
$\mathrm{Mo}(\cdot)$	mode operator
n	discrete time or quefrency index
N_c	number of cyclic prefix samples in an OFDM symbol
N_d	number of data samples in an OFDM symbol
N_r	point size of DFT or IDFT

N_s	total number of samples in an OFDM symbol
$\mathcal{N}$	normal distribution
$\mathcal{N}_c$	complex normal distribution
$P(A\|B)$	conditional probability of A given that B has occured
P_d	probability of detection
P_f	probability of false alarm
$\mathcal{R}\{x\}$	real part of a complex value x
$s(n)$	transmitted OFDM signal
$S(k)$	discrete Fourier transform of $s(n)$
t	continuous time variable
$\mathcal{T}$	test statistic
u_i	u^{th} cooperating sensor
U	total number of cooperating sensors
$\mathbb{V}\text{ar}[\cdot]$	variance operator
$w(n)$	additive white Gaussian noise
$x(n)$	received signal
$X(k)$	discrete Fourier transform of $x(n)$
$X(\omega)$	discrete-time Fourier transform of $x(n)$
$\mathbb{Z}$	set of all integers
$\mathbb{Z}_+$	set of all positive integers
$Z(k)$	$\log \lvert X(k) \rvert$
β^2	location parameter for Log-Rayleigh distribution
η	detector threshold value
γ	Euler's constant
μ_n	expected value of the n^{th} coefficient of $c(n)$
μ_z	expected value of a Log-Rayleigh distributed random variable Z
ω	angular frequency
σ_k^2	variance of the k^{th} coefficient of $X(k)$
σ_n^2	variance of the n^{th} coefficient of $c(n)$
σ_s^2	OFDM signal variance
σ_w^2	noise variance
σ_x^2	variance of the received signal $x(n)$
σ_z^2	variance of a Log-Rayleigh distributed random variable Z
τ	time delay
$\lfloor \cdot \rfloor$	floor operator
$[\cdot]_{\mathcal{A}}$	operator for rounding towards the nearest value in $\mathcal{A}$

Contents

Chapter 1

Introduction

1.1 Background

The usable radio frequency (RF) spectrum has become crowded due to the rigid spectrum allocation policy and the rapid growth of wireless technologies. In addition, some licensed spectrum bands are in fact highly underutilized, which makes the overall spectrum utilization inefficient [1,2]. Cognitive radios (CR) are developed to overcome this underutilization problem by allowing the secondary users (SUs) to exploit unoccupied primary bands opportunistically through dynamic spectrum access (DSA) along with flexible allocation policy. Furthermore, the number of heterogeneous networks is going to rise in the future [1]. In such scenarios, acquiring awareness of the spectrum state such as identifying idle spectrum and classifying different users (for example primary or secondary users) in the network is of utmost importance.

Orthogonal frequency division multiplexing (OFDM) is a key wideband digital transmission technology for the present as well as future wireless systems [3]. Therefore, it is reasonable to assume that many licensed and secondary spectrum users will transmit OFDM waveforms with different parameters. Thus, detection and classification of OFDM waveforms are important research problems for spectrum monitoring and coexistence of heterogeneous networks.

The cepstrum can capture information on periodicities or on the rate of change in different spectrum bands in a signal. Cepstral processing was first used for characterizing the seismic echoes resulting from earthquakes [4]. Since then, it has also been used in various applications such as radar and sonar, speech processing, and deconvolution of two or more signals [5]. It has often been used in speech processing applications such as pitch estimation for voice coding, voice activity detection or speech recognition [6,7].

The cepstrum has the ability to distinguish periodicities in a signal. The insertion of the cyclic prefix (CP) in an OFDM symbol induces periodicities in the signal which can be detected by the cepstrum. This property motivates the use of cepstrum when sensing OFDM signals. It is shown that there are distinct differences in the mean and the variance of the cepstra of OFDM signal

and additive white Gaussian noise (AWGN), which is a property that can be utilized both in detection and classification purposes.

1.2 Contributions of the thesis

In this thesis, the use of cepstral analysis for OFDM signal sensing is studied in detail. A theoretical analysis of the distributions of the cepstral coefficients for an OFDM signal in a noisy channel is presented. Moreover, novel algorithms are proposed for detecting OFDM signals and estimating their transmission parameters based on cepstral analysis. The performances of the proposed algorithms as well as the results from theoretical analysis are examined and justified by extensive simulations. A few of the results related to the proposed algorithms for cepstrum-based detection and parameter estimation were published in [8].

The main contributions of this thesis are summarized as follows:

- The distributions of cepstral coefficients for AWGN only and OFDM signal in AWGN are derived theoretically. It is shown that in addition to the DC peak, the mean of the OFDM cepstrum has peaks at the indices of integer multiples of the data length in an OFDM symbol. In addition, the variance of the cepstrum when OFDM signal is present has triangular shaped peaks that appear at the indices corresponding to the symbol length. On the other hand, the mean (except the DC index) and the variance are constant valued when only AWGN is received.

- Based on the differences between the cepstra of an OFDM signal and noise, two OFDM detection schemes are proposed in this thesis. The distributions of the two test statistics are established so that both the threshold value and the probability of detection for a Neyman-Pearson detector can be calculated analytically. The performances of these detectors are compared with the classical energy detector (ED) both in the absence and the presence of noise uncertainty. It is shown that the first detector is robust to noise uncertainty and outperforms the energy detector even in the case of small noise uncertainty while the performance of the second detector is closer to that of the ED.

- Algorithms for estimating the data length and the CP length of an OFDM symbol based on cepstral analysis are proposed. The parameters of data length and CP length in an OFDM symbol are generally distinct for different wireless standards and therefore can be used for classifying OFDM signals. This is an added advantage over the energy detection scheme which cannot distinguish between different signals. It is shown through simulations that the expected values of the proposed estimates converge to their desired values and their variances converge to zero as the SNR increases.

- The proposed local signal detection and parameter estimation algorithms are extended into a cooperative scenario where multiple distributed sensors operate simultaneously and their sensing results are combined in a fusion center. Cooperation is shown to improve both detection and estimation performances over the single-user scenario.

1.3 Outline of the thesis

The organization of this thesis is as follows. In Chap. 2, a brief introduction to CR systems, its functions and dynamic spectrum access is given. After that, the basics of cepstrum analysis and OFDM waveforms are presented in Chap. 4. In Chap. 5, the analytical distributions of the cepstral coefficients are derived for both AWGN and for OFDM signal in AWGN. In Chapters 6 and 7, novel cepstrum-based detection and parameter estimation algorithms are presented for both single-user and cooperative sensing scenarios. Moreover, the performance results of each proposed algorithm are presented with Matlab simulations. Chap. 8 concludes the thesis.

Chapter 2

Overview on Cognitive Radio Systems

The usable RF spectrum is a valuable natural source - which unfortunately is of limited extent. Problematically, the ever increasing demand for high-speed wireless communication results in a growing need for the spectrum. In addition, it has been shown that the current rigid spectrum allocation cannot meet the increased demand for usable frequency bands and is also partly causing the lack of usable spectrum [9]. Furthermore, there is significant underutilization in the spectrum since many licensed users do not use their frequency bands most of the time [10]. *Cognitive radio* CR systems are developed to offer a novel solution to the spectrum underutilization since they aim to utilize the available RF spectrum in an efficient way through acquiring awareness of the spectrum and accessing free spectrum dynamically [11]. In CR systems, also unlicensed users have a possibility to use licensed spectrum, as long as they do not harm the licensed users.

In this chapter, the main concepts of CR systems are discussed. First, a brief introduction to the definitions of CR is given, after which the framework and the most important functions of CR systems are introduced. After that, the usage of CR in dynamic spectrum access and the current regulatory and standardization efforts regarding CR are reviewed. Additional information on CR systems and DSA can be found for instance in [11–14].

2.1 Introduction

The term CR was first introduced by Joseph Mitola III in 1998, while he had already promoted the term soft-ware defined radio (SDR) five years earlier [14]. Practically, a software-defined radio means *a multiband radio that supports multiple air interfaces and is reconfigurable through software run on digital signal processor or general-purpose microprocessors* [15]. In 1999, Mitola published an article where CR was introduced to be an enhancement for the flexibility of personal wireless systems, and it was discussed more in detail

in Mitola's doctoral dissertation in May 2000 [15]. Simon Haykin defined CR in his survey [15] as *an intelligent wireless communication system that learns from the environment by understanding-by-building methodology.* By Haykin *et al.* [11], the objective of CR is twofold:

- provide highly reliable communication for all users whenever and wherever needed;
- facilitate efficient utilization of the radio spectrum in a fair-minded and cost-effective manner.

Another popular definition of CR systems is given by the Federal Communications Commission (FCC), which states that CR is *a radio or system that senses its operational electromagnetic environment and can dynamically and autonomously adjust its radio operating parameters to modify system operation, such as maximize throughput, mitigate interference, facilitate interoperability, access secondary markets* [16].

The main idea in CR systems is to exploit opportunities in the licensed spectrum bands. The cognitive SUs try to detect whether the primary users (PUs) are transmitting or not so that they could utilize primary frequency bands. According to the CR approach, the SUs can use spectrum bands allocated for the PUs as long as their secondary transmissions do not interfere with the PUs.

Next, the basic CR framework and its main functions are briefly introduced. After that the general concepts regarding DSA, the main application of CR networks, are discussed.

2.2 Cognitive radio framework

In order to provide reliable communication and maintain the required quality of service (QoS) for primary users, CR networks have to follow certain design challenges. According to [17], CR networks should avoid interfering with the PUs, provide seamless communication regardless of the appearance of the PUs, and support QoS-aware communication considering the dynamic and heterogeneous network. To address these challenges, one can divide the spectrum management process into four different categories: spectrum sensing, spectrum decision, spectrum sharing and spectrum mobility [17]. Fig. 2.1 presents how the CR network can be modeled with these four categories.

The first step in the cognitive cycle is **spectrum sensing** where cognitive SUs try to obtain awareness of the state of the spectrum and whether the PU transmission is present or not. The goal of spectrum sensing is to find exploitable spectrum holes and to determine how to access licensed spectrum without causing harmful interference to the PU receivers [18]. Spectrum sensing is one of the most essential functions in CR systems, for which it is discussed more in detail in Chap. 3.

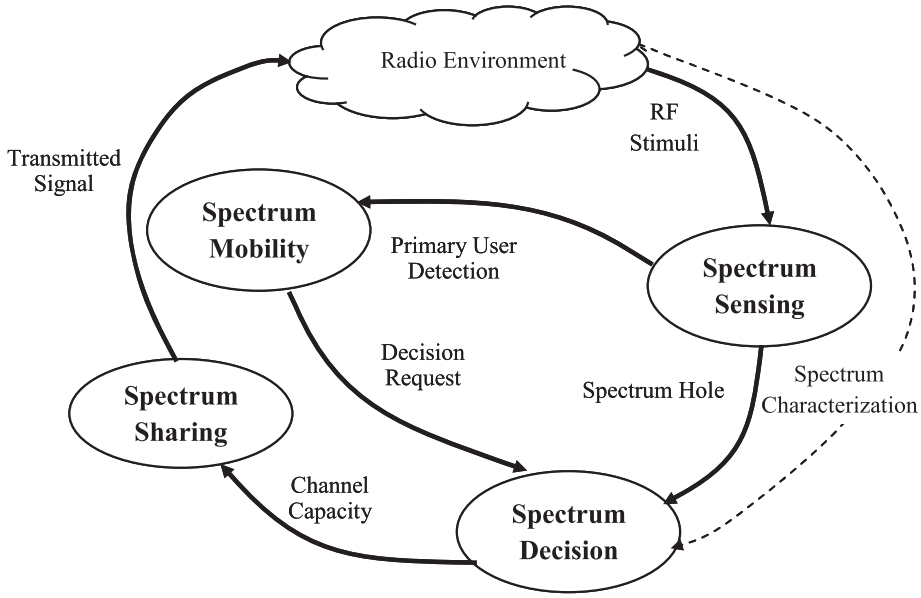

Figure 2.1: The main functions in CR networks, from [19].

Spectrum decision is done based on spectrum sensing data. During this phase, the SU basically decides when to start operation and chooses the operating frequency and its corresponding transmission parameters [20]. It is essential to select the most appropriate band according to the QoS requirements and channel characteristics [19, 21]. Based on those requirements, the data rate, acceptable error rate, delay bound, transmission mode, and the transmission bandwidth can be determined [21].

Spectrum mobility is related to the change of operating frequency band of the SUs [13]. When a PU starts transmitting in a frequency band that is currently being used by a SU, the SU must immediately vacate the spectrum band and change its transmission frequency. In order to maintain seamless communication, the function of spectrum mobility must try to ensure that the secondary transmission can continue without errors in the new spectrum band.

The final component of the categorized CR functions is **spectrum sharing**, which handles the situations where multiple cognitive users operate in the same frequency band. CR network access should be coordinated in such way that the collisions between users transmitting in overlapping frequency bands would be prevented [17]. Efficient spectrum sharing can be managed by implementing different DSA strategies which are explained in the next section.

2.3 Dynamic spectrum access

Currently, the RF spectrum is strictly allocated for different licensed users. The allocation is done and supervised in each country by some national organization, for example FCC in the USA or Finnish Communications Regulatory

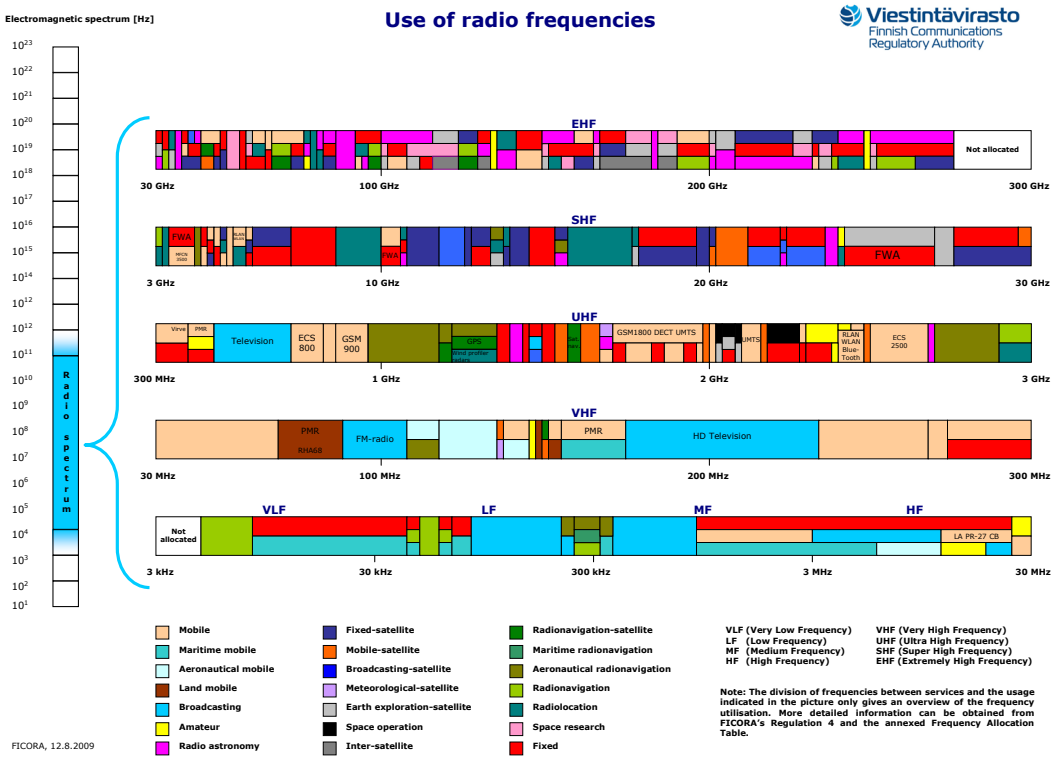

Figure 2.2: The current RF spectrum allocation in Finland [22].

Authority (FICORA) in Finland. Fig. 2.2 shows the current RF spectrum allocation in Finland regulated by FICORA.

As the number of wireless transmission technologies has grown significantly, it is clear that the rigid spectrum allocation cannot meet the growing demand for free spectrum bands [12]. In addition, some of the spectrum bands are not used frequently by their licensed PUs. According to measurements done by the FCC's Spectrum Policy Task Force [10], the rigidly allocated RF spectrum is in fact heavily underutilized, which gives opportunity for cognitive users to exploit bands that are unoccupied. The frequency bands that are allocated to, but in some location at some times are not utilized by their licensed users are called *spectrum holes* or spectrum opportunities [13].

The classic approach is that the spectrum holes can be exploited in three different dimensions: time, frequency and space. However, in [2] it is suggested that one can also exploit such dimensions as code (spread spectrum signals, time or frequency hopping codes), angle (beamforming) or polarization. An effective cognitive system should be able to identify opportunities in all dimensions for the most efficient spectrum utilization.

The approach of opportunistically utilizing idle spectrum and therefore improving the spectral efficiency is termed as *dynamic spectrum access*. In contrast to the legacy wireless systems that were designed to operate on a

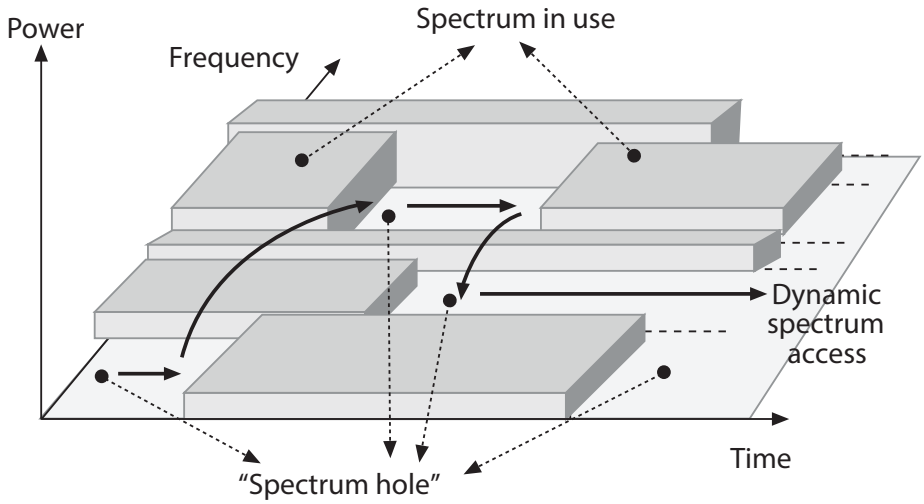

Figure 2.3: The concepts of dynamic spectrum access and spectrum holes, from [17].

certain frequency band, the main objective of CR is to optimize the wireless transmission by adaptively changing its transmission parameters [13]. Fig. 2.3 illustrates how DSA can be performed by utilizing spectrum holes.

The DSA strategies can be divided into three different models: dynamic exclusive use model, open sharing model and hierarchical access model [14,18], which are briefly explained next.

Dynamic exclusive use model is based on the current static spectrum regulation policy where spectrum band are licensed to PUs for exclusive use. However, the spectrum efficiency is improved by introducing flexibility with two ways: *spectrum property rights* and *dynamic spectrum allocation*. The first of these approaches allows users to sell and trade technology and to freely choose technology [14]. On the other hand, dynamic spectrum allocation tries to improve spectral efficiency by utilizing the spatial and temporal statistics of different services [18].

Open sharing model (also referred to spectrum commons model) assumes that all users have equal rights to use the spectrum. Thus, the spectrum can be shared with cooperation - or simply by co-existing. When the spectrum is shared cooperatively, users need to employ a common inter-networking protocol and communicate with each other [20].

Hierarchical access model gives all SUs free access to licensed spectrum bands with a constraint that the interference caused to the PUs is limited [20]. This can be done using one of the three approaches: interweave, spectrum underlay or spectrum overlay [23]. In spectrum underlay approach, the SUs operate below the noise floor of PUs for example by spreading the transmission power over a wide frequency band [20]. An overlay approach allows also

higher transmit powers for SUs but permits the transmission only at times or locations where the spectrum is unutilized by the PUs [18]. The interweave strategy uses the spatial domain for spectrum exploitation by utilizing the primary spectrum in locations where primary activity is absent, for example in TV broadcasting and cellular networks [18]. Especially in hierarchical access model, the interference management should be carefully taken into consideration.

Interference management

The main constraint in opportunistic spectrum reuse is the fact that the opportunistic secondary transmission must not cause harmful interference to the primary receivers. One approach to reduce the caused interference is to specify and to obey a set of two parameters: maximum level of interference power perceived by a PU and a maximum probability that the interference level exceeds that [14]. Another method in measuring interference was proposed by the FCC. It includes a parameter called *interference temperature* that serves as an upper bound of the interference caused to PUs and consists of both random noise power level and interference level from other transmitters [13]. According to the model, each PU has a limit temperature that guarantees a certain quality of service [23]. However, the locations of the primary receivers may not be known and they can be passive. Hence, the interference levels may be difficult to characterize in practice. The interference management in CR systems is studied in more detail in [24].

2.4 Cognitive radio in wireless transmission standards

In recent years, the interest in cognitive radio systems as a part of the wireless transmission standards has risen significantly. Various cognitive features have already been included in current wireless communication standards. Several standardization organizations such as the International Telecommunication Union (ITU), the Institute of Electrical and Electronics Engineers (IEEE), European Telecommunications Standards Institute (ETSI), SDR forum and European Association for Standardizing Information and Communication Systems (ECMA) are all working on CR related standards in different scenarios [25]. Next, a few of the main standards that incorporate CR techniques are presented.

IEEE 802.22 standard (known as *cognitive radio standard*) is one of the earliest standardization efforts that is developed based on cognitive radios [12]. It defines techniques to exploit white spaces in TV broadcast bands in wireless regional area networks (WRANs). The same IEEE 802 working group has also prepared the IEEE standards 802.11y/af and 802.19 that define how to share wireless local area network (WLAN) frequency bands with other

users and how to operate in the coexistence of networks belonging to various different wireless standards in the unlicensed band [12]. Dynamic Spectrum Access Networks Standards Committee (DySPAN - SC) (formerly known as the IEEE Standardization Coordination Committee 41, SCC41) has also developed definitions, architecture and conditions for dynamic spectrum access in wireless communication. [23, 25].

Other international standards that involve CR are for example ITU-R WP 1B and ITU-R WB 5A that include definitions on spectrum management and DSA as well as description of CR systems in the land mobile service [12, 25]. ETSI TC RSS group also provided standardization for regulatory aspects of CR systems and coexistence architecture for CR networks in ultra high frequency (UHF) white space frequency bands [25].

Chapter 3

Spectrum Sensing in Cognitive Radio

As stated earlier, in a CR system, the opportunistic SUs must sense the spectrum in order to determine whether the primary receiver is transmitting or not. Spectrum sensing is defined in [2] as *the task of obtaining awareness about the spectrum usage and existence of PUs in a geographical area.* The awareness indicates in this context both measuring the RF content in the spectrum as well as acquiring information about the type of the transmitted signals [2].

In order to apply DSA and not to cause harmful interference to the primary transmission, SUs must be able to detect the presence of the PUs effectively, which implies that spectrum sensing is one of the most essential elements in CR [26]. Hence, an advanced SU should both be able to detect other radio transmissions in its proximity and to be capable of classifying whether the detected signal is a primary or another secondary transmission or some other interfering signal.

This chapter is organized as follows. In the next two sections, an overview of the currently used detection and classification techniques in CR is presented. The final section of the chapter introduces the aspects in collaborative spectrum sensing.

3.1 Signal detection

In this section, a brief overview of classical signal detection theory is presented, after which some commonly used signal detection techniques are introduced. In this section, only a single sensor case is considered and the detection is performed under a binary hypothesis test which is explained next.

3.1.1 Binary hypothesis test

The detection of a PU signal is essentially a classical statistical problem that can be formulated as a binary hypothesis test. In a binary hypothesis test, the absence of the target signal is denoted as a null hypothesis H_0 whereas an

alternative hypothesis H_1 states that the target signal is present. Therefore the binary hypothesis problem can be written as:

$$\begin{cases} H_0: & x(n) = w(n) \\ H_1: & x(n) = s(n) + w(n), \end{cases} \tag{3.1}$$

where $x(n)$ is the received signal, $w(n)$ denotes AWGN and $s(n)$ is the signal to be detected. Here n stands for the discrete time index. Since the measurements are affected by random noise, they can be modeled as random variables with a certain distribution. The distributions associated with both hypotheses are assumed to be different which allows for the detection of the distribution from which an observed sample is generated.

In a binary hypothesis test, the receiver always decides based on some decision statistic whether the observed data come from H_0 (decision D_0) or from H_1 (decision D_1). Since the received signal is affected by random continuously distributed noise, an observed value can in fact be drawn from either of the possible distributions. Therefore, there can occur four different decision cases that are shown in Table 3.1.

Table 3.1: Four different decision scenarios under a binary hypothesis test.

Decision	True Hypothesis	
	H_0 (only noise)	H_1 (noise and target signal)
D_0	Correct Decision Probability: $P(D_0\|H_0)$	Missed Detection Probability: $P_m = P(D_0\|H_1)$
D_1	False alarm Probability: $P_f = P(D_1\|H_0)$	Correct Detection Probability: $P_d = P(D_1\|H_1)$

Optimally, the decision rule should be formulated so that it would minimize the decision errors. However, in practice the suitable detection strategy depends on the nature of the decision making problem at hand. For example, in telecommunication applications it may be irrelevant whether the error happens when detecting 0 bit or 1 bit, whereas in radar detection numerous false alarms may overwhelm the whole radar system. There exists many different design criteria for detection. For more information, one can refer to [23,27–29].

If the distributions of the received signal under both hypotheses are known, the optimal test based on the i.i.d. observations $x(1), x(2), \ldots, x(M)$ is a likelihood ratio test (LRT) which is given by

$$\Lambda(\mathbf{x}) = \frac{\prod_{n=1}^{M} f(x(n)|H_1)}{\prod_{n=1}^{M} f(x(n)|H_0)} = \frac{L(\mathbf{x}|H_1)}{L(\mathbf{x}|H_0)} \underset{\text{choose } H_0}{\overset{\text{choose } H_1}{\gtrless}} \eta \tag{3.2}$$

where $f(x(n)|H_i)$ denotes the conditional probability density function (PDF) of $x(n)$ under H_i $(i = 0, 1)$ and η denotes a (scalar) threshold value. The

likelihood function (LF) under H_i $(i = 0, 1)$ for a given observation vector $\mathbf{x}$ is marked with $L(\mathbf{x}|H_i)$. The test statistic $\Lambda(\mathbf{x})$ is said to be a *simple* likelihood ratio (LR) when both of the distributions are completely known. However, if the distributions contain unknown parameters, it is said to be a *composite* LR. If one uses maximum likelihood estimates for the unknown parameters in the LRT, the test is then called the generalized LRT (GLRT) which is not necessarily optimal test but often works highly reliably.

In spectrum sensing, controlling the false alarm rate parameter is crucial since false alarms can lead to inefficient spectrum reuse [23, 30]. On the other hand, a good detector should also have high probability of detection since missed detections lead to retransmissions by PU and SU and may reduce the QoS for PU, too. Therefore, the detection criterion considered in this thesis is Neyman-Pearson (NP) criterion which maximizes the probability of detection with a constraint on the maximum false alarm probability P_f [27]. Thus, the NP lemma is given as *"the LRT that rejects H_0 in favor of H_1 when"* [13]:

$$\Lambda(\mathbf{x}) = \frac{L(\mathbf{x}|H_1)}{L(\mathbf{x}|H_0)} \geq \eta \quad \text{where} \quad P(\Lambda(\mathbf{x}) \geq \eta|H_0) = \alpha, \tag{3.3}$$

where α denotes the specified maximum allowed P_f. It should be noted that in order to design a NP detector one needs to know only the distribution of the received signal under H_0 [23].

There exists also other common approaches for the detection criteria. For example, *Bayesian* strategy uses prior probabilities and conditional densities of the two hypotheses in order to minimize the Bayesian risk. The approach where the Bayes decision rule corresponding to the least favorable prior probability assignment is used to minimize the Bayes risk is called *minimax* strategy [23]. However, these and other possible decision strategies are not covered here in more detail for brevity. Detailed information on different detection criteria can be found for example in [27, 28].

3.1.2 Signal detection techniques

Signal detection techniques for CR can be roughly divided into three categories: energy detectors, matched filter detectors and feature detectors [23, 30]. In this section, the basics of each detector group are briefly given. Naturally, there also exists numerous other detection techniques. For more information on the current state-of-the-art detection techniques, one can for example refer to [2, 12, 23, 26, 30]. It should also be noted that since the field of spectrum sensing is still relatively new, novel methods are still being developed.

Energy detection (ED), which is also known as a radiometry, is probably the most elementary signal detection technique [28]. Basically, the ED just measures the energy of the received signal over a given time interval and compares the result to a threshold value that is based on the energy of the background noise.

The main benefit of the ED is its simplicity and applicability to all kinds of signals. It is also stated that assuming i.i.d. Gaussian noise channel with known noise power, the ED is at least a GLRT for unknown random signals or even optimal detector when the signal is an uncorrelated Gaussian signal [30]. However, the ED cannot distinguish between different waveforms (e.g. between primary and secondary users or interference) and is highly susceptible to noise power uncertainties. When the signal-to-noise ratio (SNR) falls under a certain level of noise power uncertainty (known as *the SNR wall*), it is impossible to detect the signal even with infinitely long measuring time [31]. The ED technique is fairly well researched detection technique and interested readers can find more details on it in [32, 33].

Matched filtering is the optimal detection method when the transmitted waveform is completely known as it maximizes the SNR in AWGN transmission channel [34]. In matched filtering, the received signal is correlated with a known signal sequence and the result of that is then compared with a predefined threshold value. Due to the coherent nature of the detector, detection can be very fast with matched filters [13].

As matched filtering works for only one type of a known signal, one needs a bank of them for detecting several types of waveforms, which naturally causes implementation issues [23]. Another limitation in practical use is the fact that a matched filter needs to know the properties of the detected waveform (i.e. preambles, pilot signals) and background noise statistics perfectly in order to operate. In addition, matched filtering is highly sensitive to synchronization errors [30].

Feature-based detectors look for certain features in the received signal in order to detect them. Since most man-made signals are cyclostationary and have periodic patterns caused by modulation and coding operations, for example by symbol rate, chip rate or channel coding, they can also be detected based on them [26]. For example, the insertion of the CP in an OFDM signal induces nonstationarity, which makes its autocorrelation function (ACF) time-varying and nonzero valued at time lags corresponding to the symbol length. This nonstationary feature can be exploited and used as a basis for signal detection. Such ACF-based detectors are proposed in a number of papers, e.g. [35–37]. The detection schemes that are proposed in Chap. 6 are likewise based on the cyclostationary features of OFDM signals.

The benefit of feature-based detectors is that they can distinguish between different waveforms. In addition, feature-based detectors can be used for detecting a wide variety of different waveforms. However, they can be relatively complex to design as compared to the ED, and the detection time can be rather long in comparison to the matched filtering. Typically, the signal also needs to be oversampled with relation to the chip or symbol rate to detect cyclostationarity.

3.2 Signal classification

Different modulation techniques are used in different wireless communication systems. Moreover, many wireless systems employ adaptive modulation and coding in link adaption. Thus, the automatic recognition of the used waveform done by an intelligent radio receiver can prove to be very useful both in civilian and military applications [38]. For example, in military applications signal classification can be used in threat analysis or electronic warfare to classify adversary radio emitters, whereas some commercial applications are spectrum management in spectrum surveillance and signal source identification [39, 40].

Identifying different kinds of signal waveforms is also an important part of CR networks [11]. If a cognitive user has detected a wireless transmission signal, it is valuable to distinguish what type it is, since it can be transmitted by either primary or secondary users. In some cases, there can even exist malicious SUs that ignore or disobey the spectrum sharing rules. In those situations, one needs to identify such users in order to locate and exclude them. Thus, utilizing signal classification techniques for hostile user identification is also considered as a major task in CR networks [41].

In addition, the coexistence of heterogeneous networks where many different types of signals are transmitted simultaneously gives another motivation for developing signal classification methods. In order to control dynamic spectrum access efficiently and to optimize the coordination and coexistence among different SUs in heterogeneous networks, one needs not only to detect different wireless transmissions but also to distinguish among them [42]. Furthermore, an intelligent SDR can also adjust its demodulator part of the receiver if it successfully classifies the received signal modulation type [43].

In this section, the basics of automatic modulation classification and signal identification are presented. For additional information on signal classification in CR systems, one can refer [38, 40, 44–47].

3.2.1 Automatic modulation classification techniques

Automatic modulation classification (AMC) is a method that targets to identify the modulation type of a given wireless communication system with high probability, short decision time, and large SNR range [38, 46]. Typically the modulation types that are used in wireless communications and need to be classified are amplitude shift keying (ASK) phase shift keying (PSK), frequency shift keying (FSK) and quadrature amplitude modulation (QAM) with different constellation sizes. *Inter-class* modulation classification refers to the case where the identified modulation types can vary (e.g. ASK, FSK or PSK), whereas in *intra-class* modulation classification identification is done within a single modulation class (e.g. BPSK or QPSK) [48].

AMC techniques can be traditionally divided into two broad classes: likelihood-based methods and feature-based methods [44, 46]. From these the former introduces a statistical decision theoretical approach, while the latter offers

more practically oriented statistical pattern recognition approach [40]. Next, the elementary information about these two categories is presented. Further information on AMC can be found in [49–51].

Likelihood-based modulation classification is basically a multiple composite hypothesis testing problem, which is based on the idea that the PDF of the observed waveform, conditioned on the embedded modulated signal, contains all information required for the modulation classification done with a composite LRT [38, 44]. In this multiple hypothesis problem each hypothesis H_i corresponds to the case that the signal is of i^{th} modulation type ($i = 1, \ldots, N_{mod}$, where N_{mod} is the total number of modulation types). The unknown parameters in the composite LRT, depending on the classification scheme, can be for example carrier phase, timing offset, phase jitter, signal level, signal power, signal power spectral density or some combination of them [38].

In likelihood-based AMC, the likelihood function is calculated for each modulation type. Under the assumption of equal priors, the decision is made based on which modulation type maximizes the likelihood function [43]. In the literature, three different variations of LRTs for the likelihood-based AMC are usually proposed : average likelihood ratio test (ALRT), generalized likelihood ratio test (GLRT) and hybrid likelihood ratio test (HLRT) [38].

In ALRT, all unknown parameters (assumed to be mutually independent of each other) are treated as random variables with certain PDFs which are then used for averaging the LF under each modulation type (or hypothesis) [43]. The LF under hypothesis H_i is then given by [38]:

$$L_A^{(i)}[x(n)] = \int L[x(n)|\mathbf{v}_i, H_i] p(\mathbf{v}_i|H_i) \mathrm{d}\mathbf{v}_i, \tag{3.4}$$

where $L[x(n)|\mathbf{v}_i, H_i]$ is the conditional LF of the noisy received signal $x(n)$ under H_i, conditioned on the unknown parameter vector $\mathbf{v}_i$, and $p(\mathbf{v_i}|H_i)$ is the a priori PDF of $\mathbf{v}_i$ under H_i. In Bayesian sense, if the chosen a priori PDF is the same as the true PDF of $\mathbf{v}_i$, ALRT results in an optimal classifier [52]. Furthermore, if the PDF of $\mathbf{v}_i$ is known, the problem reduces to a simple hypothesis-testing problem by integrating over $\mathbf{v}_i$ [38]. However, usually the problem with ALRT is the high computational complexity of multidimensional integration that may render it to be impractical in many practical situations [38].

In GLRT based classification the unknown parameters are treated as unknown deterministic quantities and are estimated. For example, maximum likelihood estimates (MLEs) of the parameters are typically used in the LRT. The LF under H_i in this case is then given by [38]:

$$L_G^{(i)}[x(n)] = \max_{\mathbf{v}_i} L[x(n)|\mathbf{v}_i, H_i]. \tag{3.5}$$

Now, instead of multidimensional integration, the LF consists of multidimensional maximization. Unfortunately, the estimation of the unknown pa-

rameters may lead to the same LF value for the nested constellations (e.g. BPSK and QPSK or 16-QAM and 64-QAM), which may cause classification errors [38].

HLRT approach is basically a combination of ALRT and GLRT techniques. Thus, the LF in HLRT approach is [38]:

$$L_H^{(i)}[x(n)] = \max_{\mathbf{v}_{i1}} \int L[x(n)|\mathbf{v}_{i1}, \mathbf{v}_{i2}, H_i]p(\mathbf{v}_{i2}, |H_i)\mathrm{d}\mathbf{v}_{i2}, \tag{3.6}$$

where $\mathbf{v}_i = [\mathbf{v}_{i1}^T, \mathbf{v}_{i2}^T]^T$ and $\mathbf{v}_{i1}$ and $\mathbf{v}_{i2}$ are vectors of unknown quantities modeled as unknown deterministic parameters and random variables respectively. Hence, HLRT offers a reasonably reliable classification performance without the computational complexity of ALRT [43]. It should be noted that there are also proposed quasi-HLRT schemes which are based on non-MLE estimation methods to avoid heavy computational workload [43].

Feature-based modulation classification is the broader and more diverse class of AMC. Basically, the classification is now done based on different features that uniquely represent each modulation format [43]. For example, modulation classification schemes have been proposed based on such features as signal statistics [52], higher order signal statistics (e.g. moments, cumulants, kurtosis) [53, 54], wavelet transform [48], cyclostationarity [55], zero crossing intervals [56], multi-fractals [57] and time-frequency analysis [58]. Some proposed AMC techniques also include techniques based on entropy, fuzzy logic, moment matrix and constellation shape recovery [38]. In [39], it is suggested that the classification based on different features can be done with pattern recognition tools. The procedure consists then of three parts: sensing, feature extraction and decision procedures. The pattern recognition based decision procedures can also include use of neural networks or subspace classifiers.

There are many different algorithms for feature-based modulation classification. A survey of cyclostationarity feature-based modulation classification techniques can be found in [59]. In [38], a comprehensive list of different feature-based AMC methods is presented. Additional information on feature-based AMC in CR can also be found in [40, 44, 47].

As shown, there are numerous different techniques for signal modulation classification. However, in practice, the algorithm must be chosen based on the scenario at hand since there is not a single method that can distinguish among all different modulation types optimally [44]. AMC can be utilized also in signal detection purposes. For example, a detection scheme utilizing AMC is proposed in [60]. It is based on the fact that all PU signals use one modulation form or another, and hence the ability of detecting any modulation scheme is sufficient for declaring the presence or absence of the PU. There have also been proposed such spectrum sensing schemes that combine both detection and AMC, for instance in [52].

3.2.2 Signal transmission parameter estimation

In situations where the receiver knows the type of the received signal it is also important to distinguish or estimate what transmission parameters are being used. This problem is usually referred to *signal parameter estimation*. As cognitive networks are usually based on exploiting the frequency band of a certain known primary signal with known transmission parameters (for example terrestrial digital video broadcasts), by estimating some waveform parameters one can easily determine whether the received signal consists of the primary signal or not. Furthermore, and similarly as with the AMC, estimating signal transmission parameters helps in spectrum monitoring and distinguishing adversary or illegal transmissions [61].

In heterogeneous networks, various different transmissions that use the same modulation method can be present simultaneously. For example, secondary cellular Worldwide Interoperability for Microwave Access (WiMAX) or Long-Term Evolution (LTE) transmissions can operate in the same network with terrestrial digital video broadcasting (DVB-T and DVB-T2) signals, all of which utilize OFDM modulation. However, each signal uses its own OFDM transmission parameters such as the number of subcarriers, symbol duration, or the length of the CP. Thus, by estimating the transmission parameters of the received signal, cognitive users can distinguish among different waveforms. For example, a joint detection and classification of mobile LTE and WiMAX OFDM signals in CR networks is proposed in [62]. In addition, a method for distinguishing between DVB-T and LTE signal (OFDM-based) as well as programme-making and special events (PMSE) signal (QPSK modulated) is proposed in [63].

Various techniques for estimating OFDM transmission parameters have been proposed in the literature. Usually, the estimation is performed based on the cyclostationarity that is induced by the insertion of the CP [61]. For example, methods for finding the symbol duration based on the distance between peaks in the autocorrelation function and for estimating the CP length based on the entropy of the time-frequency transform of the received signal are proposed in [64]. On the other hand, in [65], symbol duration estimation may be done based on cyclic correlation algorithm and the CP length is found by performing a correlation test. When the symbol length is known, a method for finding the CP length using autocorrelation of the received signal with its delayed copy is proposed in [66]. As shown later in Sec. 4.2.1, in theory such autocorrelation function has non-zero elements only at the part that falls into the guard interval. Thus, by calculating the power ratio between guard time and symbol duration, one can estimate the CP length (assuming that the SNR level is known) [66].

The performance of a given estimator can be measured with basic estimation theory tools. It is desirable that an estimate $\hat{\theta}$ of an unknown parameter θ would on average be as close as possible to the true value. *The bias* of an estimator is the average error that it gives:

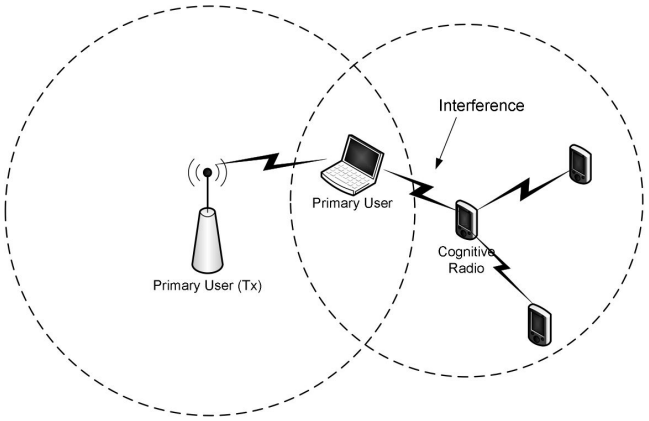

Figure 3.1: The hidden PU problem, from [2].

$$B(\hat{\theta}) = \mathbb{E}[\hat{\theta}] - \theta. \tag{3.7}$$

An estimator is said to be *unbiased* if its bias is equal to zero for all values of parameter θ. However, the unbiasedness itself does not guarantee the good quality of the estimator, since a preferable estimator should have the smallest variance possible. Thus, a useful measure of the quality of an estimator is *the mean squared error* (MSE), which can be calculated as

$$\mathrm{MSE}(\hat{\theta}) = \mathbb{E}[(\hat{\theta} - \theta)^2] = \mathrm{Var}(\hat{\theta}) + B(\hat{\theta})^2. \tag{3.8}$$

Alternatively, one can apply a constraint that the estimator is unbiased and minimize the variance under such constraint. For unbiased estimator, the MSE is simply its variance.

3.3 Collaborative spectrum sensing in cognitive radio

It is shown that the spectrum sensing performance can be improved significantly with cooperation [23, 26]. In cooperative sensing, multiple geographically distributed SUs cooperate in sensing a common PU transmission [23]. For example, such multipath propagation effects as shadowing or fading can be mitigated with cooperation [23,26]. The increased spatial diversity of many cooperating sensors help addressing these problems, since it is highly improbable that all cooperating SUs experience a radio channel in deep fade or shadowing simultaneously. Cooperation also helps in improving the detection sensitivity, robustness to non-idealities and addressing the situation called the hidden PU problem. [23, 26]

The hidden PU problem (or the hidden node problem), depicted in Fig. 3.1, is a common situation that can be very problematic in single-user spectrum

sensing. It happens when the cognitive user is located outside the reach of the primary transmitter and hence does not detect the PU transmission. However, if the SU starts transmitting at that frequency band, it may disrupt the primary receivers that are both in the reach of the primary and the secondary transmission. The hidden primary user problem can also occur for example because of severe multipath fading or shadowing [2].

In cooperative sensing, many cognitive users share their spectrum sensing information with others. The architecture of cooperative sensing can follow either *centralized* or *decentralized* strategy [12, 23]. In centralized strategy, one cognitive user serves as a fusion center (FC) and makes decisions based on the collected data that contains all the observations from all other users in the collaborative network [12, 23]. After the FC has made a decision whether the primary signal is present or not it communicates it to all cooperating CR users. On the other hand, the decentralized strategy introduces a more sophisticated structure where the individual sensors process the data locally before sending a summary of it to the FC [12, 23]. Usually, the algorithms for data fusion in the FC are derived under the assumption of the independence of the local observations conditioned on either of the possible hypotheses [23].

The centralized topology offers a simple network where classical optimization theory can be applied in order to solve the most efficient cooperative spectrum access [13]. However, because in a centralized system each user sends all its observations to the FC, it requires more bandwidth for reporting than the decentralized strategy. Furthermore, the power consumption is also higher when more data is being transmitted [23]. It is also stated that the information loss in summarizing the local observations causes minimal performance degradation for the decentralized system compared with the centralized system [23].

The data that is sent to the FC can consist of either binary decisions (*hard decisions*) or some other representation (for example some sufficient statistic) of the current state of the sensed spectrum band (*soft decisions*). After receiving the data, the FC then combines the received data with some fusion rule in order to make decisions. For example, in the case of hard combining can be done based on traditional Boolean fusion rules (OR, AND or MAJORITY) [67]. In the case of soft combining, such existing receiver diversity techniques as equal gain combining (EGC) and maximal ratio combining (MRC) can be utilized, for example [67].

Further reading about collaborative spectrum sensing can be found for example in [23,67] and about distributed detection in [68,69]. A survey regarding the performance analysis of hard decision and soft decision based cooperative sensing in imperfect reporting channels is presented in [70].

Chapter 4

Basics of Cepstral Analysis and OFDM Signals

In this chapter, the basics of the cepstral processing and its applications are introduced. After that, a brief overview of the popular OFDM transmission method is given.

4.1 Cepstrum

The cepstrum was first introduced by Bogert, Healy and Tukey in 1963 [4] to detect echoes in a time-series of seismic waves. They discovered that a logarithmic spectrum of a signal containing echos has an additive periodic component depending only on the size and the delay of the echo, and taking a further spectrum of that log-spectrum allows for detecting the presence and the "frequency" of that echo [4,71]. At the same time, they also introduced the paraphrased terms *the cepstrum* to represent the spectrum of the log-spectrum and *the quefrency* to stand for the frequency of the spectral ripples caused by the echoes and thus to be the unit of the cepstrum [72].

4.1.1 Cepstrum definitions

There exists different definitions for the cepstrum in the literature. Commonly, the cepstrum is defined to be an inverse Fourier transform of the logarithmic magnitude spectrum of a signal [4, 7, 71, 73, 74]. Because of the different definitions, there exists also different nomenclature for it such as the complex cepstrum, the real cepstrum, the power cepstrum, and the phase cepstrum. Next, the different cepstrum forms are briefly presented. Interested readers are suggested to refer [71, 75] for more details.

Complex cepstrum

Sometimes the cepstrum is defined as the Fourier transform of the logarithmic spectrum of a signal [76, 77]. Since taking the spectrum of a signal gives

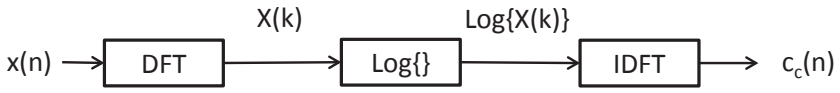

Figure 4.1: Block diagram of the complex cepstrum.

complex output, the logarithmic operation must be the complex logarithm, which yields the nomination *the complex cepstrum*. The exact definition of the complex cepstrum $c_c(n)$ of the discrete-time input signal $x(n)$ is given by [71, 75]

$$c_c(n) = \frac{1}{2\pi} \int_{-\pi}^{\pi} \mathrm{Log}\big\{X(\omega)\big\} e^{j\omega n} \mathrm{d}\omega, \tag{4.1}$$

where $X(\omega)$ is the discrete-time Fourier transform (DTFT) of $x(n)$ given by

$$X(\omega) = \sum_{n=-\infty}^{\infty} x(n) e^{-j\omega n}, \tag{4.2}$$

where ω denotes the angular frequency ($-\pi < \omega \leq \pi$). The complex logarithm Log{Z} of a complex quantity Z is defined as

$$\mathrm{Log}\big\{Z\big\} = \log|Z| + j \arg[Z], \tag{4.3}$$

where log stands for the natural logarithm and arg for the argument operator. However, in practice, the cepstrum is usually computed using the discrete Fourier transformation (DFT) instead of the DTFT. In addition, it is typically computed using the fast Fourier transform (FFT) algorithm. The definition of the complex cepstrum in terms of DFT and inverse discrete Fourier transform (IDFT) is then the following [78]:

$$\begin{aligned} \hat{x}(n) &= \mathcal{F}^{-1}\Big\{\mathrm{Log}\big\{\mathcal{F}\{x(n)\}\big\}\Big\} \\ &= \frac{1}{\sqrt{N_r}} \sum_{k=0}^{N_r-1} \big(\log|X(k)| + j \arg[X(k)]\big) e^{j\frac{2\pi kn}{N_r}} \end{aligned} \tag{4.4}$$

for $n = 0, 1, \ldots, N_r - 1$, where $\mathcal{F}$ and $\mathcal{F}^{-1}$ denote the DFT and the IDFT respectively and N_r is the number of data points used in the transforms when computing the cepstrum. The term $X(k)$ represents the DFT of $x(n)$ which is computed as [71]

$$X(k) = \sum_{n=0}^{N_r-1} x(n) e^{-j\frac{2\pi kn}{N_r}}. \tag{4.5}$$

The process of calculating the complex cepstrum with the DFT and the IDFT is illustrated in Fig. 4.1. It should be noted that since the DFT is

a sampled version of the DTFT, the complex cepstrum calculated with the DFT is due to the quefrency domain aliasing (resulting from the sampling) an approximation of the "true" complex cepstrum defined in Eq. (4.1) [71]. However, by utilizing FFT algorithms, one can make the quefrency aliasing reasonably insignificant by using sufficiently large values of N_r [79].

The main issue in computing the complex cepstrum is the implementation of the complex logarithm, and more specifically the computation of the phase angle $\arg[X(k)]$ of the spectrum $X(k)$ [71, 80]. Usually, the angle of a complex value is specified as a modulo of 2π (called the principal value of the angle). This causes problems as a proper and invertible complex cepstrum would need a continuous phase function which would need an "unwrapping" of the phase function [71, 77, 81]. Unfortunately, the implementation of accurate unwrapping has proven to be challenging and hence the use of the complex cepstrum might be impractical. However, because of the invertibility property of the complex cepstrum, it is used frequently in such processing that involve homomorphic deconvolution or homomorphic filtering for example in speech processing, image processing or seismic data processing [5].

Real cepstrum

The difficulties in the implementation of the complex cepstrum, the real cepstrum is usually used in practice instead of the complex cepstrum [77]. In fact, in the literature the term *cepstrum* generally refers to the real cepstrum. The exact definition of the real cepstrum is given by [71]

$$c_r(n) = \frac{1}{2\pi}\int_{-\pi}^{\pi} \log\left|X(\omega)\right| e^{j\omega n} \mathrm{d}\omega, \tag{4.6}$$

Again, using the DFT instead of the DTFT, one can write the real cepstrum as

$$\begin{aligned} c_r(n) &= \mathcal{F}^{-1}\{\log|\mathcal{F}\{x(n)\}|\} \\ &= \frac{1}{\sqrt{N_r}} \sum_{k=0}^{N_r-1} \log|X(k)| e^{j\frac{2\pi kn}{N_r}}. \end{aligned} \tag{4.7}$$

Now, as $|X(k)|$ is a real valued function, the phase argument is ignored and hence unwrapping is not needed. Fig. 4.2 shows the block diagram of the cepstral process, which is now simpler than with the complex cepstrum.

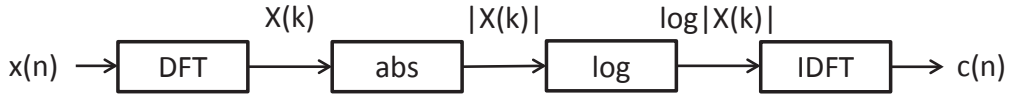

Figure 4.2: Block diagram of the real cepstrum.

It should be noted that discarding the phase components creates the output of the DFT to be symmetric across the zero-point [82]. Hence, the real cepstrum is also always symmetrical. It can also be proved that the real cepstrum sequence is in fact the even part of the complex cepstrum [82], i.e.,

$$c_r(n) = \frac{c_c(n) + c_c(-n)}{2}. \tag{4.8}$$

Note also that throughout this thesis, the real cepstrum that is computed with the DFT/IDFT implementation shown in Eq. (4.7) is used. Since the real cepstrum is symmetrical, only the first half of the cepstrum sequence need to be taken into account in derivations. Furthermore, the real cepstrum is also referred simply as *the cepstrum* and $c_r(n)$ is denoted by $c(n)$ for convenience.

Power cepstrum

The power cepstrum was first described by Bogert *et al.* in their article [4] in 1963, in which the whole concept of the cepstrum was first introduced. The power cepstrum is defined as a square magnitude of an inverse Fourier transform of the logarithmic square magnitude spectrum (i.e. logarithmic power spectrum) of a signal [4, 5, 83]:

$$c_p(n) = \left|\mathcal{F}^{-1}\{\log|\mathcal{F}\{x(n)\}|^2\}\right|^2 = \left|\frac{1}{\sqrt{N_r}}\sum_{k=0}^{N_r-1}\log\left|X(k)\right|^2 e^{j\frac{2\pi kn}{N_r}}\right|^2. \tag{4.9}$$

Fig. 4.3 shows the algorithm of computing the power cepstrum.

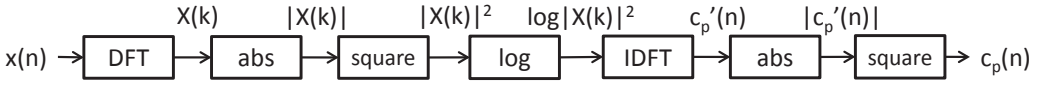

Figure 4.3: Block diagram of the power cepstrum.

Among different cepstrum definitions, the power cepstrum is a relatively frequently used technique in practical applications. For example, it is used to analyze the periodic effects that are caused by a vibrating machine (e.g. fault detection in a turbine blade or a gearbox) [84].

Phase cepstrum

The phase cepstrum is defined as an inverse DFT of the phase of the complex logarithm [5]. Hence it is given by

$$c_a(n) = \mathcal{F}^{-1}\left\{\mathcal{I}\Big[\log\left\{\mathcal{F}\{x(n)\}\right\}\Big]\right\} = \frac{1}{\sqrt{N_r}}\sum_{k=0}^{N_r-1}\arg[X(k)]e^{j\frac{2\pi kn}{N_r}}, \tag{4.10}$$

where $\mathcal{I}\{\cdot\}$ and arg[·] denote the imaginary part and the argument of a complex number. Fig. 4.4 illustrates the algorithm of computing the phase cepstrum. The arg-operator in Eq. (4.10) is simply the imaginary part of the complex logarithm.

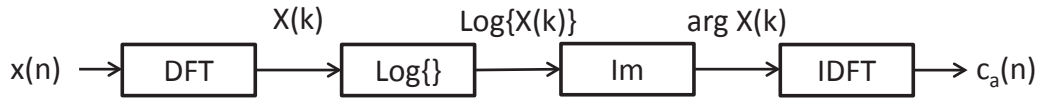

Figure 4.4: Block diagram of the phase cepstrum.

Unfortunately, the phase cepstrum is as difficult to compute as the complex cepstrum since they both require the unwrapping of the phase. It is also shown in [5] that empirical experiments have shown that the phase cepstrum does not perform as well as the power cepstrum in the determination of echo arrival times. Hence, the usage of the phase cepstrum in practical applications is relatively minimal.

4.1.2 Applications of cepstral analysis

The cepstrum has found most of its usage in the field of speech processing. For example, applications such as pitch estimation, voice activity detection, voiced/unvoiced speech detection, speech recognition and vocoding utilize the properties of the cepstrum [6,7,85,86]. Another remarkable area where the cepstrum is used is the analysis of different kinds of signals that include harmonic components, such as seismic waves [4], motor vibration signals [83, 84, 87] or electrocardiograph (ECG) signals [88].

Next, the main applications that use cepstral analysis are presented. First, the speech processing applications are discussed, after which the applications in the field of communications and cognitive radios are introduced. Finally, other cepstrum applications are briefly presented.

Applications in speech processing

The cepstrum has properties that are extremely suitable for the processing of speech signals. Traditionally, a speech signal is considered to consist of a source signal which is convolved with a filtering vocal tract impulse response function [71, 75, 86, 88]. After taking a DFT and a logarithm, the convolution turns into a simple addition, which allows for easy separation of the cepstra of the excitation signal and the vocal tract impulse function.

The process of removing one of the above mentioned components of the speech production model is called *homomorphic filtering* [71, 75, 79, 86]. Fig. 4.5 shows an example of homomorphic filtering where an envelope of a voice spectrum is obtained by cutting out the high quefrencies of the cepstrum. When the resulting cepstrum is converted back to the spectral domain, the

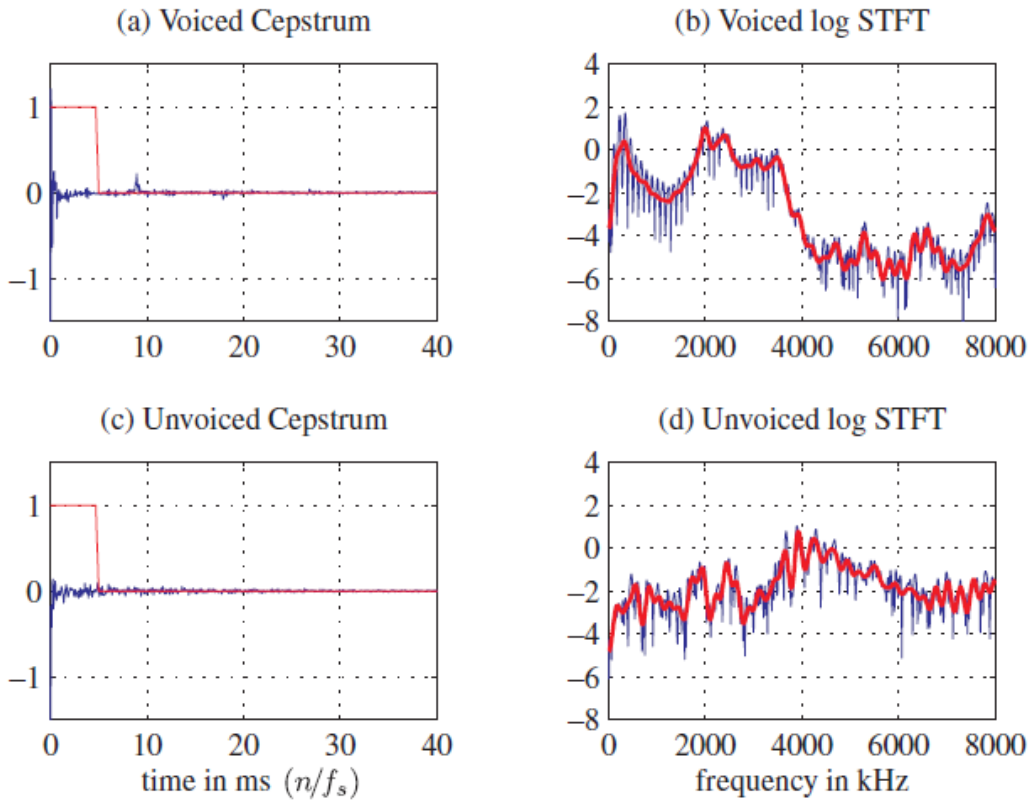

Figure 4.5: Cepstra (a, c) and logarithmic spectra (b, d) of a voiced speech signal and an unvoiced speech signal, from [71].The red curves illustrate the homomorphic filtering process.

smoothened spectrum that represents the slow-varying vocal tract transfer function has remained.

Since the behaviour of the vocal tract transfer function can be efficiently presented with only a few cepstral coefficients, it is a useful tool in applications such as speech coding (vocoding) [72, 89] and speech recognition [90, 91]. Especially in speech recognition applications, the spectrum of the speech signal is mapped to a mel-frequency spectrum that corresponds better with the human hearing system [91]. Hence, those applications utilize special cepstral coefficients called the mel-frequency cepstral coefficients (MFCC).

Another remark from the Fig. 4.5 is that the voiced sound induces a peak in the cepstrum, which corresponds with the fundamental period of the speech. This distinctive feature can be used for applications such as pitch detection [72], voiced/unvoiced speech detection [92, 93] and voice activity detection [94].

Applications in communications

The homomorphic abilities of cepstral analysis have been utilized also in communications applications. For example, in [95] the channel response of a frequency selective multipath channel is estimated utilizing cepstral analysis. In

addition, prefiltering for time delay estimation in reverberant environment for two or more microphones is implemented utilizing cepstral processing in [96]. In both cases, the homomorphic deconvolution offered by cepstral processing is used for determining channel properties.

The use of the cepstrum in cognitive radio systems or radio frequency signal detection or classification purposes has been relatively minimal. In [97], the authors propose a method for the automatic recognition of different OFDM waveforms based on cepstral features. In 2012, Al-Makhlasawy *et al.* [98] suggested a method for an automatic OFDM signal modulation type detector based on MFCCs. To my knowledge, there are not any other cognitive radio applications that use cepstral analysis, which makes the scope of this thesis relatively novel.

Other applications

Cepstral processing is also utilized in many other applications that involve periodic signals. Historically, it was used for analyzing seismic waves [4]. In machine and power industry, the cepstrum is used to discriminate failures in a rotating machine from the vibration signal, since most of the abnormalities cause harmonic vibration that can be distinguished with the cepstrum [83, 84, 87]. Also medical applications use cepstral analysis. In [88], it is shown that homomorphic filtering and cepstral analysis can be used for example in diastolic heart sound analysis for the detection of coronary artery disease and ECG pattern classification. In addition, also applications, such as radar for determining the arrival time of the incoming wavelet and marine exploration for ocean bottom mapping both use cepstral analysis [88].

4.2 OFDM signal model

Current mobile and wireless transmission applications are in need of high rate transmission schemes. Multicarrier modulations are used in most of the current and emerging high data rate wireless system such as LTE, WiMAX and WLAN. The key idea in multicarrier transmission is to reduce channel distortion by spreading the useful data over a large number of carriers. That way, the symbol duration could be guaranteed to be longer than the maximum delay of the channel [99]. This feature is used to reduce the distortion caused by multipath propagation as a frequency selective broadband channel was turned into multiple narrowband subchannels that experience flat fading.

OFDM is a widely used multicarrier transmission scheme in current wireless communications. For example, it is the basis of digital radio broadcasting (DAB in Europe), digital video broadcasting (DVB-T and DVB-T2) transmissions, 4G mobile transmissions (LTE), wireless local or metropolitan area networks (WLAN and WMAN) as well as wired digital subscriber line (DSL) internet access schemes. Hence, the vast popularity of the OFDM waveform

in current communication systems justifies why this study is concentrated in processing of OFDM signals.

Next, the basics of OFDM transmission and its properties are given. In addition, some popular standards that use OFDM waveforms are introduced and the criteria to choose different transmission parameters is briefly presented. Interested readers can refer [3] for more details on OFDM systems.

4.2.1 OFDM implementation

Fig. 4.6 shows the OFDM system model on a discrete time baseband level. The transmitter side of it includes a serial-to-parallel transformation, N_d-point IDFT, insertion of N_c samples long CP and a parallel-to-serial transformation. After that the digital baseband data is fed to a RF transmitter through a digital-to-analog converter. If $S(0), \ldots, S(N_d - 1)$ are N_d complex QAM (or PSK) symbols, then the output of the IDFT is given by

$$s(n) = \frac{1}{\sqrt{N_d}} \sum_{k=0}^{N_d-1} S(k) e^{\frac{j2\pi kn}{N_d}} \tag{4.11}$$

for $n = 0, 1, \ldots, N_d - 1$. Here n is the discrete time index while k is the discrete frequency index. Generally, the FFT/IFFT are used instead of the DFT/IDFT for efficient implementation [3].

The receiver side of the OFDM transceiver is an inversed version of the transmitter. Thus, after RF transmitter, analog-to-digital converter and timing and frequency synchronization, an OFDM receiver includes serial-to-parallel transformation, removing of the CP, N_d-point DFT, parallel-to-serial transformation and symbol detection. More detailed information of OFDM transceiver implementation can be found in [3].

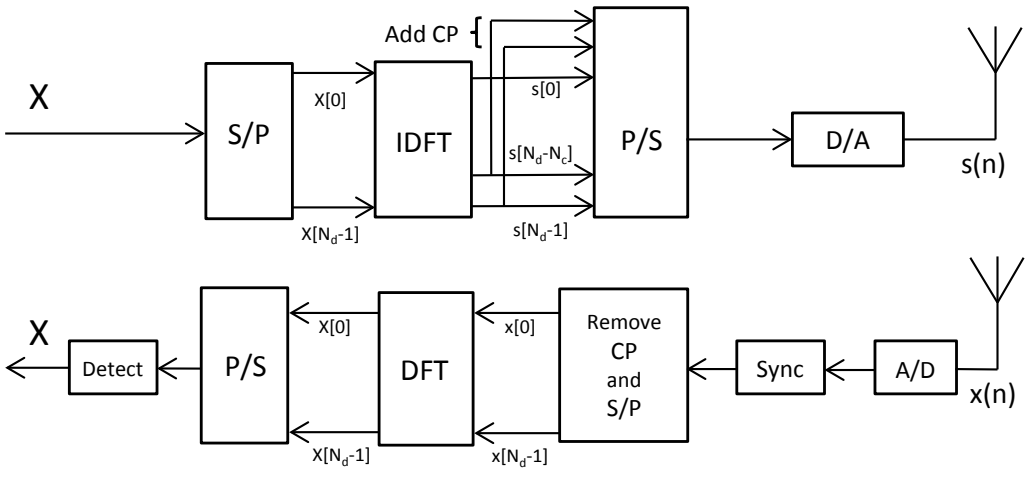

Figure 4.6: A simplified discrete-time-baseband model of an OFDM transceiver.

In an OFDM signal, a high-rate serial data stream is split up into a set of low-rate substreams [3]. Thanks to the orthogonality used in OFDM, subcarri-

ers can overlap in frequency domain without causing interference to each other, which guarantees near optimal spectral efficiency [99]. Naturally, this gives a better spectral efficiency than with traditional frequency division multiplexing (FDM) scheme which has to use guard bands between subcarrier to prevent inter-carrier-interference (ICI). The bandwidth saving in OFDM scheme can be almost 50 % compared to the FDM transmission [3].

However, due to the required orthogonality, OFDM is relatively sensitive to the synchronization errors, phase noise or frequency offset caused by imperfections in the transceiver hardware or Doppler shift [3, 100]. According to [3], one additional drawback with OFDM compared to the single carrier modulation schemes is a relatively large peak-to-average power ratio, which may reduce the efficiency of the RF power amplifier.

In order to increase cyclic redundancy and to decrease inter-block interference (IBI) from previous OFDM blocks caused by the delay spread of the transmission channel a CP is inserted in an OFDM symbol [101]. A complete OFDM symbol is created by prefixing the N_d symbols long IDFT output with its own last N_c samples as shown in Fig. 4.7. If OFDM signal contains B OFDM symbols each of $N_s = N_c + N_d$ samples, then the total number of samples in an OFDM signal is $M = B(N_c + N_d)$.

The samples in a CP in an OFDM symbol are copies from the last N_c data samples, which naturally induces correlation in the signal. Using $n = p + bN_s$, the accurate correlation of an OFDM signal for different lags $\tau \in \mathbb{Z}$ is simply:

$$\mathbb{E}[s(p+bN_s)s^*(p+bN_s-\tau)] = \begin{cases} \sigma_s^2 & \tau = \pm N_d, \quad p = 0, 1, \ldots, N_c - 1 \\ 0 & \text{otherwise,} \end{cases} \tag{4.12}$$

where σ_s^2 represents OFDM signal power, p is a sample index inside an OFDM symbol and b is the index of that OFDM symbol ($b = 1, \ldots, B$).

Techniques based on this correlation have been used for various purposes related to OFDM systems. For example, it may be utilized in synchronization and estimation of different channel parameters [36].

4.2.2 OFDM applications and standards

OFDM is used in various wireless applications. It was first used in digital audio broadcast (DAB) systems, for example in Digital Radio Mondiale (DRM) and EUREKA 147. Nowadays, OFDM is included in numerous IEEE standard working groups, such as IEEE 802.11a/g/n/ac/ad (WLAN), IEEE 802.15.3a (wireless personal area networks, WPAN) and IEEE 802.16d/e (WiMAX) [101]. Furthermore, OFDM is used in terrestrial TV systems such as DVB-T, DVB-T2, T-DMB and ISDB-T and in current mobile communication standards 3GPP LTE, 3GPP UMTS, 4G and Flash-OFDM cellular systems. Table 4.1 shows the basic transmission parameters for three popular current wireless digital communication standards that use OFDM waveforms.

OFDM is also used in some wireline applications such as Asymmetric Digital Subscriber Line (ADSL) and Very high speed Digital Subscriber Line

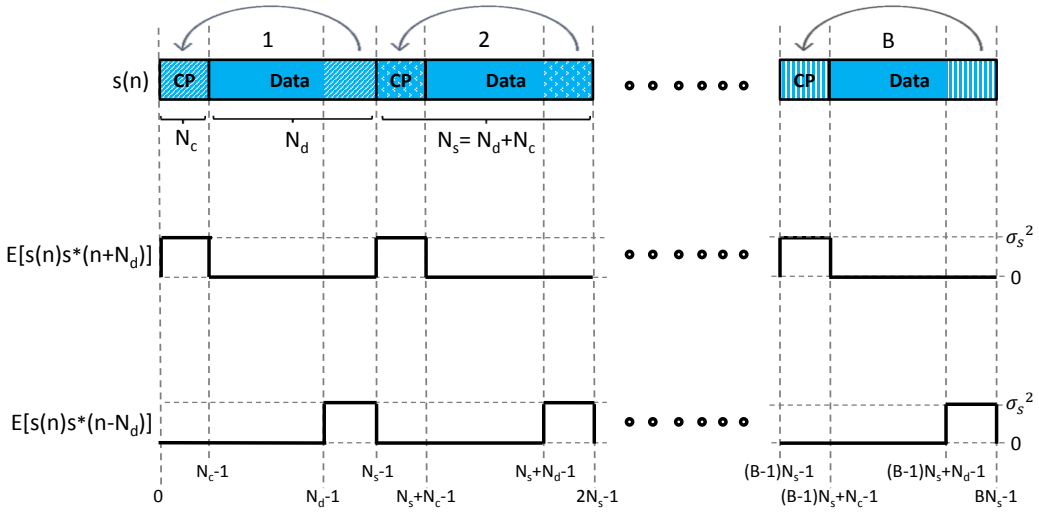

Figure 4.7: $\mathbb{E}[s(n)s^*(n+N_d)]$ and $\mathbb{E}[s(n)s^*(n-N_d)]$, when $s(n)$ is an OFDM signal. Expressions have nonzero outcome σ_s^2 only at the indices where the samples in the data match with the samples in the cyclic prefix.

Table 4.1: Basic parameters of three different OFDM standards [103–105].

Standard name	DVB-T2	IEEE 802.11ac (WLAN)	IEEE 802.16e (WiMAX)
Year	2007	2013	2005
Bandwidth, B, (MHz)	1.7, 5, 6, 7, 8, 10	20, 40, 80, 160	1.75, 3.5, 5.5, 7
Subcarrier spacing, f_{SC}, (kHz)	279 – 8929	312.5	10.9
FFT size, N_d, (k = 1024)	1k, 2k, 3k, 4k, 8k, 16k, 32k	64, 128, 256, 512	256
$\frac{\text{CP length}}{\text{symbol length}}$	1/4, 1/8, 1/16, 1/32	1/4, 1/8	1/4, 1/8, 1/16, 1/32
Modulation types	QPSK, 16QAM, 64QAM, 256QAM	BPSK, QPSK, 16QAM, 64QAM, 256QAM	QPSK, 16QAM, 64QAM

(VDSL) broadband internet access and Multi-media over Coax Alliance (MoCA) home networking.

Choice of OFDM transmission parameters

When choosing the suitable parameters for an OFDM transmission, one should take the delay spread of the channel and the Doppler shift due to movement into account. The symbol frequency in an OFDM transmission should

be significantly greater than the Doppler frequency to prevent inter-carrier-interference (ICI), which gives [3, 101]

$$T_s \ll \frac{1}{f_d}, \tag{4.13}$$

where T_s and f_d represent the symbol duration and the Doppler frequency respectively. Furthermore, in order to decrease ISI, one should guarantee that the guard interval T_c is greater than the maximum channel delay τ_c. Hence, we can set the limit for the cyclic prefix length

$$T_c > \tau_c. \tag{4.14}$$

However, increasing the CP length increases transmission overhead. Hence, also the payload data length in an OFDM symbol should be taken into account when choosing the CP length. Usually, T_c is an integer fraction of the payload data length T_d (for example in DVB-T: $\frac{T_c}{T_d} = \frac{1}{4}, \frac{1}{8}, \frac{1}{16}, \frac{1}{32}$) [107].

Usually, the DFT/IDFT used in OFDM modulation and demodulation is implemented as the FFT/IFFT, which gives a significant benefit in the computational complexity [3]. Hence, it is a reasonable assumption that the subcarrier length N_d is [101]

$$N_d = 2^m, \quad m = \lceil \log_2 M \rceil, \ M \in \mathbb{Z}_+, \tag{4.15}$$

since facilitating an efficient FFT involves such a point length.

Chapter 5

Cepstral Analysis of OFDM Signals

This chapter involves studying the cepstrum of an OFDM signal in additive white Gaussian noise (AWGN) channel. The basic observations of the cepstrum for both AWGN and OFDM in AWGN are stated and their distributions are derived using analytical tools. The results obtained from the analysis are verified with simulations.

5.1 Cepstrum of an OFDM signal

In this section, the basic observations of the cepstrum when the processed signal is either AWGN or OFDM signal in AWGN are shown. The motivation for using cepstum in sensing purposes lies in the fact that the periodicity inducing CP is typically inserted into an OFDM signal. This periodicity may be seen as a distinct peak in cepstrum when an OFDM signal is present. If the received signal is only uncorrelated noise, no such peak occurs. Furthermore, traditional speech processing applications pitch detection and voiced/unvoiced detection are analogous to the methods proposed in this thesis and have thus inspired the use of the cepstrum for detecting and classifying OFDM signals.

Fig. 5.1a shows the mean of the cepstral coefficients for AWGN and an OFDM signal in AWGN channel for the SNR of 10 dB (SNR $= 10\log_{10}\frac{\sigma_s^2}{\sigma_w^2}$). There can be found clear differences when OFDM signal is either present or not in the received signal. The mean of the real part of the cepstrum for AWGN has only one peak appearing at the zeroth index (or the DC index) while other values are zero. On the other hand, the mean of the real part of the OFDM cepstrum shows distinct peaks at the indices of the integer multiples of N_d in addition to the DC peak. It can be suggested that this property can be exploited in designing detection and classification methods for OFDM signals. However, the peaks do not appear in the imaginary part of the cepstrum, which justifies the use of the real part of the cepstrum only. Furthermore, if the CP is removed from the OFDM signal, all additional peaks disappear from the

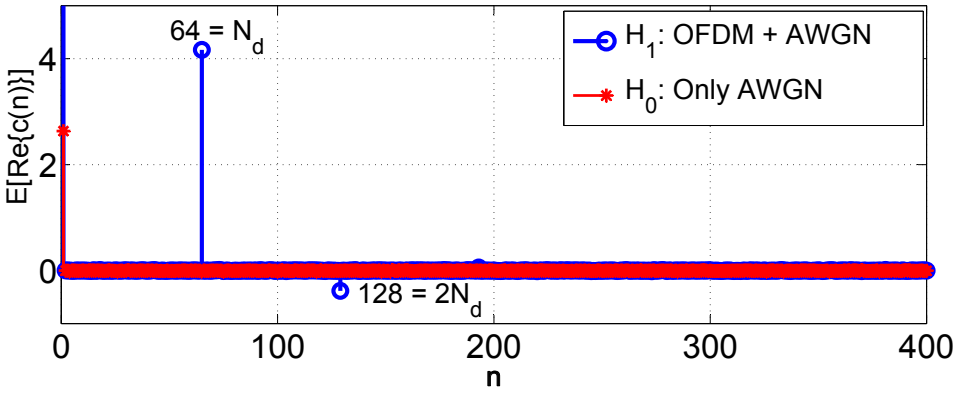

(a) The mean of the AWGN cepstrum has only one peak at the DC peak, while all other coefficients are zero mean. When an OFDM signal is present, there are additional peaks at the indices of multiples of N_d.

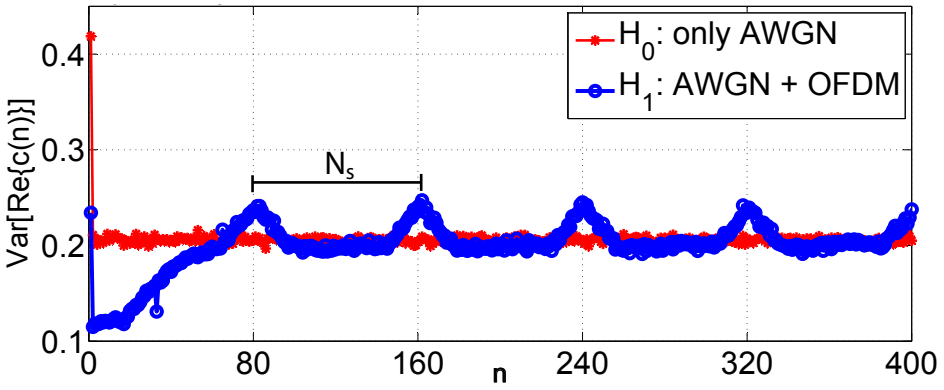

(b) The presence of OFDM causes the variance of the cepstrum to have triangular shapes peaking at the integer multiples of N_s while for AWGN it is constant valued.

Figure 5.1: a) The mean and b) the variance of the real part of the cepstrum $c(n)$ (zoomed to only first 400 indices) when the received signal is AWGN and OFDM signal in AWGN under hypotheses H_0 and H_1. The results are averaged over 10000 realizations and the simulation parameters are $N_d = 64$, $N_c = 16$, $B = 26$, $N_r = 2048$ and SNR $= 10$ dB.

cepstrum sequence. This implies that the additional peaks are caused by the periodicity that is induced by the insertion of the CP in an OFDM symbol.

It can be seen from Fig. 5.1b that also the variance of the cepstrum sequence is distinctively different with noise only or OFDM signal in AWGN. The real parts of the coefficients have constant variance under H_0, which is not the case under H_1. When OFDM signal is present the variances start to rise at the indices of $lN_s - N_d$ ($l = 1, 2, 3, \ldots$), peaking at the indices of lN_s. Also variances at the indices smaller than N_d are significantly lower than under H_0. Similar behavior is observed also in the imaginary parts of the coefficients. It can be suggested that these effects can be for example used to estimate the CP length of an OFDM symbol.

The variance sequence of $c(n)$ is found to be dependent on the FFT size used in calculating the cepstrum. It is observed that when the used FFT size is too large and the received signal samples are zero-padded to match the length of the FFT, the base level of the variances stops being constant for AWGN. It is observed from Fig. 5.2 that the base level of the variance sequence stops being flat when the FFT size is larger than the total number of the received signal samples $M = BN_s$. Furthermore, in that case the triangular peaks seem to decrease as the index increases. The effect is observed to appear stronger as the FFT size increases with relation to M.

From these observations, we can conclude that the used FFT size should be less than or near to the total data sample size in order to maintain the flat base level of variances. Hence, it is assumed in all simulations that regardless of the OFDM transmission parameters the number of the received signal samples is equal to the FFT size N_r used in cepstral processing and hence no zero-padding is performed.

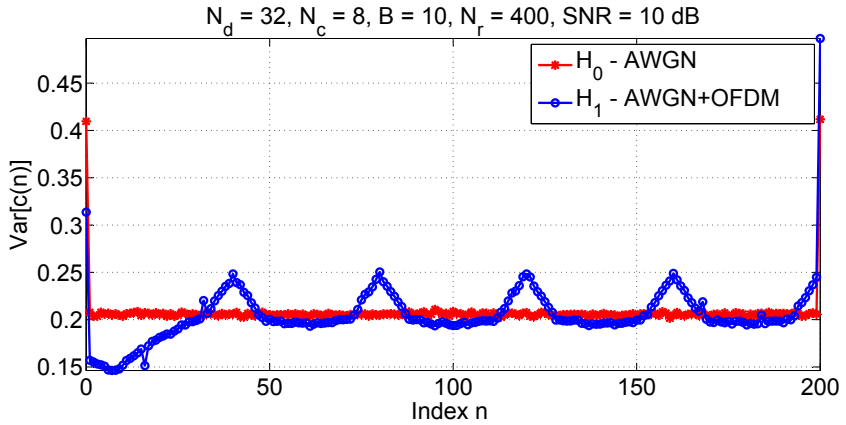

(a) Here, $N_r = M$, which means that DFT is used instead of FFT. The base line is flat and the peaks are similar with each other.

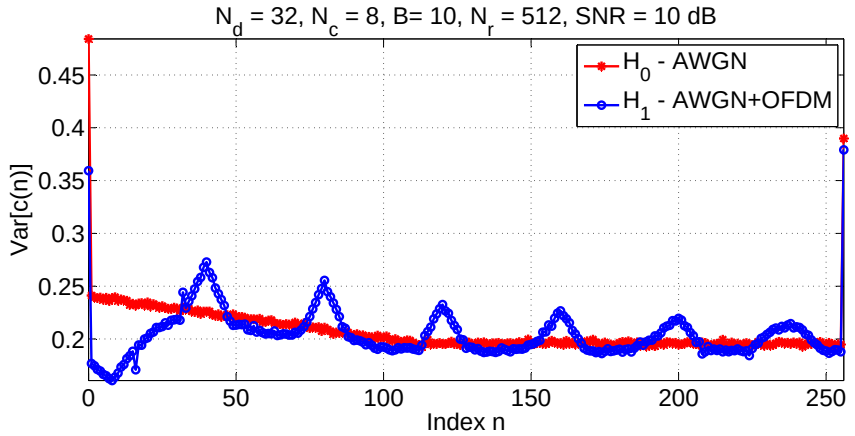

(b) Here, $N_r/2 \leq M \leq N_r$. The base level of variances is not flat anymore. There is descending slope at the beginning which reaches to the index of $N_r - M$. After that the variances are at constant level.

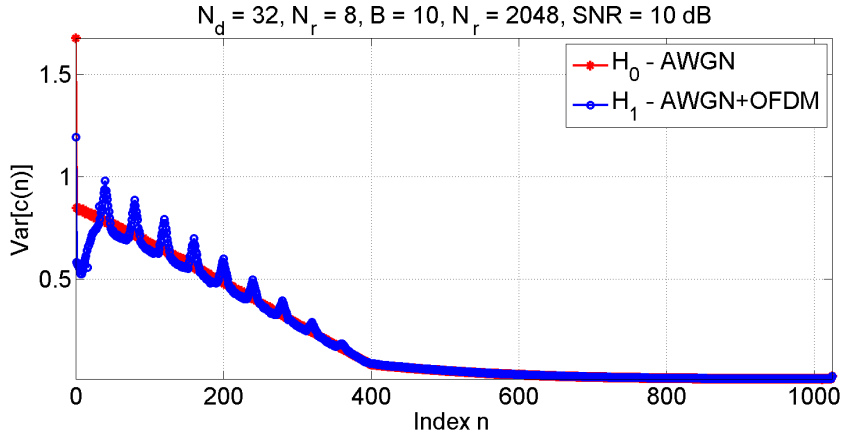

(c) Here, $M \leq N_r/2$. The level of variances decreases linearly until the index M, after which the decrease is nonlinear.

Figure 5.2: Illustration of how the receiver FFT size affects the variances of the cepstral coefficients.

5.2 Distributions of cepstral coefficients

In this section, the distribution of the cepstrum $c(n)$ is derived under the two hypotheses. We begin with the null hypothesis, after which the alternative hypothesis is considered. In both cases, the obtained results are verified with simulations.

5.2.1 Distributions of cepstral coefficients under H_0

In this subsection, the noise only case is considered. Hence, the received signal $x(n) = w(n)$, where

$$w(n) \sim \mathcal{N}_c(0, \sigma_w^2) \tag{5.1}$$

and σ_w^2 is the noise variance. After taking the unitary DFT transform, the distribution remains the same and therefore

$$X(k) \sim \mathcal{N}_c(0, \sigma_w^2). \tag{5.2}$$

Since $X(k)$ is a zero mean complex circular Gaussian random variable with variance σ_w^2, its absolute value $|X(k)|$ follows a Rayleigh-distribution with the scale parameter $\sigma_X = \sigma_w/2$. Hence,

$$|X(k)| \sim \text{Rayleigh}(\sigma_X). \tag{5.3}$$

The next step in the cepstral process involves taking a natural logarithm of the $|X(k)|$. In [108], the logarithm of a Rayleigh distributed random variable is shown to follow circular Log-Rayleigh distribution, i.e.,

$$Z(k) = \log|X(k)| \sim \text{Log-Rayleigh}(\sigma_X^2/2), \tag{5.4}$$

where $\sigma_X^2 = \sigma_w^2$ in the presence of AWGN only. The probability distribution function for a circular Log-Rayleigh random variable Z is given in [108] by

$$p_Z(z) = \frac{(e^z)^2}{\beta^2} \exp\left(-\frac{(e^z)^2}{2\beta^2}\right), \tag{5.5}$$

where $\beta^2 = \sigma_X^2/2$ is the location parameter. The circular Log-Rayleigh distribution is characterized by a property that all its central moments of order higher than one are independent of localization parameter [108]. The mean and the variance of Z are given by

$$\begin{aligned} \mu_z &= \log\beta + \frac{\log 2}{2} - \frac{\gamma}{2} \\ \text{and} \quad \sigma_z^2 &= \frac{\pi^2}{24}, \end{aligned} \tag{5.6}$$

where γ is the Euler's constant ($\gamma \approx 0.577216$). Now, $c(n)$ is the IDFT of $\log|X(k)|$. Substituting $Z(k) = \log|X(k)|$, we can rewrite Eq. (4.7) as

$$c(n) = \frac{1}{\sqrt{N_r}} \sum_{k=0}^{N_r-1} Z(k) e^{j\frac{2\pi kn}{N_r}}. \tag{5.7}$$

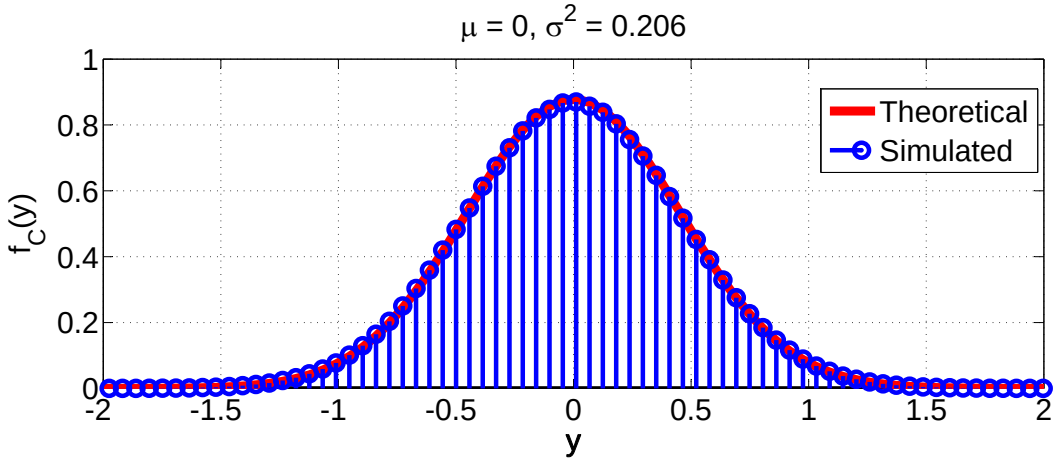

Figure 5.3: Distribution of $\mathcal{R}\{c(N_d)\}$ when only AWGN signal is present. The theoretical and the simulated distributions are on par.

Since $c(n)$ is a sum of i.i.d. rotated Log-Rayleigh random variables $Z(k)e^{j\frac{2\pi kn}{N_r}}$, assuming N_r to be sufficiently large we can use the central limit theory (CLT) to infer that the distribution of $c(n)$ under the null hypothesis is Gaussian. The mean of $c(n)$ is:

$$\mathbb{E}[c(n)] = \frac{1}{\sqrt{N_r}} \sum_{k=0}^{N_r-1} \mathbb{E}[Z(k)]e^{j\frac{2\pi kn}{N_r}} = \frac{1}{\sqrt{N_r}}\mu_z \sum_{k=0}^{N_r-1} e^{j\frac{2\pi kn}{N_r}}. \tag{5.8}$$

Noting that $\sum_{k=0}^{N_r-1} e^{j\frac{\pi kn}{N_r}} = N_r$ for $n = 0$ and 0 otherwise, we get

$$\mathbb{E}[c(n)] = \begin{cases} \mu_z\sqrt{N_r}, & n = 0 \\ 0 & n \neq 0. \end{cases} \tag{5.9}$$

Since the DFT is a unitary transform, the variances of all $c(n)$ coefficients come straight from the Log-Rayleigh distribution

$$\mathbb{V}\text{ar}[c(n)] = \frac{1}{N_r} \sum_{k=0}^{N_r-1} \text{Var}[Z(k)] = \sigma_z^2 = \frac{\pi^2}{24}. \tag{5.10}$$

Hence, we get the following distribution for $c(n)$ for AWGN

$$c(n) \sim \begin{cases} \mathcal{N}(\mu_z\sqrt{N_r}, \pi^2/24), & n = 0 \\ \mathcal{N}(0, \pi^2/24), & n \neq 0. \end{cases} \tag{5.11}$$

The results from the analysis are verified by simulations in Fig. 5.3. It can be seen that the theoretical and simulated distributions are on par. Note that $\mathcal{R}\{c(N_d)\} \sim \mathcal{N}(0, \pi^2/48) \approx 0.2056$. Note also that irrespective of the noise power σ_w^2 the variance of $c(n)$ for AWGN is a constant $\sigma_z^2 = \pi^2/24$. Hence, the distribution of $c(n)$ remains the same for any noise power under the AWGN assumption (when $n \neq 0$).

5.2.2 Distributions of cepstral coefficients under H_1

In this subsection, the analytical expressions for the distributions of cepstral coefficients are derived under hypothesis H_1. It is shown that the coefficients of the real cepstrum follow Gaussian distribution also under H_1, but in order to have the explicit expressions one needs to know their means and variances.

Now, we assume that the received signal consists of an OFDM signal and AWGN, i.e., $x(n) = s(n) + w(n)$. Assuming sufficiently large IDFT size for the OFDM signal and invoking the CLT, $s(n)$ can be said to be Gaussian distributed

$$s(n) \sim \mathcal{N}_c(0, \sigma_s^2). \tag{5.12}$$

Therefore, the distribution of the received signal under H_1 is given by

$$x(n) \sim \mathcal{N}_c(0, \sigma_s^2 + \sigma_w^2). \tag{5.13}$$

Since $c(n)$ is the DFT of $\log|X(k)|$, assuming a sufficiently large DFT size N_r and invoking the CLT, the distribution of $c(n)$ can be approximated to be Gaussian. Therefore, the distribution of $c(n)$ is fully specified by its mean and variance. For this purpose the distributions of $X(k)$, $|X(k)|$, $\log|X(k)|$ and $c(n)$ are derived step-by-step in that order.

Since $X(k)$ is the DFT of $x(n)$, assuming sufficiently large DFT size N_r and invoking the CLT, $X(k)$ also follows a complex Gaussian distribution. Noting that $\mathbb{E}[x(n)] = 0$, the mean of $X(k)$ is also

$$\mathbb{E}[X(k)] = 0, \quad \forall k. \tag{5.14}$$

The variance of $X(k)$ is given by

$$\begin{aligned} \mathbb{V}\mathrm{ar}[X(k)] &= \mathbb{E}[|X(k)|^2] - \mathbb{E}^2[X(k)] = \mathbb{E}[X(k)X^*(k)] \\ &= \mathbb{E}\Big[\frac{1}{N_r}\sum_{n=0}^{N_r-1}\sum_{m=0}^{N_r-1} x(n)x^*(m)e^{-j\frac{2\pi k(n-m)}{N_r}}\Big] \\ &= \frac{1}{N_r}\sum_{n=0}^{N_r-1}\sum_{m=0}^{N_r-1} \mathbb{E}[x(n)x^*(m)]e^{-j\frac{2\pi k(n-m)}{N_r}}. \end{aligned} \tag{5.15}$$

As shown in Sec. 4.2.1, the insertion of the CP induces periodicity, for which we have the following correlation in an OFDM signal in AWGN:

$$\mathbb{E}[x(p+bN_s)x^*(p+bN_s-\tau)] = \begin{cases} \sigma_x^2 & \tau = 0 \\ \sigma_s^2 & \tau = \pm N_d, \quad p = 0, 1, \ldots, N_c - 1 \\ 0 & \text{otherwise,} \end{cases} \tag{5.16}$$

where p is a sample index inside an OFDM symbol and b is the index of that OFDM symbol ($b = 1, \ldots, B$). Using Eq. (5.16), and solving $\mathbb{V}\mathrm{ar}[x(n)]$ in three parts, where $m = n$, $m = n - N_d$ and $m = n + N_d$, we get:

$$\mathbb{V}\mathrm{ar}[X(k)] = \sigma_x^2\big(1 + 2\rho_x \cos(\tfrac{2\pi k N_d}{N_r})\big), \tag{5.17}$$

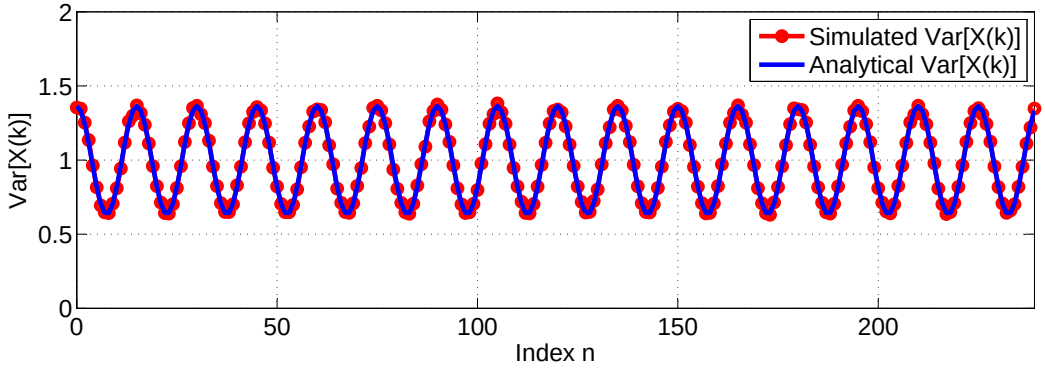

Figure 5.4: Analytical and simulated variance of $\mathcal{R}\{X(k)\}$ sequence. The analytical and simulated results are on par. Simulation parameters are: $N_d = 16, N_c = 4, B = 12, N_r = 240$, SNR $= 0$ dB and $\sigma_x^2 = 1$.

where $\rho_x = \frac{N_c}{N_c+N_d}\frac{\sigma_s^2}{\sigma_w^2+\sigma_s^2}$ [36]. The detailed derivation of Eq. (5.17) is given in Appendix A. Therefore, the distribution of $X(k)$ can be written as

$$X(k) \sim \mathcal{N}_c(0, \sigma_k^2), \tag{5.18}$$

where $\sigma_k^2 = \mathbb{V}\text{ar}$. Fig. 5.4 shows the analytical and the simulated variance of the real part of $X(k)$ sequence. It shows that the results match very well.

Now, $X(k)$ and $X(l)$ are correlated random variables and therefore finding cross-correlation between them is important. The cross-correlation between $X(k)$ and $X(l)$ is given by

$$\mathbb{E}[X(k)X^*(l)] = \mathbb{E}\left[\frac{1}{N_r}\sum_{n=0}^{N_r-1}\sum_{m=0}^{N_r-1} x(n)x^*(m)e^{-j\frac{2\pi(kn-lm)}{N_r}}\right]. \tag{5.19}$$

Using Eq. (5.16), and again solving $\mathbb{E}[X(k)X^*(l)]$ in three parts, where $m = n$, $m = n + N_d$, and $m = n - N_d$, we have:

$$\mathbb{E}[X(k)X^*(l)] = \sigma_x^2\delta(k-l) + \frac{\sigma_s^2\Delta}{N_r}\left(e^{j\frac{2\pi lN_d}{N_r}} + e^{-j\frac{2\pi kN_d}{N_r}}\right). \tag{5.20}$$

Here, $\delta(n)$ represents the discrete unit impulse function

$$\delta(n) = \begin{cases} 1, & n = 0 \\ 0, & n \neq 0 \end{cases} \tag{5.21}$$

and Δ is defined as

$$\Delta = \begin{cases} BN_c, & |k-l|=0, \\ Be^{-j\theta_{kl}(N_c-1)}\frac{\sin(\theta_{kl}N_c)}{\sin(\theta_{kl})}, & |k-l|=B,2B,\ldots,(N_s-1)B \\ 0, & \text{otherwise.} \end{cases} \tag{5.22}$$

where

$$\theta_{kl} = \frac{\pi(k-l)}{N_r}. \tag{5.23}$$

The full derivation of Eq. (5.20) can be found in Appendix B. It should be noted that for $k = l$, the equation collapses to that for variance of $X(k)$.

Fig. 5.5 shows theoretical $\mathbb{E}[X(k)X^*(l)]$ matrix and a Frobenius norm from squared error matrix between simulated and analytically derived matrices. The Frobenius norm is calculated with the following equation:

$$\| \mathbf{A} \|_F^2 = \sqrt{\sum_{i=1}^{N_r}\sum_{j=1}^{N_r} |a_{ij}|^2}, \tag{5.24}$$

where a_{ij} is the $(i,j)^{\text{th}}$ element of the squared error matrix $\mathbf{A}$. It can be observed from Fig. 5.5 that the analysis matches well with simulation and the Frobenius norm of the error matrix is small-valued and stays constant as the SNR changes.

When $\mathbb{E}[X(k)X^*(l)]$ is known, one can easily calculate the cross-correlation matrix $\rho_{X,kl}$ of $X(k)$:

$$\begin{aligned}
\rho_{X,kl} &= \frac{\mathbb{E}[(X(k)-\mu_k)(X(l)-\mu_l)^*]}{\sigma_k\sigma_l} \\
&= \frac{\mathbb{E}[X(k)X^*(l)]}{\sigma_k\sigma_l} \\
&= \delta(k-l) + \frac{\sigma_s^2\Delta\left(e^{j\frac{2\pi l N_d}{N_r}} + e^{-j\frac{2\pi k N_d}{N_r}}\right)}{N_r(\sigma_s^2+\sigma_w^2)},
\end{aligned} \tag{5.25}$$

for $k, l = 0, 1, \ldots, N_r - 1$.

Since $X(k)$ is Gaussian distributed, $Z(k) = \log|X(k)|$ follows Log-Rayleigh distribution [108], i.e.,

$$Z(k) \sim \text{Log-Rayleigh}(\sigma_X^2/2). \tag{5.26}$$

The next step in the cepstrum process involves finding $\mathbb{E}[Z(k)Z^*(l)]$. The second moment of Log-Rayleigh distributed random variables $Z(k)$ and $Z(l)$ can be calculated with using a probability density function of bivariate Rayleigh distribution given in [109]:

$$\begin{aligned}
&f_{R_1R_2}(r_1, r_2|\Omega_1, \Omega_2, \rho_r) \\
&= \frac{4r_1r_2}{\Omega_1\Omega_2(1-\rho_r)} \exp\left(-\frac{1}{1-\rho_r}\left(\frac{r_1^2}{\Omega_1} + \frac{r_2^2}{\Omega_2}\right)\right) \\
&\quad \times I_0\left(\frac{2\sqrt{\rho_r}r_1r_2}{(1-\rho_r)\sqrt{\Omega_1\Omega_2}}\right),
\end{aligned} \tag{5.27}$$

where r_1 and r_2 are Rayleigh distributed random variables, $\Omega_i = \mathbb{E}[r_i^2]$, and ρ_r is the correlation coefficient between r_1^2 and r_2^2. $I_0(\cdot)$ stands for the zeroth

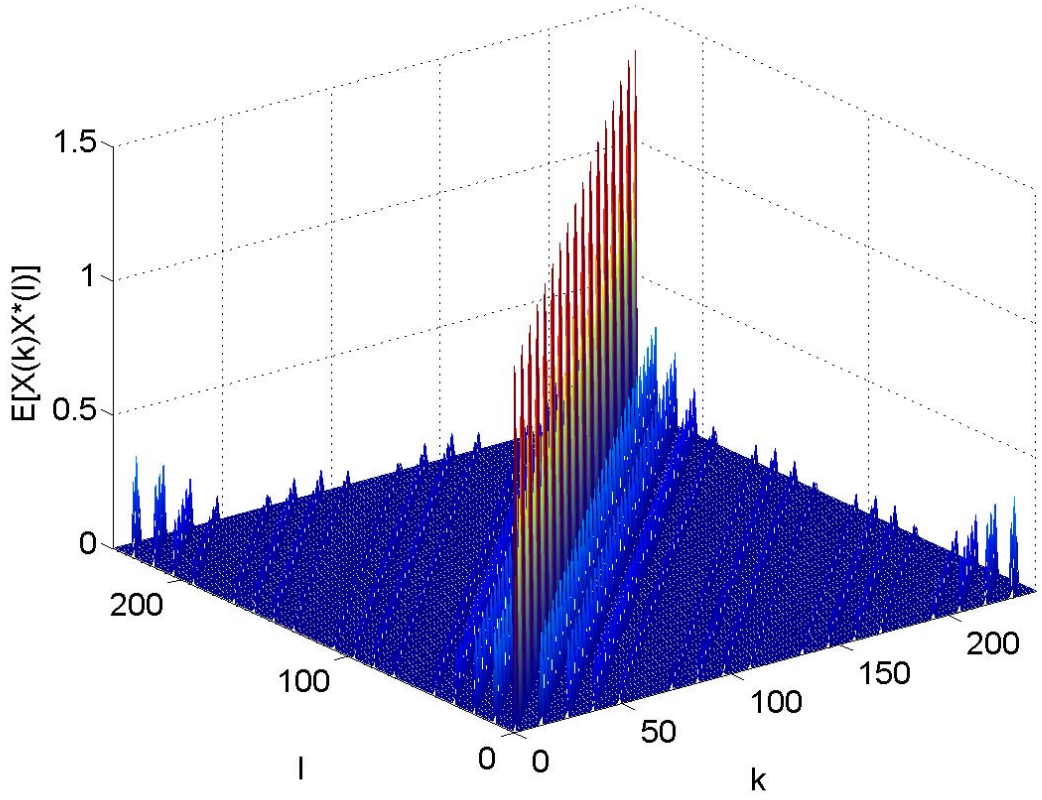

(a)

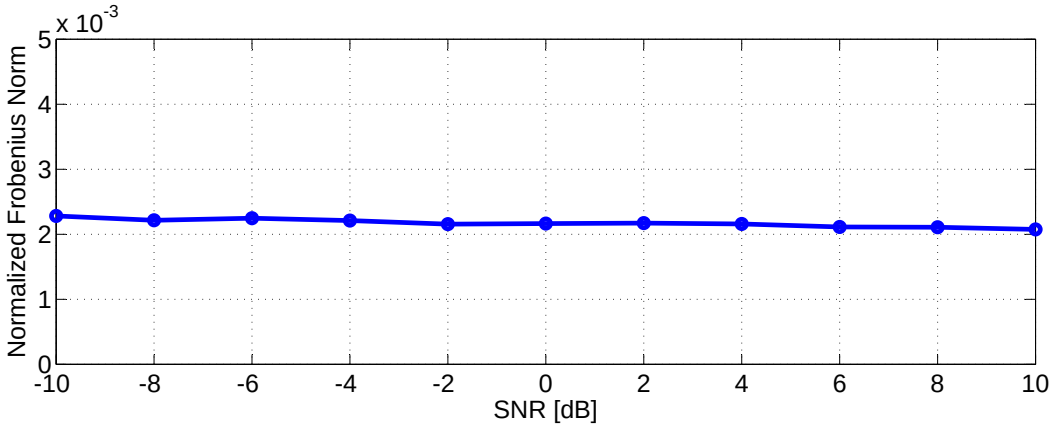

(b)

Figure 5.5: a) Analytical $\mathbb{E}[X(k)X^*(l)]$ matrix. b) The Frobenius norm of the squared error matrix between simulated and analytical $\mathbb{E}[X(k)X^*(l)]$ for different SNR values. Values in the plot are normalized with a Frobenius norm of the analytical matrix. Simulation matches with the analysis very well. Simulation parameters are: $N_d = 16, N_c = 4, B = 12, N_r = 240$, SNR $= 10$ dB and $\sigma_x^2 = 1$. The results are averaged over 10000 realizations.

order modified Bessel function of the first kind. In [110], it is suggested that if ρ_n is the correlation coefficient between normal bivariate random vectors, then the correlation coefficient between the squared sum of the random vectors is $\rho_c = \rho_n^2$. Using Eq. (5.27) with $\rho_r = \rho_{X,kl}^2$, one can calculate the second moment between $Z(k)$ and $Z(l)$

$$\begin{aligned} &\mathbb{E}[Z(k)Z^*(l)] \\ &= \int_0^\infty \int_0^\infty \log r_1 \log r_2 \; f_{R_1R_2}(r_1, r_2|\Omega_1, \Omega_2, \rho_r)\mathrm{d}r_1\mathrm{d}r_2 \end{aligned} \tag{5.28}$$

Unfortunately, there is no closed form solution for Eq. (5.28) and it has to be solved numerically. Fig. 5.6 shows theoretical $\mathbb{E}[Z(k)Z^*(l)]$ matrix and a Frobenius norm from squared error matrix between simulated and analytical matrices. It can be seen, that the analysis matches well with the simulation result.

Note that $c(n)$ is the sum of N_r random variables. Therefore its distribution can be approximated to be Gaussian using the CLT. The mean of $c(n)$ is given by

$$\begin{aligned} \mathbb{E}[c(n)] = \mu_n &= \frac{1}{\sqrt{N_r}} \sum_{k=0}^{N_r-1} \mathbb{E}[Z(k)] e^{j\frac{2\pi kn}{N_r}} \\ &= \frac{1}{\sqrt{N_r}} \sum_{k=0}^{N_r-1} \mu_z(\beta_1) e^{j\frac{2\pi kn}{N_r}} \\ &= \frac{1}{\sqrt{N_r}} \sum_{k=0}^{N_r-1} \left[\log\sqrt{\frac{\sigma_1^2}{2}} + \frac{\log(2)}{2} - \frac{\gamma}{2} \right] e^{j\frac{2\pi kn}{N_r}} \\ &= \frac{1}{2\sqrt{N_r}} \sum_{k=0}^{N_r-1} \left[\log\frac{\sigma_x^2}{2} + \log 2 - \gamma \right] e^{j\frac{2\pi kn}{N_r}} \\ &\quad + \frac{1}{2\sqrt{N_r}} \sum_{k=0}^{N_r-1} \log\left(1 + 2\rho_x \cos(\tfrac{2\pi kN_d}{N_r})\right) e^{j\frac{2\pi kn}{N_r}} \end{aligned} \tag{5.29}$$

where $Z(k)$ is Log-Rayleigh distributed random variable and $\mu_z(\beta_1)$ is the mean of Log-Rayleigh distribution with location parameter $\beta_1^2 = \sigma_k^2/2$. From Eq. (5.29) we can easily derive the expressions for the real and the imaginary parts of $c(n)$. Noting that the sum of rotating cosine makes the expected value of $c(n)$ zero when $n \neq 0, N_d, 2N_d, \ldots$, we can write the expected value of the real part of $c(n)$ as

$$\mathbb{E}[\mathcal{R}\{c(n)\}] = \begin{cases} \frac{1}{\sqrt{N_r}} \sum_{k=0}^{N_r-1} \mu_z(\beta_1) \cos(\frac{2\pi kn}{N_r}) & n = 0, N_d, 2N_d, \ldots \\ 0 & \text{otherwise.} \end{cases} \tag{5.30}$$

The sum of rotating sine makes the expected value of the imaginary part of $c(n)$ zero with all n:

$$\mathbb{E}[\mathcal{I}\{c(n)\}] = \frac{1}{\sqrt{N_r}} \sum_{k=0}^{N_r-1} \mu_z(\beta_1) \sin(\tfrac{2\pi kn}{N_r}) = 0. \tag{5.31}$$

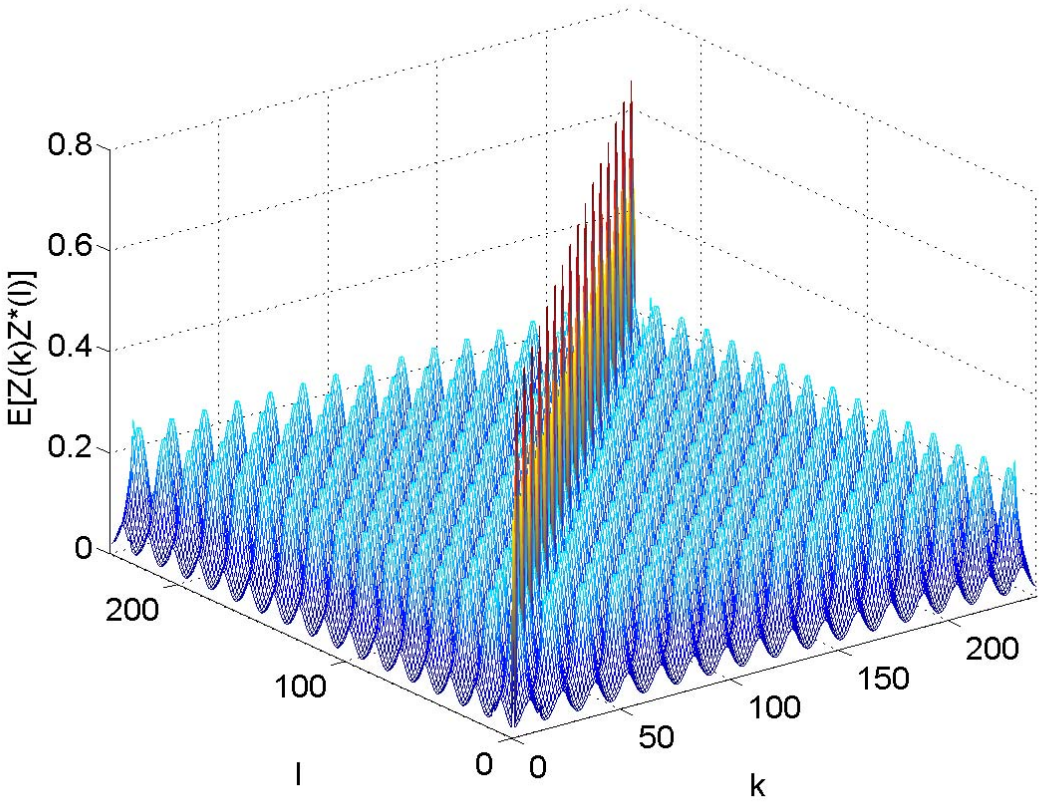

(a)

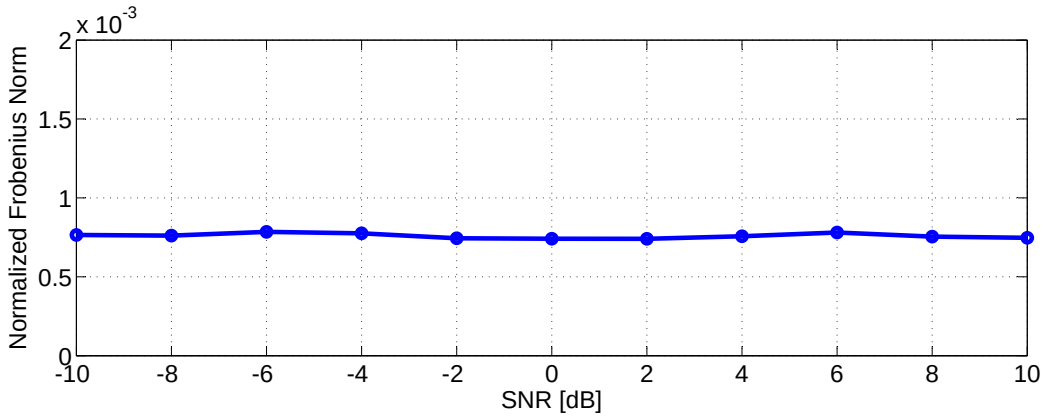

(b)

Figure 5.6: a) Analytical $\mathbb{E}[Z(k)Z^*(l)]$ matrix. b) Frobenius norm of the squared error matrix between simulated and analytical $\mathbb{E}[Z(k)Z^*(l)]$ for different SNR values. Values in the plot are normalized with a Frobenius norm of the analytical matrix. Simulation matches with the analysis very well. Simulation parameters are: $N_d = 16, N_c = 4, B = 12, N_r = 240$, SNR = 10 dB and $\sigma_x^2 = 1$. The results are averaged over 10000 realizations.

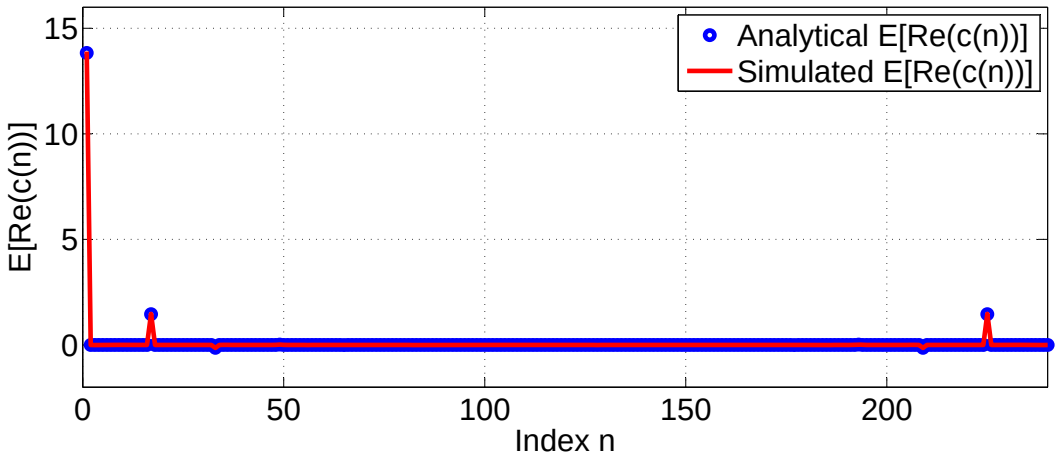

(a)

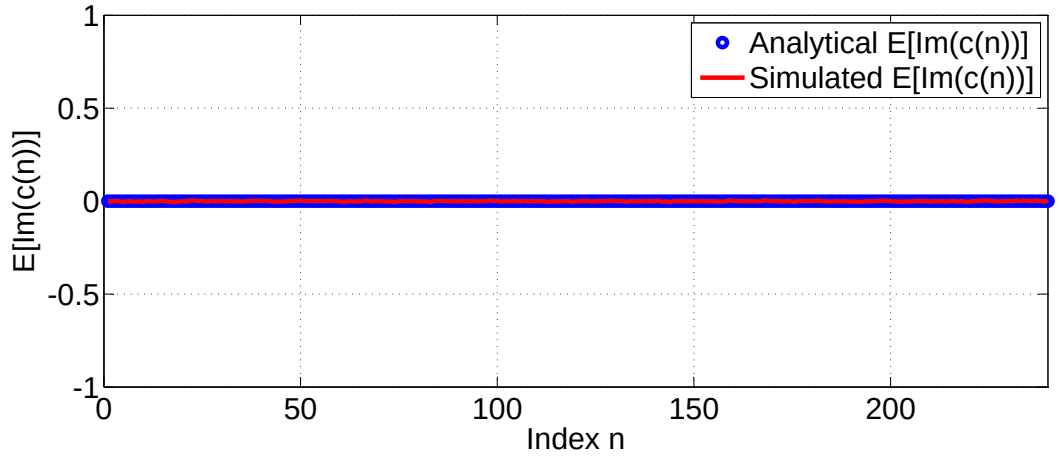

(b)

Figure 5.7: a) Analytical and simulated means of the real parts of the cepstral coefficients under hypothesis H_1. b) Analytical and simulated means of the imaginary parts of the cepstral coefficients under hypothesis H_1. In both cases the simulated results match the analysis very well. Simulation parameters are: $N_d = 16, N_c = 4, B = 12, N_r = 240$, SNR $= 10$ dB and $\sigma_w^2 = 1$.

Fig. 5.7 shows the analytical and simulated means of cepstral coefficients. The results match very well.

The variance of the cepstrum sequence $c(n)$ is

$$\mathbb{V}\text{ar}[c(n)] = \sigma_n^2 = \mathbb{E}[|c(n)|^2] - \mathbb{E}^2[c(n)]. \tag{5.32}$$

where the second moment of the real cepstrum $c(n)$ is given by

$$\begin{aligned}\mathbb{E}[|c(n)|^2] &= \mathbb{E}\left[\frac{1}{\sqrt{N_r}}\sum_{k=0}^{N_r-1} Z(k)e^{j\frac{2\pi kn}{N_r}}\frac{1}{\sqrt{N_r}}\sum_{l=0}^{N_r-1} Z^*(l)e^{-j\frac{2\pi ln}{N_r}}\right] \\ &= \frac{1}{N_r}\sum_{k=0}^{N_r-1}\sum_{l=0}^{N_r-1}\mathbb{E}[Z(k)Z^*(l)]e^{j\frac{2\pi(k-l)n}{N_r}}.\end{aligned} \tag{5.33}$$

The variance of $c(n)$ can now be calculated with Eq. (5.32). Fig. 5.8 shows the numerically solved analytical and the simulated variance of the cepstrum sequence $c(n)$ for an OFDM signal in AWGN. The analytical version can be seen to match the simulated result quite well except at the end points of the sequence. The difference very likely results from the numerical errors in the implementation of Eq. (5.28).

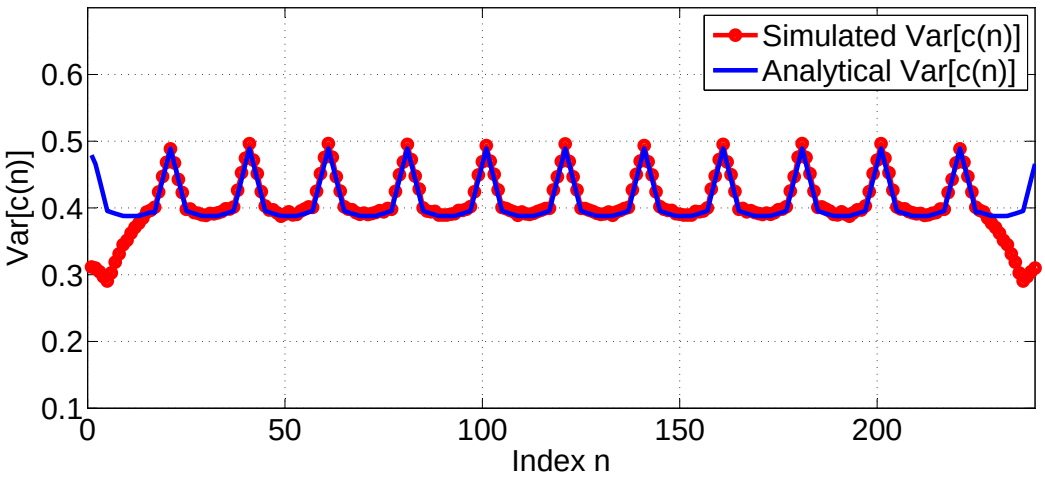

Figure 5.8: Analytical and simulated variance of the real cepstrum sequence $c(n)$. The analytical version matches quite well with the simulated one except at the end points of the sequence, which results from the numerical errors in the implementation of (5.28). Simulation parameters are: $N_d = 16, N_c = 4, B = 12, N_r = 240$, SNR $= 10$ dB and $\sigma_w^2 = 1$.

5.3 Summary of the statistical properties of the cepstrum

In Sect. 5.2.1 the distribution of the cepstrum $c(n)$ is derived step-by-step for AWGN and an OFDM signal in AWGN. The distributions in each step of the cepstrum process are summarized in Table 5.1. Note that for AWGN, $x(n) = w(n)$ and σ_z^2 is constant $\frac{\pi^2}{24}$. For OFDM signal in AWGN, $x(n) = w(n) + s(n)$, $\mu_n = \mathbb{E}[c(n)]$ and $\sigma_n^2 = \mathbb{V}\text{ar}[c(n)]$.

Figs. 5.9 and 5.10 show the simulated and the analytical distributions of AWGN and OFDM signal in AWGN in each step of the cepstrum process. Index n is selected to be $0, N_d, 2N_d$ and an arbitrary irrelevant index 34 in the example. In all situations, the analytical and the simulated distributions match very well.

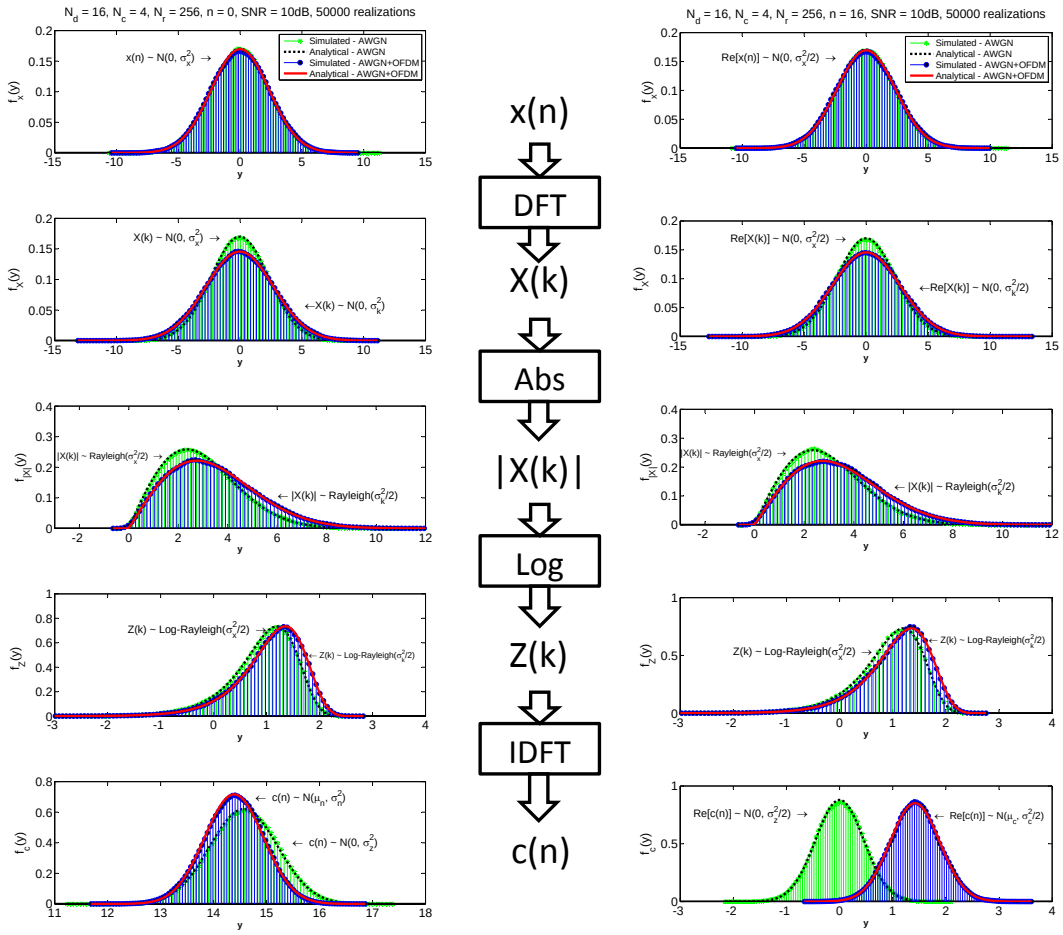

(a) Distributions when $n = 0$ (b) Process (c) Distributions when $n = N_d$

Figure 5.9: Simulated and analytical distributions of AWGN and OFDM signal in AWGN (SNR = 10 dB) in each step of the cepstrum process. Note that only the real parts of $x(n)$, $X(k)$ and $c(n)$ are displayed. Also, the noise power is adjusted so that the both received signals have the same power. In all situations, analytical and simulated distributions are on par.

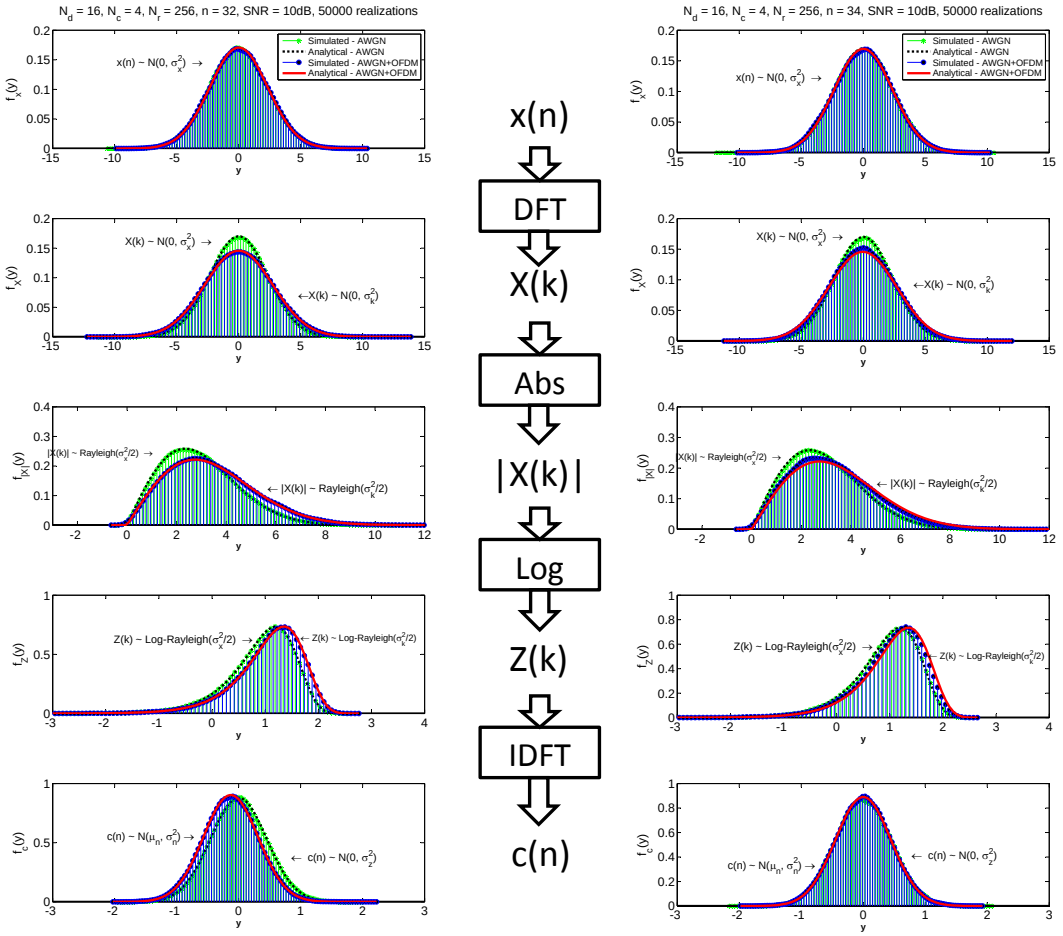

(a) Distributions when $n = 2N_d$ (b) Process (c) Distributions when $n = 34$

Figure 5.10: Simulated and analytical distributions of AWGN and OFDM signal in AWGN (SNR = 10 dB) in each step of the cepstrum process. Note that only the real parts of $x(n)$, $X(k)$ and $c(n)$ are displayed. Also, the noise power is adjusted so that the both received signals have the same power. In all situations, analytical and simulated distributions are on par.

Table 5.1: Distributions of the output at each step in the cepstrum process for AWGN and ODFM signal in AWGN.

	AWGN	OFDM in AWGN
1. Received signal	$x(n) \sim \mathcal{N}_c(0, \sigma_x^2)$	$x(n) \sim \mathcal{N}_c(0, \sigma_x^2)$
2. DFT	$X(k) \sim \mathcal{N}_c(0, \sigma_x^2)$	$X(k) \sim \mathcal{N}_c(0, \sigma_k^2)$
3. ABS	$\lvert X(k)\rvert \sim \text{Rayleigh}(\sigma_x^2/2)$	$\lvert X(k)\rvert \sim \text{Rayleigh}(\sigma_k^2/2)$
4. LOG	$Z(k) \sim \text{Log-Rayleigh}(\sigma_x^2/2)$	$Z(k) \sim \text{Log-Rayleigh}(\sigma_k^2/2)$
5. IDFT	$c(n) \sim \begin{cases} \mathcal{N}_c(\mu_z\sqrt{N_r}, \sigma_z^2) & n = 0 \\ \mathcal{N}_c(0, \sigma_z^2) & n \neq 0. \end{cases}$	$c(n) \sim \mathcal{N}_c(\mu_n, \sigma_n^2)$

Chapter 6

Cepstrum-Based Detection of OFDM Waveforms

In this chapter, two cepstrum based schemes for detecting OFDM waveforms in AWGN channel are proposed. The detection schemes are first proposed assuming that a single SU is sensing, after which they both are extended into a collaborative sensing scenario where multiple distributed sensors are observing the spectrum simultaneously.

The detection of an OFDM signal is formulated as a binary hypothesis test introduced in Sec. 3.1 and the assumed detection strategy is chosen to follow the Neyman-Pearson criterion. Now, the target signal $s(n)$ in the binary hypothesis test is an OFDM signal. Thus, the distribution of $x(n)$ under the two hypotheses is given by

$$\begin{aligned} H_0 &: x(n) \sim \mathcal{N}_c(0, \sigma_w^2) \\ H_1 &: x(n) \sim \mathcal{N}_c(0, \sigma_s^2 + \sigma_w^2). \end{aligned} \tag{6.1}$$

where $x(n)$ is the received signal, $s(n)$ is an OFDM signal and $w(n)$ is AWGN. Furthermore, it is assumed that $s(n)$ and $w(n)$ are independent of each other. For the distribution of the cepstrum under the binary hypothesis assumption we have:

$$\begin{aligned} H_0 &: \mathbf{c} \sim \mathcal{N}_c(\boldsymbol{\mu}_0, \mathbf{C}_0) \\ H_1 &: \mathbf{c} \sim \mathcal{N}_c(\boldsymbol{\mu}_1, \mathbf{C}_1) \end{aligned} \tag{6.2}$$

where $\mathbf{c}$ is a vector containing all cepstrum coefficients $c(n)$, $\boldsymbol{\mu}_0 = \mathbb{E}[\mathbf{c}|H_0]$, $\boldsymbol{\mu}_1 = \mathbb{E}[\mathbf{c}|H_1]$ and the covariance matrices $\mathbf{C}_0 = \mathbb{E}[(\mathbf{c} - \boldsymbol{\mu}_0)(\mathbf{c} - \boldsymbol{\mu}_0)^T|H_0]$ and $\mathbf{C}_1 = \mathbb{E}[(\mathbf{c} - \boldsymbol{\mu}_1)(\mathbf{c} - \boldsymbol{\mu}_1)^T|H_1]$. When dealing with a Gaussian problem, the optimal decision test statistic would be [27]:

$$T_{\text{opt}} = (\mathbf{c} - \boldsymbol{\mu}_0)^T \mathbf{C}_0 (\mathbf{c} - \boldsymbol{\mu}_0) - (\mathbf{c} - \boldsymbol{\mu}_1)^T \mathbf{C}_1 (\mathbf{c} - \boldsymbol{\mu}_1). \tag{6.3}$$

Since obtaining a closed form solution of $\mathbf{C}_1$ is difficult, the suboptimal test would be a generalized log likelihood ratio (GLLRT) where the covariance

matrix of the cepstrum under H_1 is estimated to be the same as under H_0 (i.e. $\hat{\mathbf{C}}_1 = \mathbf{C}_0$). In that case, the test statistic for the GLLRT is as follows [27]:

$$T_{\mathrm{G}} = \mathbf{c}^T \mathbf{C}_0 \Delta\boldsymbol{\mu} \tag{6.4}$$

where $\Delta\boldsymbol{\mu} = \boldsymbol{\mu}_1 - \boldsymbol{\mu}_0$. Since $\mathbf{C}_0$ is in fact a diagonal matrix with constant diagonal values of $\frac{\pi^2}{24}$, we can ignore the multiplicative constant and rewrite Eq. (6.4) as [27]:

$$T_{\mathrm{G}} = \Delta\boldsymbol{\mu}^T \mathbf{c}. \tag{6.5}$$

As shown earlier, most of the elements of $\Delta\boldsymbol{\mu}$ are zeros, which motivates us to design detectors based on only those cepstral coefficients that have non zero means (i.e. indices $n = 0,\ N_d,\ 2N_d,\ \dots$). Next, two simple cepstrum based detection algorithms which are based on two of the most significant non zero meaned cepstral coefficients $c(N_d)$ and $c(0)$ are proposed.

6.1 Detection based on the cepstral coefficient $c(N_d)$

The mean of the real part of the OFDM cepstrum has peaks at integer multiples of N_d in addition to the DC peak while those peaks are not present in AWGN cepstrum. The first cepstrum based sensing scheme is proposed on this distinguishing factor. Note that although there are multiple peaks, the magnitudes of the peak values decrease rapidly after the first peak at index N_d. Therefore, it is suggested to use the following test statistic based on only the first peak at index N_d

$$T_1 = \mathcal{R}\{c(N_d)\}. \tag{6.6}$$

As seen in Eq. (5.11), a real part of a cepstral peak value $c(N_d)$ follows zero mean Gaussian distribution with a variance of $\pi^2/48$ for AWGN. Using this knowledge, we can calculate a threshold value η for NP detection strategy. Starting from Gaussian distributed cumulative distribution function and inserting $\mu = 0$ and $\sigma^2 = \pi^2/48$ we have:

$$F(x) = \frac{1}{2}\left[1 + \mathrm{erf}\left(\frac{x-\mu}{\sqrt{2\sigma^2}}\right)\right] = \frac{1}{2}\left[1 + \mathrm{erf}\left(\frac{x}{\sqrt{\pi^2/24}}\right)\right], \tag{6.7}$$

where erf denotes the error function. A value for a fixed probability of false alarm P_f can be calculated with Eq. (6.7):

$$P_f = 1 - F(\eta) = 1 - \frac{1}{2}\left[1 + \mathrm{erf}\left(\frac{\eta}{\sqrt{\pi^2/24}}\right)\right] = \frac{1}{2}\mathrm{erfc}\left(\frac{\eta}{\sqrt{\pi^2/24}}\right), \tag{6.8}$$

where erfc denotes the complementary error function. Therefore, the desired threshold value η for a given P_f is

$$\eta_1 = \sqrt{\frac{\pi^2}{24}}\mathrm{erfc}^{-1}(2P_f), \tag{6.9}$$

where erfc^{-1} denotes the inverse of the complementary error function.

It can be seen that the threshold value is independent of the noise power σ_w^2. Hence, the proposed detector is a constant false-alarm rate (CFAR) detector, which states that the prespecified P_f can be maintained without knowing the noise power [26]. Moreover, that property is very valuable in practical scenarios since it means that the proposed detector is robust to noise power uncertainty.

Assuming that for low SNR values $\mathbb{V}\text{ar}[\mathcal{R}\{c(N_d)\}] \approx \frac{\sigma_z^2}{2} = \frac{\pi^2}{48}$, we can write the probability of detection $P_{d,1} = P(T_1 > \eta_1 | H_1)$ as

$$P_{d,1} = \frac{1}{2}\text{erfc}\left(\frac{\eta_1 - \mu_1}{\sqrt{\pi^2/24}}\right), \tag{6.10}$$

where $\mu_1 \triangleq \mathbb{E}[\mathcal{R}\{c(N_d)|H_1\}]$ given by Eq. (5.30).

6.2 Detection based on the cepstral coefficient $c(0)$

It was seen in Sec. 5.1 that the mean of the cepstral coefficient $c(0)$ increases in the presence of OFDM signal as compared to AWGN alone. Using this property, a detection scheme with the following test statistic is proposed

$$T_2 = c(0). \tag{6.11}$$

From the distribution of Eq. (5.11), $T_2 \sim \mathcal{N}(\mu_z\sqrt{N_r}, \pi^2/24)$. Using Eqs. (6.7) and (6.8) and inserting $\mu = \mu_z\sqrt{N_r}$ and $\sigma^2 = \pi^2/24$, the threshold for a NP detector using test statistic T_2 is given by

$$\eta_2 = \sqrt{\frac{\pi^2}{12}}\text{erfc}^{-1}(2P_f) + \sqrt{N_r}(\log\beta + \frac{\log 2}{2} - \frac{\gamma}{2}). \tag{6.12}$$

In this scheme, the location parameter $\beta^2 = \sigma_w^2/2$ and thus the threshold depends on the noise power σ_w^2. Therefore the algorithm is not robust to the noise power uncertainty, which is a drawback when compared to the scheme based on $c(N_d)$.

Assuming that for low SNR values $\mathbb{V}\text{ar}[c(0)] \approx \sigma_z^2 = \frac{\pi^2}{24}$, we can write the probability of detection $P_{d,2} = P(T_2 > \eta_2 | H_1)$ as

$$P_{d,2} = \frac{1}{2}\text{erfc}\left(\frac{\eta_2 - \mu_2}{\sqrt{\pi^2/12}}\right), \tag{6.13}$$

where $\mu_2 \triangleq \mathbb{E}[c(0)|H_1]$ given by Eq. (5.29).

6.3 Collaborative detection using multiple sensors

In this section, the two proposed detection methods are extended to a collaborative sensing with multiple distributed sensors. The main aim of this section is to demonstrate, through simulations, the improvement obtained by extending the proposed detection schemes to the collaborative scenario. The topic of optimality of the cooperative detection strategy is out of the scope of this thesis and is not therefore discussed in detail.

The considered distributed sensing system follows a parallel topology with a FC as shown in Fig. 6.1. In this scenario, each SU sends the decision statistics corresponding to the two proposed single-sensor detection schemes (i.e. T_1 and T_2) to the FC where they are fused to obtain the test statistics for collaborative sensing. Since the proposed detectors are based on the GLLRT given in Eq. (6.5), a reasonable fusion rule is the SUM rule.

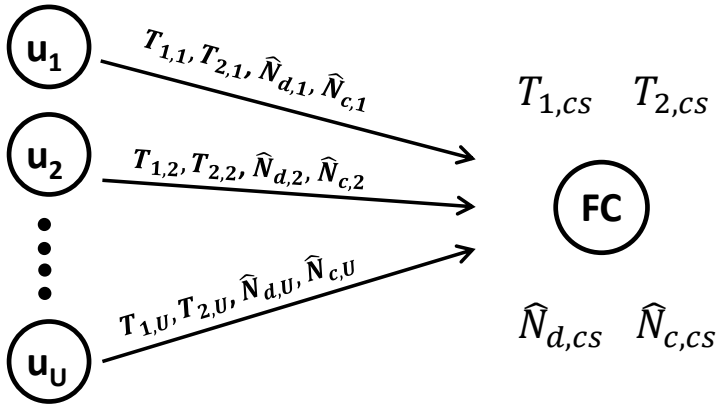

Figure 6.1: System model for the proposed cooperative sensing and estimation schemes. We consider the parallel topology with a fusion center (FC). Values that are sent to the FC by each u^{th} single sensor are: $T_{1,u}, T_{2,u}, \hat{N}_{d,u}$ and $\hat{N}_{d,u}$.

It is now assumed that all test statistics from all individual sensors are conditionally independent, conditioned on either of the two hypotheses. Using the SUM rule, the combined test statistic T_{cs} of U number of single user test statistics T_u is as follows:

$$T_{cs} = \sum_{u=1}^{U} T_u, \tag{6.14}$$

where u denotes the cooperating user index. With the first scheme, which uses

the real part of $c(N_d)$ cepstral coefficient, we have:

$$T_{1,cs} = \sum_{u=1}^{U} T_{1,u}, \tag{6.15}$$

where $T_{1,u} = \mathcal{R}\{c_u(N_d)\}$. Since all $T_{1,u} \sim \mathcal{N}(0, \pi^2/48)$ are independent and the combined test statistic is a sum of them, we can say that $T_{1,cs} \sim \mathcal{N}(0, U\pi^2/48)$. The threshold value has then similar form as Eq. (6.9):

$$\eta_{1,cs} = \sqrt{\frac{U\pi^2}{24}}\mathrm{erf}^{-1}(2P_f). \tag{6.16}$$

Again, the threshold does not depend on the noise power σ_w^2, which makes this collaborative scheme also robust to noise power uncertainty.

For the second scheme, which uses $c(0)$ cepstral coefficient, we have:

$$T_{2,cs} = \sum_{u=1}^{U} T_{2,u}, \tag{6.17}$$

where $T_{2,u} = c_u(0)$. Since all $T_{2,u} \sim \mathcal{N}(\sqrt{N_r}\mu_z, \pi^2/24)$ and the combined test statistic is a sum of them, we can say that $T_{2,cs} \sim \mathcal{N}(U\sqrt{N_r}\mu_z, U\pi^2/24)$. Again, it is assumed that conditional independence, conditioned on the two hypotheses, holds for the individual test statistics. The threshold value has then similar form as Eq. (6.12):

$$\eta_{2,cs} = \sqrt{\frac{U\pi^2}{12}}\mathrm{erf}^{-1}(2P_f) + U\sqrt{N_r}\Big(\log\sqrt{\frac{\sigma_w^2}{2}} + \frac{\log 2}{2} - \frac{\gamma}{2}\Big). \tag{6.18}$$

Again, the threshold does in this case depend on the noise power σ_w^2, which makes the collaborative scheme susceptible to noise power uncertainty.

6.4 Simulation results

In this section, simulation results for all of the proposed cepstrum based schemes for detecting OFDM waveforms in AWGN channel are presented. The schemes are simulated both under single-user as well as cooperative sensing scenario. In all simulations, NP strategy is used. Simulations are implemented in Matlab environment, and the parameters shown in Table 6.1 are used in all of the simulations unless stated otherwise. It is also assumed that synchronization is not needed when receiving the processed signal.

Fig. 6.2 shows a plot for the probability of detection with respect to the SNR for both proposed detection schemes in a single-user case. It can be seen that the results from the theoretical analysis and from the simulations are very close for both detectors. The scheme based on $c(0)$ is observed to perform better than the scheme based on $c(N_d)$ when the noise power in AWGN channel is assumed to be known perfectly.

Table 6.1: Simulation parameters.

Parameter	Value
FFT size, N_r	2048
Data length, N_d	64
Cyclic prefix length, N_c	16
Number of blocks, B	26
False alarm rate, P_f	0.05
Noise power, σ_w^2	1
Num. of realizations	10000

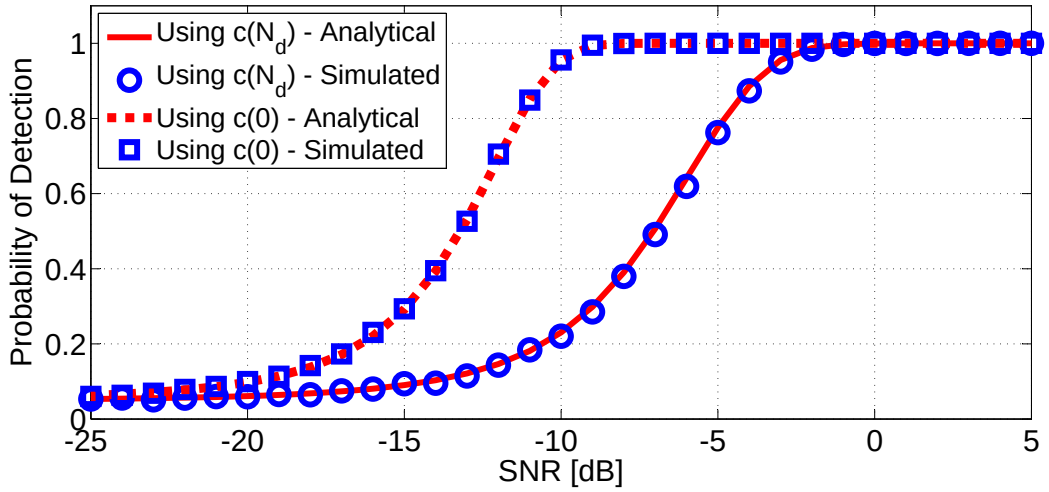

Figure 6.2: Probability of detection with respect to the SNR for both proposed detection schemes. Theoretical analysis and simulated results are close. Noise power is assumed to be known and NP strategy is used.

Next, the performances of the proposed single-user detectors are compared to the traditional ED method. Fig. 6.3 shows the probability of detection vs SNR curves for the proposed cepstrum based schemes and the ED when the noise power is assumed to be known. However in practice, noise level is always uncertain and needs to be estimated [31]. Hence, detection results are also included with noise power uncertainty of 1 dB. It can be seen that the detection scheme based on the cepstral coefficient $c(N_d)$ performs worse than the ED when the noise power is perfectly known. However, even when a small uncertainty of 1 dB is present in the noise power, the performance of the ED degrades drastically. On the other hand, the scheme based on $c(N_d)$ is insensitive to noise uncertainty and is very valuable for practical scenarios as it provides a good trade-off between detection performance and robustness. Although the performance of the detection scheme using $c(0)$ is close to that of the energy detector, the performance degrades similar to energy detector in the presence of noise uncertainty. When compared to the empirical GLLRT

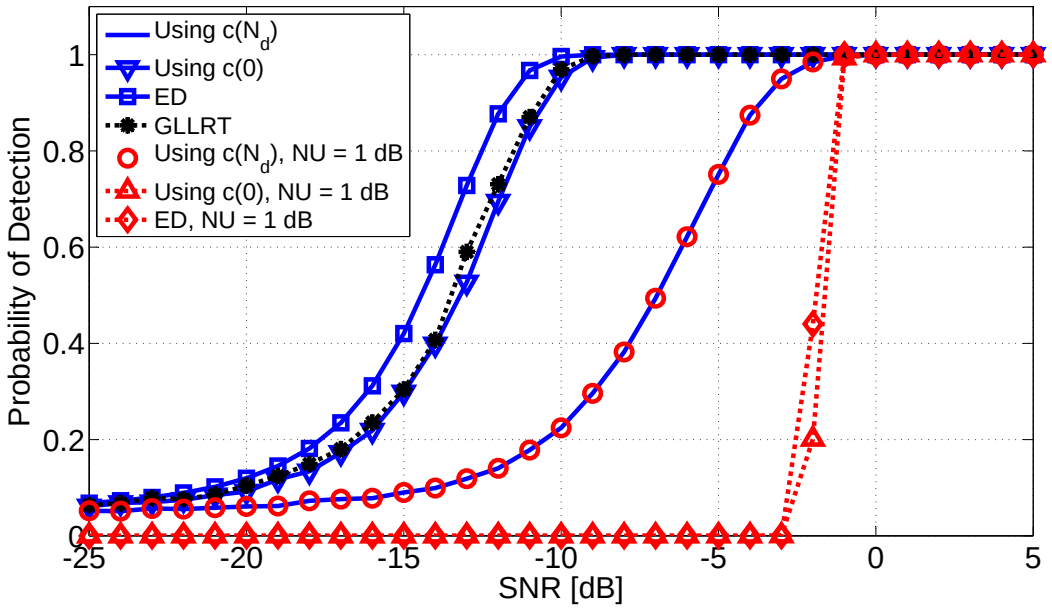

Figure 6.3: Probability of detection vs. SNR for the two proposed cepstrum based sensing schemes in addition to the ED. Neyman-Pearson detection strategy is used for all of the detectors. Under low SNR, the probability of detection for each detector does not rise above the desired false alarm rate. The scheme based on the cepstral coefficient $c(N_d)$ is robust to noise uncertainty and performs better than the ED even in the presence of noise uncertainty of only 1 dB. The performance of the proposed scheme based on the cepstral coefficient $c(0)$ is close to that of the ED and empirical GLLRT based cepstrum detector.

based cepstrum detector, the proposed scheme using $c(0)$ does not perform significantly worse.

Fig. 6.4 shows how the proposed detection schemes perform with different OFDM transmission parameters. In the example, we consider the following two existing wireless standards: LTE [106] and WLAN IEEE 802.11a [104]:

- LTE: $N_d = 256$, $N_c = 18$, $\mu = 0.07$
- WLAN: $N_d = 64$, $N_c = 16$, $\mu = 0.2$

It can be seen that the detection performance depends highly on the proportion of the CP length from the data length, which is marked as $\mu = \frac{N_c}{N_c+N_d}$. In this case, WLAN signal ($\mu = 0.2$) is detected significantly better than LTE signal ($\mu = 0.07$), even when the processed sample size remains the same ($N_r = 2048$).

The detection performance is notably improved when collaborative sensing is introduced, which can be seen in Fig. 6.5 that shows the probability of detection curves for 1 user and 5 or 10 collaborative users.

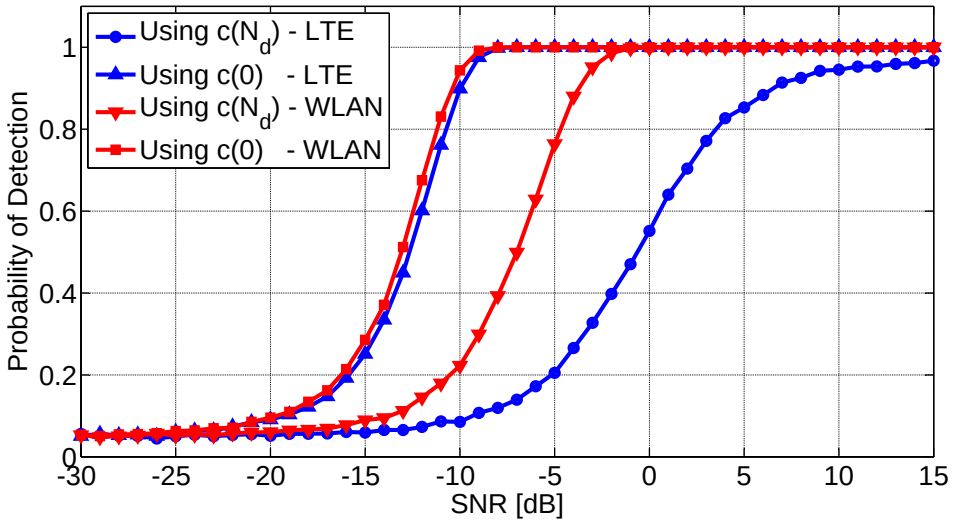

Figure 6.4: Probability of detection vs. SNR for the two proposed cepstrum based sensing schemes with LTE ($\mu = 0.07$) and WLAN ($\mu = 0.2$) signals. The performance improves when μ is higher, i.e. when the correlation is stronger in the signal.

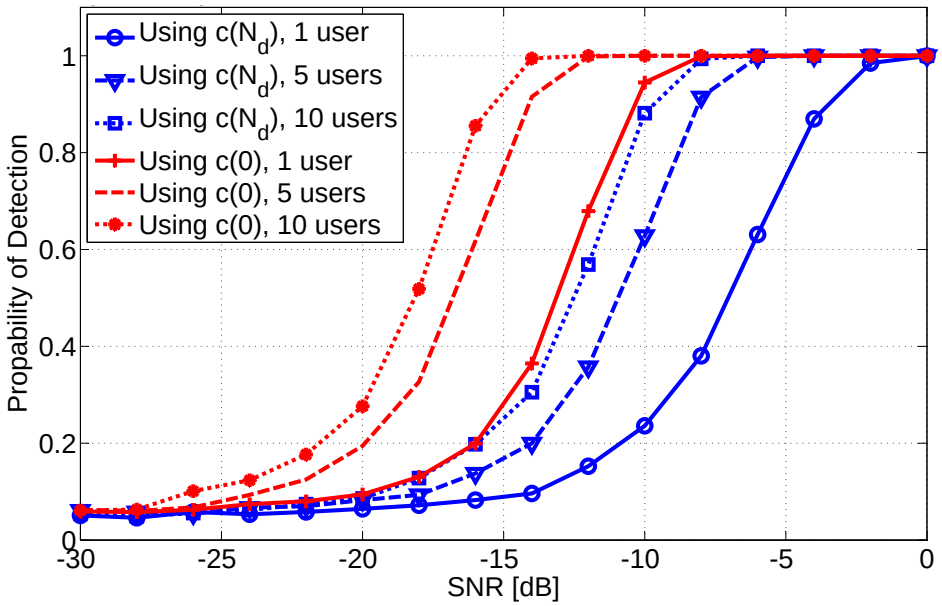

Figure 6.5: Probability of detection vs. SNR for the two proposed cepstrum based sensing schemes with single user and 5 or 10 cooperating users. The performance improves notably when more users are collaborating, which shows as SNR gain and steeper slopes of the P_d curves.

Chapter 7

Cepstrum-Based Estimation of OFDM Parameters

In this chapter, estimation methods for finding the data length and the CP length in an OFDM symbol based on the cepstrum features of OFDM are proposed. Like in the previous chapter, the schemes are first derived for a single-user case, after which they are extended into a collaborative scenario. Finally, the performances of the derived estimation methods are displayed with simulations.

7.1 Estimation of OFDM data length

It was seen in Fig. 5.1a that the mean of the real part of the OFDM cepstrum has a dominant peak at N_d in addition to the DC peak. This feature can be used to extract data size N_d from an unknown OFDM signal by searching the index of the highest real cepstral coefficient value excluding the DC peak. Therefore the estimate of N_d is given by

$$\hat{N}_d = \arg\max_{\mathrm{n}} \ \mathcal{R}\{c(n)\}, \quad n = 1, \ldots, \left\lfloor \frac{N_r}{2} \right\rfloor . \tag{7.1}$$

Note that being the DFT of a real signal, the cepstrum is symmetrical and hence only the first half of the cepstral coefficients are used for classification purposes.

The error of the estimate will depend on the set of allowed values. Generally there are only few possible values of N_d and N_c for each OFDM signal. For example, DVB-T has option of 2048 and 8192 values for N_d while N_c can take values from 1/4, 1/8, 1/16 and 1/32 of N_d [107]. The accuracy of the estimate can be improved if the estimate $\hat{N}_d$ is limited to take values from a finite set of possible values. Without loss of generality, we consider a set containing powers of two because generally the number of subcarriers in an OFDM symbol is a power of 2 since it facilitates efficient FFT/IFFT implementation [101].

Limiting the set of values allowed for $\hat{N}_d$, the estimate of N_d is given by

$$\hat{N}_d = \arg\max_{\mathrm{n}} \ \mathcal{R}\{c(n)\}, \quad n = 2^m, m \in (1, 2, \ldots, \log_2 \left\lfloor \frac{N_r}{2} \right\rfloor). \tag{7.2}$$

7.2 Estimation of the CP length in OFDM

As seen in Fig. 5.1b, the variance sequence of the cepstrum has a repetitive pattern when an OFDM signal is present. The period of the triangular peaks is N_s samples, which can be estimated by finding the highest correlation for different lags τ by

$$\hat{N}_s = \arg\max_{\tau \in \mathcal{A}} \sum_{n=N_d}^{N_d+M_v} V_c(n) V_c(n+\tau), \tag{7.3}$$

where $V_c(n)$ is the variance of $\mathcal{R}\{c(n)\}$, $M_v < N_r/2 - N_d$ and $\mathcal{A}$ is set of all integers between $N_d + 1$ and $\frac{3N_d}{2}$ under a reasonable assumption that N_c can take integer values between 1 and $\frac{N_d}{2}$, and N_d is an even number. Finally, the estimate of the CP length can be easily calculated with $\hat{N}_s$:

$$\hat{N}_c = \hat{N}_s - N_d. \tag{7.4}$$

Similar to the case of N_d, it is also possible to limit the possible values for $\hat{N}_c$ to be integer powers of 2 less or equal than $N_d/2$. In such case, $\mathcal{A} = N_d + 2^m$, where $m = \{0, 1, 2, \ldots, \ \log_2 \left\lfloor \frac{N_d}{2} \right\rfloor\}$.

7.3 Collaborative estimation of OFDM parameters

In this section the proposed two detection methods introduced in Secs. 7.1 and 7.2 are extended into a collaborative sensing scenario for demonstrating the improvement in the estimation performance that is obtained by collaboration. The considered distributed sensing system follows the same topology that was introduced with the cooperative detection and shown in Fig. 6.1. In that scenario, each SU sends values of the local estimates $\hat{N}_d$ and $\hat{N}_c$ to the FC. At the FC, cooperative estimates ($\hat{N}_{d,cs}$ and $\hat{N}_{c,cs}$) are calculated from the received values from each individual sensor.

When multiple estimates of the same parameter are available and it is assumed the estimates are uncorrelated and have similar statistical properties (i.e. same mean and variance), it is a reasonable procedure to combine them by averaging [102]. If the mean of each local estimator is $\mathbb{E}[\hat{\theta}_u]$ and the variance is $\mathbb{V}\mathrm{ar}[\hat{\theta}_u]$, the mean of the combined estimate $\hat{\theta}$ is

$$\mathbb{E}[\hat{\theta}] = \mathbb{E}[\hat{\theta}_u] \tag{7.5}$$

and the variance is

$$\mathbb{V}\mathrm{ar}[\hat{\theta}] = \frac{\mathbb{V}\mathrm{ar}[\hat{\theta}_u]}{U}, \tag{7.6}$$

where U is the total number of local estimates. Thus, as more estimates are averaged, the variance will decrease [102].

Hence, assuming that the above mentioned conditions are met, the proposed cooperative estimate of N_d is a *sample mean* of U number of SU estimates that is rounded towards the nearest value belonging to the allowed set of values.

$$\hat{N}_{d,ave} = \left[\frac{1}{U} \sum_{u=1}^{U} \hat{N}_{d,u} \right]_{\mathcal{A}}, \tag{7.7}$$

where $[\cdot]_{\mathcal{A}}$ denotes the operator of rounding towards the nearest value in the set of allowed values $\mathcal{A}$. Using the same strategy, the cooperative estimate of N_c is:

$$\hat{N}_{c,ave} = \left[\frac{1}{U} \sum_{u=1}^{U} \hat{N}_{c,u} \right]_{\mathcal{A}}. \tag{7.8}$$

The combination can also be done by using order statistics such as *sample median* or *mode*. In those cases we have the following combined estimates for N_d:

$$\hat{N}_{d,md} = \mathrm{Md}(\hat{\Theta}_d), \tag{7.9}$$

and

$$\hat{N}_{d,mo} = \mathrm{Mo}(\hat{\Theta}_d), \tag{7.10}$$

where $\hat{\Theta}_d = \{\hat{\theta}_{d,1}, \hat{\theta}_{d,2}, \ldots, \hat{\theta}_{d,U}\}$ and $\mathrm{Md}(\cdot)$ and $\mathrm{Mo}(\cdot)$ denote the sample median and mode operator respectively. Similarly, for N_c we have:

$$\hat{N}_{c,md} = \mathrm{Md}(\hat{\Theta}_c), \tag{7.11}$$

and

$$\hat{N}_{c,mo} = \mathrm{Mo}(\hat{\Theta}_c), \tag{7.12}$$

where $\hat{\Theta}_c = \{\hat{\theta}_{c,1}, \hat{\theta}_{c,2}, \ldots, \hat{\theta}_{c,U}\}$.

7.4 Simulation results

In this section, the simulation results for the derived estimation algorithms both in a single-user and a collaborative estimation scenario are shown. The simulation setting and the used parameters are the same as in Sec. 6.4.

Single-user estimation results

Figs. 7.1 and 7.2 show the means and the variances of the single-user estimates $\hat{N}_d$ and $\hat{N}_c$ with respect to the SNR. It can be seen that both of the estimates converge to their desired values and their variances converge to zero as the SNR increases. In both cases, limiting the set of the allowed values induces better estimation performance. Note that both N_d and N_c are integer values. The variance sequence used in the estimation of N_c is calculated from 200 cepstrum realizations in the example.

Note that in the low SNR regime, the estimates of N_d and N_c behave like uniform discrete random variables and hence their mean and variance depend on the set of their allowed values. For example, the mean and the variance for a uniform discrete random variable Y over the set $\mathcal{A}' \in \{1, 2, 4, 8, 16, 32\}$ are calculated as:

$$\mathbb{E}[Y] = \sum_{i \in \mathcal{A}'} y_i f(y_i) = \frac{1}{6}(1 + 2 + 4 + 8 + 16 + 32) = 10.5 \tag{7.13}$$

and

$$\begin{aligned} \mathbb{V}\mathrm{ar}[Y] &= \sum_{i \in \mathcal{A}'} y_i^2 f(y_i) - \mathbb{E}[Y]^2 \\ &= \frac{1}{6}(1^2 + 2^2 + 4^2 + 8^2 + 16^2 + 32^2) - 10.5^2 \\ &= 117.25, \end{aligned} \tag{7.14}$$

which match with the mean and the variance of the simulated $\hat{N}_c$ under low SNR region in Fig. 7.2.

The variance of the estimate N_d in Fig. 7.1 slightly increases in the SNR range of -5 to -10 dB before falling to zero with higher SNR values. This is a property of a uniform distribution with one biased value that has higher probability mass than other values. Fig. 7.3 shows the distribution of $\hat{N}_d$ for SNRs of -10 dB, -5 dB and 0 dB. It can be seen that all indices except N_d behave like uniform random variables. In Fig. 7.3, analytical variances for such "biased" uniform distributions are calculated and compared to the simulated variances of $\hat{N}_d$. The results match, which explains the increase in the variance plot.

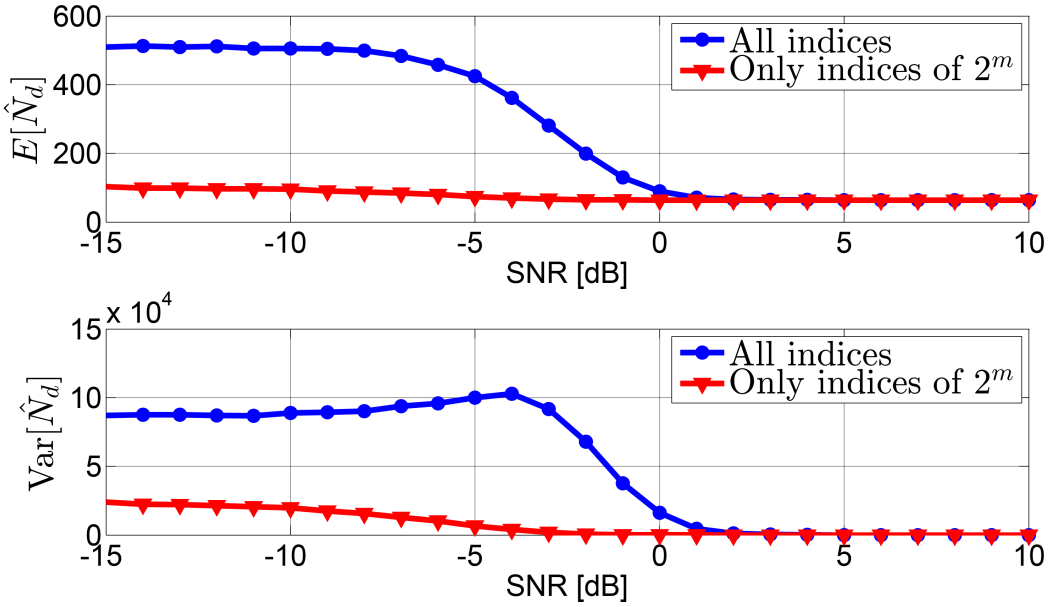

Figure 7.1: Mean and variance of the estimate $\hat{N}_d$. The mean converges to the correct value 64 and the variance converges to zero as the SNR increases.

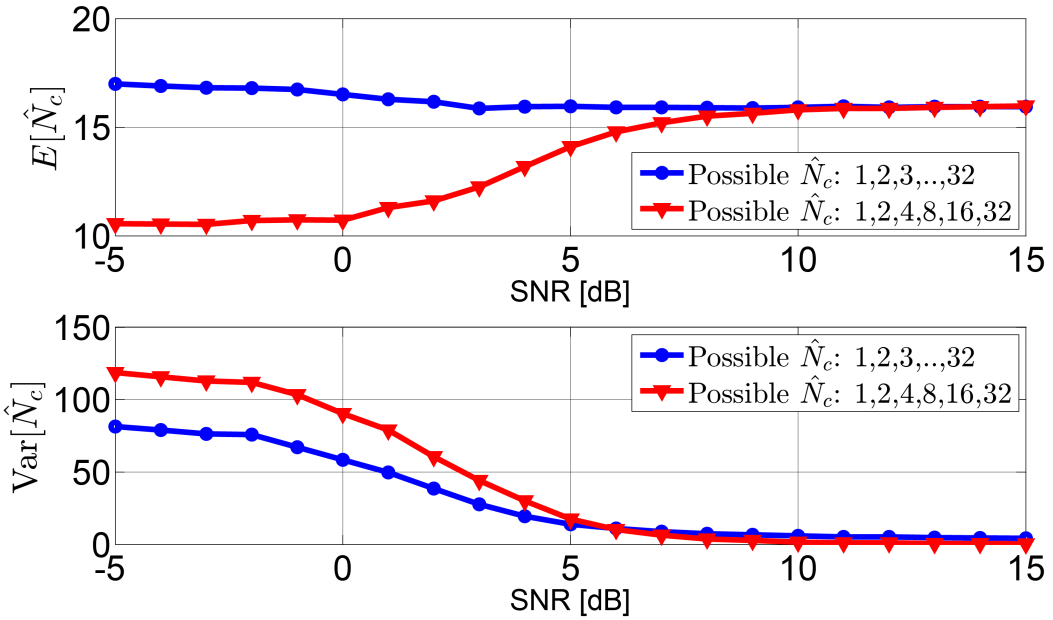

Figure 7.2: Mean and variance of the $\hat{N}_c$ value. The mean converges to the correct value 16 and the variance reduces as the SNR increases. When the set of possible N_c values is limited, the variance of $\hat{N}_c$ converges to zero.

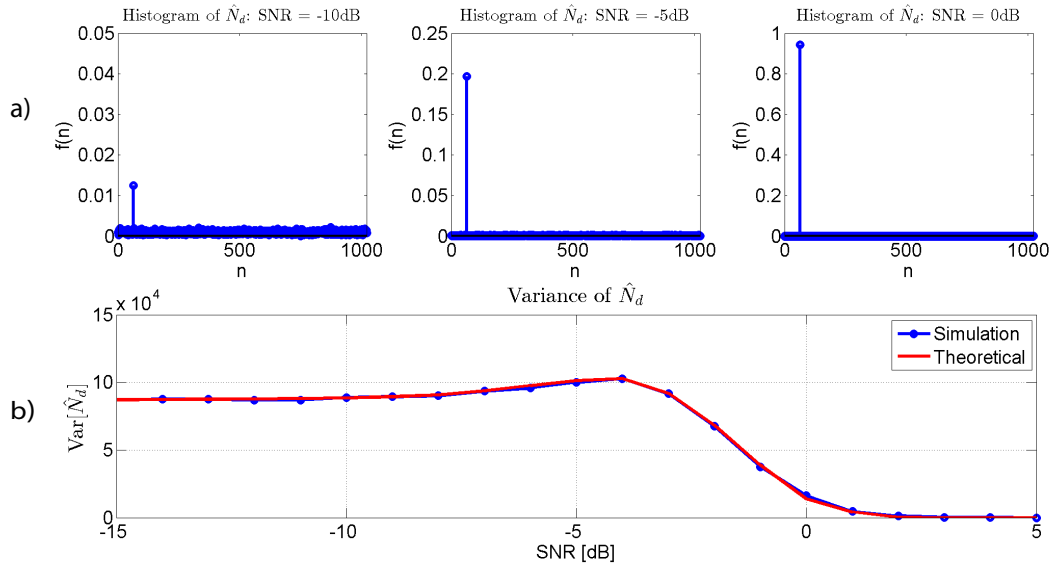

Figure 7.3: a) Histograms of $\hat{N}_d$ for the SNRs of -10 dB, - 5 dB and 0 dB. They are distributed as a uniform distribution that has one biased value. b) Simulated variance of $\hat{N}_d$ and theoretical variance of similar "biased" uniform distributions. Results match, which explains the slight increase in the variance in the middle of the plot.

Collaborative estimation results

In Fig. 7.4, the mean and the variance of the three different proposed collaborative estimators for N_d w.r.t. the SNR are presented when 5 and 10 SUs are cooperating and the set of the allowed values is either $\{1, 2, \ldots, \lfloor \frac{N_r}{2} \rfloor\}$ or 2^m, where $m \in \{1, 2, \ldots, \lfloor \log_2 \frac{N_r}{2} \rfloor\}$. As more SU estimates are combined, the variances of the cooperative estimates decrease faster, which naturally is a benefit. Fig. 7.5 presents the mean and the variance of the three different proposed collaborative estimators for N_c when 5 and 10 SUs are cooperating and the set of the allowed values is either $\{1, 2, \ldots, \lfloor \frac{N_d}{2} \rfloor\}$ or 2^m, where $m \in \{1, 2, \ldots, \lfloor \log_2 \frac{N_d}{2} \rfloor\}$. Similar observations can be done as with the collaborative estimation of N_d. Thus, the estimation results are notably improved when cooperation is introduced.

From the three proposed fusion rules, *mode* seems to perform the best as its mean converges to its desired value and its variance decreases to zero fastest as the SNR increases.

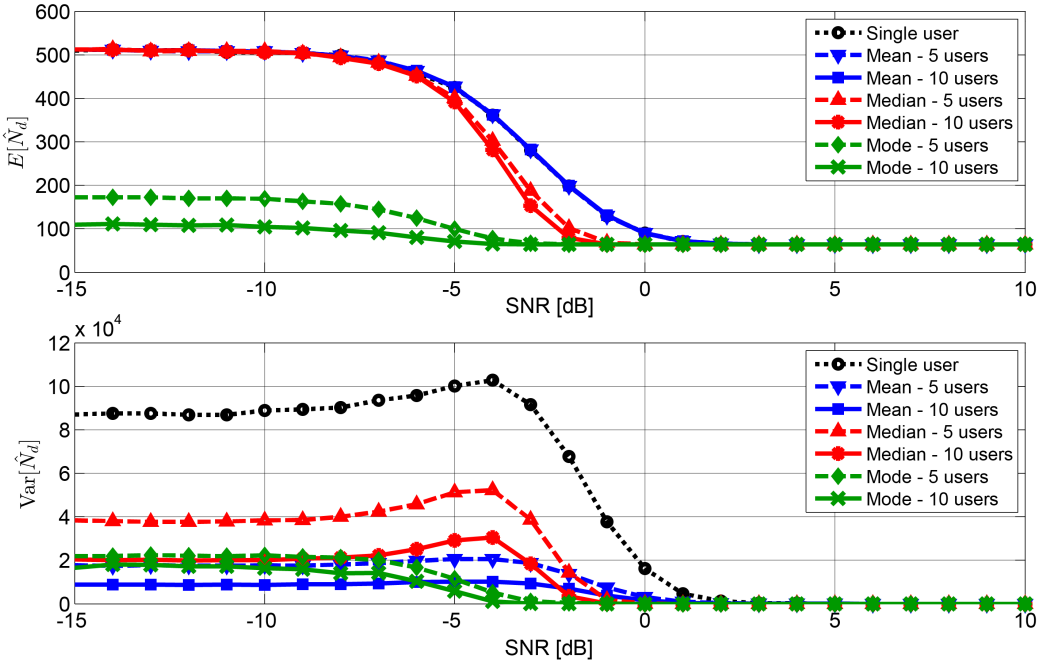

(a) Possible $\hat{N}_d$: $\{1, 2, \ldots, \lfloor \frac{N_r}{2} \rfloor\}$.

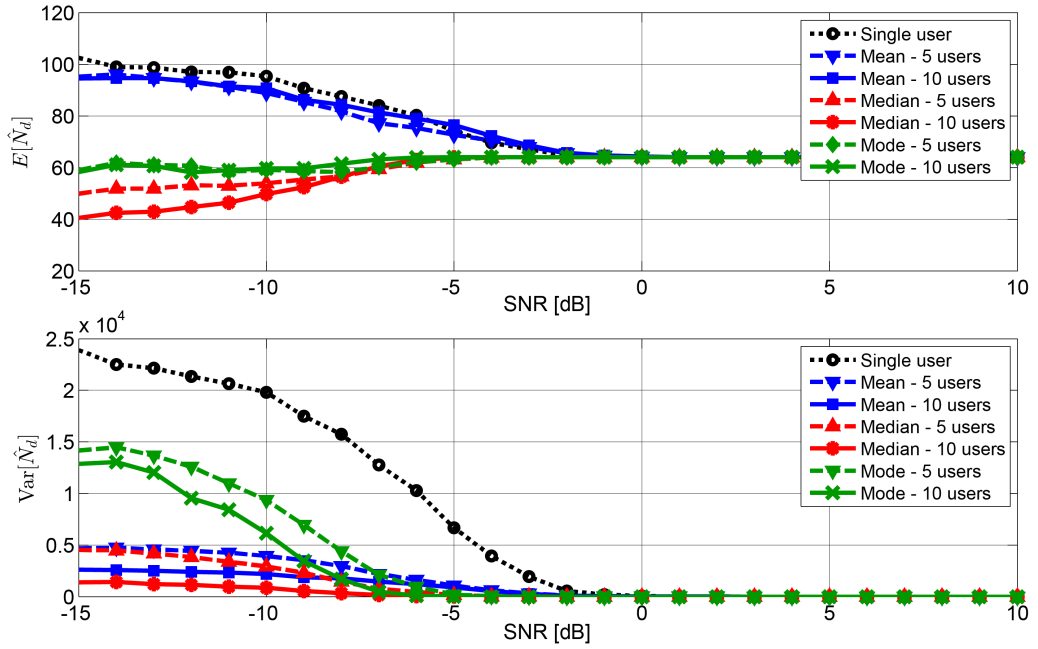

(b) Possible $\hat{N}_d$: 2^m, where $m \in \{1, 2, \ldots, \lfloor \log_2 \frac{N_r}{2} \rfloor\}$.

Figure 7.4: The mean and the variance of $\hat{N}_d$ w.r.t. the SNR for single-user and 5 or 10 cooperating users when the allowed set of values is a) $\{1, 2, \ldots, \lfloor \frac{N_r}{2} \rfloor\}$ or b) 2^m, where $m \in \{1, 2, \ldots, \lfloor \log_2 \frac{N_r}{2} \rfloor\}$. The performance improves notably when cooperation is introduced, which shows as a smaller variance and as a faster convergence to the real value with more users.

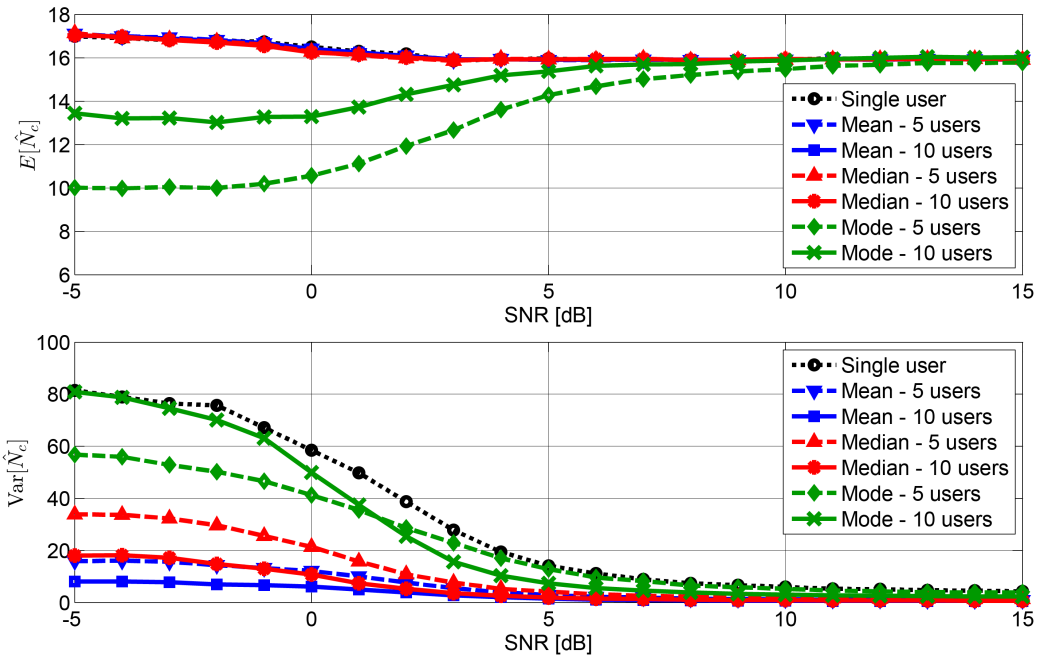

(a) Possible $\hat{N}_c$: $\{1, 2, \ldots, \lfloor \frac{N_d}{2} \rfloor\}$.

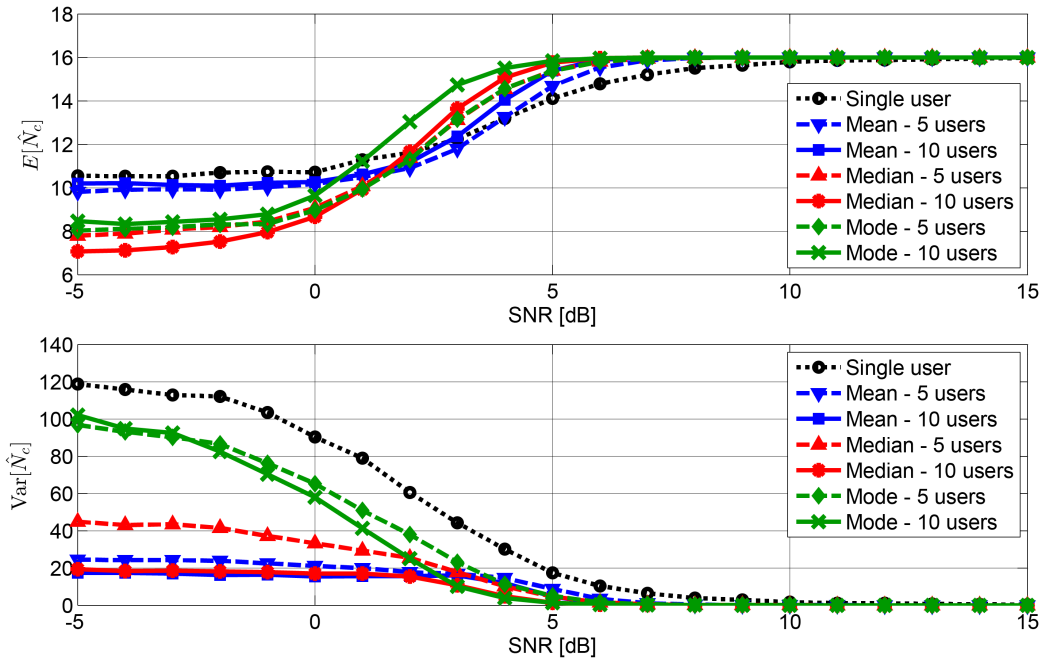

(b) Possible $\hat{N}_c$: 2^m, where $m \in \{1, 2, \ldots, \lfloor \log_2 \frac{N_d}{2} \rfloor\}$.

Figure 7.5: The mean and the variance of $\hat{N}_c$ w.r.t. the SNR for single-user and 5 or 10 cooperating users when the allowed set of values is a) $\{1, 2, \ldots, \left\lfloor \frac{N_d}{2} \right\rfloor\}$ or b) 2^m, where $m \in \{1, 2, \ldots, \left\lfloor \log_2 \frac{N_d}{2} \right\rfloor\}$. The performance improves in both cases notably when cooperation is introduced, which shows as a smaller variance and as a faster convergence to the real value with more users.

Chapter 8

Conclusions

The current wireless networks are based on a fixed spectrum allocation policy. However, in practice the overall utilization of the assigned spectrum can be very low. This underutilization of the licensed spectrum along with the limited usable radio frequency spectrum leads to problems since the need for RF spectrum is on the rise. Cognitive radios are developed to solve the inefficiency in the spectrum usage by exploiting licensed spectrum in an agile manner through dynamic spectrum access. In dynamic spectrum access, the secondary users can use the underutilized licensed spectrum as long as they do not interfere with the primary users. In order to access spectrum dynamically, cognitive users must acquire awareness of the radio environment through spectrum sensing. Spectrum sensing includes both detecting whether the spectrum is occupied or not and acquiring information about the type of the transmitted signals.

The cepstrum is a signal processing tool that is historically used mainly in speech processing applications. The ability of cepstrum to effectively distinguish periodicities in a signal is found to be useful for detecting man-made signals since almost all of them include periodicities due to modulation and coding operations.

This thesis is focused on studying how spectrum sensing can be performed based on cepstral analysis. First, the cepstrum of an OFDM signal in AWGN channel is examined. It is shown that the cepstrum has distinctive differences when an OFDM signal is either absent or present in the received signal. When OFDM transmission is present, peaks corresponding to the OFDM data length appear in the mean of the cepstrum. However, that does not occur when only AWGN is received. In addition, the variance of the cepstrum for OFDM signal shows triangular shapes related to the symbol length as opposed to the constant valued variance of AWGN cepstrum. In this thesis, the distributions for the cepstrum coefficients for both AWGN and OFDM in AWGN are derived analytically.

Based on the distinctive features in the cepstrum when OFDM transmission is either present or not, two cepstrum-based detection algorithms are proposed in this thesis. The detection is formulated as a binary hypothesis problem and a

Neyman-Pearson decision strategy is applied. The distributions of the decision statistics under two alternative hypotheses are derived analytically. The first detection scheme is based on the peak at the cepstrum coefficient at the index corresponding to the OFDM data sample length while the second detector is based on the DC cepstral coefficient that corresponds to the received signal power. For both detectors, the threshold values for decision making are derived analytically and their performances are compared with the energy detector. Based on the properties of the cepstrum of an OFDM signal, the first detector is found to be independent of the noise power, for which it is robust to noise power uncertainties and performs thus better than ED when noise power is uncertain. The second detector, based on the DC value, performs close to the classical energy detector and is thus susceptible to noise power uncertainties.

An algorithm for estimating OFDM data length is proposed based on the peak in the mean of the cepstrum. Since the peak corresponds to the data length in an OFDM symbol, the estimation can be implemented by searching the maximum cepstral coefficient, excluding the DC coefficient. Furthermore, a method for finding the cyclic prefix length is proposed based on the triangular shapes in the variance of the cepstrum when OFDM is present. An estimate for an OFDM symbol length is found by searching the lag that maximizes the autocorrelation function of the cepstrum variance sequence. The cyclic prefix length is then calculated by simply subtracting the data length value for the obtained symbol length estimate. It is shown through simulations that the expected values of the proposed estimates converge to their desired values and their variances converge to zero as the SNR increases.

All proposed detection and parameter estimation algorithms are extended into a cooperative scenario where multiple users operate simultaneously. The cooperative algorithms are designed for a distributed sensing system that follows a parallel topology. In that scenario, each individual SU processes its local decisions or parameter estimates and sends them to a fusion center. In the fusion center, a cooperative decision or estimate is calculated according to a fusion rule. In each case, the performance of the detection or the estimation is found to be better when cooperation is included.

As future work, the performances of cepstrum-based spectrum sensing techniques in different multipath channels or for sensing other waveforms than OFDM would be interesting research topics. In addition, issues regarding the practical implementation of the proposed detection and classification algorithms could be studied more deeply.

References

[1] C. Ghosh, S. Roy and D. Cavalcanti, "Coexistence Challenges for Heterogeneous Cognitive Wireless Networks in TV White Spaces," *IEEE Transactions on Wireless Communications*, vol.18, no.4, pp. 22–31, Aug. 2011.

[2] T. Yücek and H. Arslan, "A Survey of Spectrum Sensing Algorithms for Cognitive Radio Applications," *IEEE Communications Surveys & Tutorials*, vol. 11, no. 1, pp. 116–130, Mar. 2009.

[3] R. Prasad and R. Van Nee, *OFDM for Wireless Communications Systems.* Norwood, MA: Artech House, 2000, 284 pages.

[4] B. Bogert, M. Healy and J. Tukey, "The Quefrency Alanysis of Time Series for Echos: Cepstrum, Pseudo-Autocovariance, Cross-Cepstrum, and Saphe Cracking," *Proceedings of the Symposium on Time Series Analysis*, Chap. 15, pp. 209–243, Wiley, New York, 1963.

[5] D. Childers, D. Skinner and R. Kemerait, "The Cepstrum: A Guide to Processing," *Proceedings of the IEEE*, vol. 65, no. 10, pp. 1428–1443, Oct. 1977.

[6] D. O'Saughnessy, *Speech Communications: Human and Machine.* Addison-Wesley, 1987, 576 pages.

[7] B. Gold, N. Morgan and D. Ellis, *Speech and Audio Signal Processing: Processing and Perception of Speech and Music.* 2nd Ed., Wiley: New York, 2011, 660 pages.

[8] J. Jäntti, S. Chaudhari and V. Koivunen, "Cepstrum Based Detection and Classification of OFDM Waveforms," *Proceedings of the IEEE International Conference on Acoustics, Speech and Signal Processing (ICASSP '14)*, pp. 8113 – 8117, May 2014.

[9] I. Akyildiz, W. Lee, M. Vuran and S. Mohanty, "NeXt Generation/Dynamic Spectrum Access/Cognitive Radio Wireless Networks: A Survey," *Computer Networks*, vol. 50, no. 13, Elsevier, pp. 2127–2159, Sep. 2006.

[10] Federal Communications Committee, *FCC Spectrum Policy Task Force Report*. ET Docket No. 02-155, Nov. 2002.

[11] S. Haykin, D. Thomson and J. Reed, "Spectrum Sensing for Cognitive Radio," *Proceedings of the IEEE*, vol. 97, no. 5, pp. 849–877, May 2009.

[12] E. Biglieri, A. Goldsmith, L. Greenstein, N. Mandayam and V. Poor, Eds., *Principles of Cognitive Radio.* Cambridge University Press, 2013, 321 pages.

[13] E. Hossain, D. Niyato and Z. Han, *Dynamic Spectrum Access and Management in Cognitive Radio Networks.* Cambridge University Press, 2009, 487 pages.

[14] Q. Zhao and B. Sadler, "A Survey of Dynamic Spectrum Access," *IEEE Signal Processing Magazine*, vol. 24, no. 3, pp. 79–89, May 2007.

[15] S. Haykin, "Cognitive Radio: Brain-empowered Wireless Communications," *IEEE Journal on Selected Areas in Communications*, vol. 23, no. 2, pp. 201–220, Feb. 2005.

[16] Federal Communications Committee, *Notice of Proposed Rule Making and Order: Facilitating Opportunities for Flexible, Efficient, and Reliable Spectrum Use Employing Cognitive Radio Technologies*. ET Docket No. 03-108, Feb. 2005.

[17] I. Akyildiz, W. Lee, M. Vuran and S. Mohanty, "A Survey on Spectrum Management in Cognitive Radio Networks," *IEEE Communications Magazine*, vol. 46, no. 4, pp. 40–48, Apr. 2008.

[18] G. Ghosh, P. Das and S. Chatterjee, "Cognitive Radio and Dynamic Spectrum Access – A Study," *International Journal of Next-Generation Networks*, vol. 6, no. 1, pp. 43–60, Mar. 2014.

[19] I. Akyildiz, W. Lee, K. Chowdhury, "CRAHNs: Cognitive Radio Ad Hoc Networks," *Ad Hoc Networks*, Elsevier, vol. 7, no. 5, pp. 810–836, Jul. 2009.

[20] Z. Tabakovic, S. Grgic and M. Grgic, "Dynamic Spectrum Access in Cognitive Radio," *IEEE International Symposium ELMAR*, pp. 245–248, Sep. 2009.

[21] L. Khalid and A. Anpalagan, "Emerging Cognitive Radio Rechnology: Principles, Challenges and Opportunities," *Computers and Electrical Engineering*, Elsevier, vol. 36, no. 2, pp. 358–366, Mar. 2010.

[22] Finnish Communications Regulatory Authority, *Spectrum Allocation in Finland.* Aug. 2009, online: https://www.viestintavirasto.fi/attachments/Radiotaajuuksien_kaytto_EN.pdf, [Accessed in May 18, 2014].

[23] S. Chaudhari, *Spectrum Sensing for Cognitive Radios: Algorithms, Performance and Limitations.* PhD Thesis, Aalto University School of Electrical Engineering, Department of Signal Processing and Acoustics, Nov. 2012.

[24] I. Garcia, *Interference Management in Cognitive Radio Systems.* M. Sc. Thesis, Aalto University School of Science and Technology, Faculty of Electronics, Communications and Automation, 2010.

[25] S. Filin, H. Harada, H. Murakami and K. Ishizu, "International Standardization of Cognitive Radio Systems," *IEEE Communications Magazine*, vol. 49, no. 3, pp. 82-89, Mar. 2011.

[26] E. Axell, G. Leus, E. Larsson and H. Poor, "State-of-the-art and Recent Advances: Spectrum Sensing for Cognitive Radio," *IEEE Signal Processing Magazine*, vol. 29, no. 3, pp. 101–116, May 2012.

[27] M. Barkat, *Signal Detection and Estimation.* 2nd Ed., Artech House, Boston, 2005, 714 pages.

[28] V. Poor, *An Introduction to Signal Detection and Estimation.* 2nd Ed., Springer-Verlag: Berlin, 1998, 398 pages.

[29] P. Varshney, *Distributed Detection and Data Fusion.* 2nd Ed., Springer-Verlag: New York, 1997, 276 pages.

[30] J. Lundén, *Spectrum Sensing for Cognitive Radios and Radar Systems.* PhD Thesis, Helsinki University of Technology, Department of Signal Processing and Acoustics, Nov. 2009.

[31] R. Tandra and A. Sahai, "SNR Walls for Signal Detection," *IEEE Journal on Selected Topics in Signal Processing*, vol. 2, pp. 4–17, Feb. 2008.

[32] J. Lehtomäki, *Analysis of Energy Based Signal Detection.* PhD Thesis, University of Oulu, Faculty of Technology, Dec. 2005.

[33] H. Urkowitz, "Energy Detection of Unknown Deterministic Signals," *Proceedings of the IEEE*, vol. 55, no. 4, pp. 523–531, Apr. 1967.

[34] D. Cabric, S. Mishra and R. Brodersen, "Implementation Issues in Spectrum Sensing for Cognitive Radios," *Conference Record on the Thirty-Eighth Asilomar Conference on Signals, Systems and Computers, 2004*, vol. 1, pp. 772–776, Nov. 2004.

[35] E. Axell and E. Larsson, "Optimal and Sub-Optimal Spectrum Sensing of OFDM Signals in Cognitive radios," *IEEE Transactions on Signal Processing*, vol. 29, pp. 290–304, Feb. 2011.

[36] S. Chaudhari, V. Koivunen and H. Poor, "Autocorrelation-Based Decentralized Sequential Detection of OFDM Signals in Cognitive Radios," *IEEE Transactions on Signal Processing*, vol. 57, pp. 2690–2700, Jul. 2009.

[37] Z. Lei and F. Chin, "OFDM Signal Sensing for Cognitive Radios," *Proceedings of the IEEE 19th International Symposium on Personal, Indoor, Mobile and Radio Communications (PIMRC 2008)*, pp. 1–5, Sep. 2008.

[38] O. Dobre, A. Abdi, Y. Bar-Ness and W. Su, "Survey of Automatic Modulation Classification Techniques: Classical Approaches and New Trends," *IET Communications*, vol. 1, no. 2, pp. 137–156, Apr. 2007.

[39] M. Bhawna, M. Kaur and G. Lall, "Automatic Modulation Recognition for Digital Communication Signals," *International Journal of Soft Computing and Engineering (IJSCE)*, vol. 2, no. 2, pp. 110–114, May 2012.

[40] J. Venäläinen, *Modulation Recognition in Dispersive Communication Channels*. Licensiate Thesis, Tampere University of Technology, Department of Information Technology, Nov. 2004.

[41] W. Guibène and D. Slock, "Signal Separation and Classification Algorithm for Cognitive Radio Networks," *IEEE International Symposium on Wireless Communication Systems (ISWCS)*, pp. 301–305, Aug. 2012.

[42] H. Cao and J. Peissig, "A Robust Signal Classification Scheme for Cognitive Radio," *IEEE Journal of Selected Topics in Signal Processing*, vol. 6, no. 1, pp. 26–41, Feb. 2012.

[43] R. Li, *Modulation Classification and Parameter Estimation in Wireless Networks*. M. Sc. Thesis, Syracuse University, L.C. Smith College of Engineering and Computer Science, Jun. 2012.

[44] B. Ramkumar, "Automatic Modulation Classification for Cognitive Radios Using Cyclic Feature Detection," *IEEE Circuits and Systems Magazine*, vol. 9, no. 2, pp. 27–45, Jun. 2009.

[45] J. Xu, W. Su and M. Zhou, "Likelihood-ratio Approaches to Automatic Modulation Classification," *IEEE Transactions on Systems, Man, and Cybernetics, Part C: Applications and Reviews*, vol. 41, no. 4, pp. 492–495, Jul. 2011.

[46] A. Castro, L. Freitas, C. Cardoso, J. Costa and A. Klautau, "Modulation Classification in Cognitive Radio," in *Foundation of Cognitive Radio Systems*, S. Cheng, Ed., InTech, 2012, 298 pages.

[47] B. Ramkumar, *Automatic Modulation Classification and Blind Equalization for Cognitive Radios*. PhD Thesis, Virginia Polytechnic Institute and State University, Jul. 2011.

[48] K. Ho, W. Prokopiw and Y. Chan, "Modulation Identification of Digital Signals by the Wavelet Transform," *IEE Proceedings on Radar, Sonar and Navigation*, vol. 147, no. 4, pp. 169–176, Aug. 2000.

[49] J. Venäläinen, L. Terho and V. Koivunen, "Modulation Classification in Fading Multipath Channel," *Conference Record on the Thirty-Sixth Asilomar Conference on Signals, Systems and Computers, 2002*, vol. 2, pp. 1890–1894, Nov. 2002.

[50] A. Rosti and V. Koivunen, "Classification of MFSK Modulated Signals Using the Mean of Complex Envelope," *Proceedings of EUSIPCO-2000*, vol. 1, pp. 581–584, Sep. 2000.

[51] J. Lunden and V. Koivunen, "Automatic Radar Waveform Recognition," *IEEE Journal of Selected Topics in Signal Processing*, vol. 1, no. 1, pp. 124–136, Jun. 2007.

[52] N. Madhavan, A. Vinod, A. Madhukumar and A. Krishna, "Spectrum Sensing and Modilation Classification for Cognitive Radios Using Cumulants Based on Fractional Lower Order Statistics," *International Journal of Electronics and Communications (AEÜ)*, Elsevier, vol. 67, no. 6, pp. 479–490, Jun. 2013.

[53] O. Dobre, Y. Bar-Ness and W. Su, "Higher-Order Cyclic Cumulants for Higher Order Modulation Classification," *Proceedings of the IEEE Military Communications Conference*, vol. 1, pp. 112–117, Oct. 2003.

[54] A. Swami, S. Barbarossa and B. Sadler, "Blind Source Separation and Signal Classification," *Conference Record on the Thirty-Fourth Asilomar Conference on Signals, Systems and Computers, 2002*, vol. 2, pp. 1187–1191, Nov. 2000.

[55] O. Dobre, Q. Zhang, Y. Bar-Ness and W. Su, "Cyclostationarity-Based Blind Classification of Analog and Digital Modulations," *IEEE Military Communications Conference (MILCOM)*, pp. 1–7, Oct. 2006.

[56] S. Hsue and S. Soliman, "Automatic Modulation Classification Using Zero Crossing," *IEE Proceedings F, Radar and Signal Processing*, vol. 137, no. 6, pp. 459–464, Dec. 1990.

[57] H. Tao, Z. Zheng-ou and L. Xi-rong, "Modulation Classification Based on Multifractal Features," *Proceedings of the IEEE International Conference on ITS Telecommunications (ITST)*, pp. 152–155, Jun. 2006.

[58] H. Ketterer, F. Jondral and A. Costa, "Classification of Modulation Modes Using Time-Frequency Methods," *Proceedings of the IEEE International Conference on Acoustics, Speech and Signal Processing (ICASSP '99)*, pp. 2471–2474, vol. 5, Mar. 1999.

[59] A. Malady, *Cyclostationarity Feature-Based Detection and Classification.* M. Sc. Thesis, Virginia Polytechnic Institute and State University, Apr. 2011.

[60] J. Popoola and R. van Olst, "The Performance Evaluation of a Spectrum Sensing Implementation Using an Automatic Modulation Classification Detection Method with a Universal Software Radio Peripheral," *Expert Systems with Applications*, Elsevier, vol. 40, no. 6, pp. 2165–2173, May 2013.

[61] T. Yücek and H. Arslan, "OFDM Signal Identification and Transmission Parameter Estimation for Cognitive Radio Applications," *Proceedings of the IEEE Global Telecommunications Conference 2007 (GLOBECOM '07)*, pp. 4056–4060, Nov. 2007.

[62] A. Al-Habashna, O. Dobre, R. Venkatesan and D. Popescu, "Joint Detection and Classification of Mobile WiMAX and LTE OFDM Signals for Cognitive Radio," *Conference Record on the Forty-Fourth Asilomar Conference on Signals, Systems and Computers, 2010*, pp. 160–164, Nov. 2010.

[63] W. Guibène and D. Slock, "Signal Classification in Heterogeneous OFDM-based Cognitive Radio Systems," *IEEE International Conference on Telecommunications (ICT)*, pp. 1–5, May 2013.

[64] W. Akmouche, E. Kerherve and A. Quinquis, "OFDM Parameters Estimation a Time Approach," *Conference Record on the Thirty-Fourth Asilomar Conference on Signals, Systems and Computers, 2000*, vol. 1, pp. 142–146, Nov. 2000.

[65] H. Li, Y. Bar-Ness, A. Abdi and O. Somekh, "OFDM Modulation Classification and Parameters Extraction," *Proceedings of the IEEE 1st International Conference on Cognitive Radio Oriented Wireless Networks and Communications (Crowncom)*, pp. 1–6, Jun. 2006.

[66] L. Zou, "Detection of the Guard Interval Length in OFDM Systems," *Proceedings of the IEEE Consumer Communications and Networking Conference (CCNC)*, vol. 3, pp. 1048–1051, Jan. 2006.

[67] I. Akyildiz, B. Lo and R. Balakrishnan, "Cooperative Spectrum Sensing in Cognitive Radio Networks: A Survey," *Physical Communication*, vol. 4, no. 1, pp. 40–62, 2011.

[68] P. Varshney and R. Viswanathan, "Distributed Detection with Multiple Sensors: Part I – Fundamentals," *Proceedings of the IEEE*, vol. 85, no. 1, pp. 54–63, Jan. 1997.

[69] R. Blum, S. Kassam and H. Poor, "Distributed Detection with Multiple Sensors: Part II – Advanced Topics," *Proceedings of the IEEE*, vol. 85, no. 1, pp. 64–79, Jan. 1997.

[70] S. Chaudhari, J. Lundén, V. Koivunen and H. Poor, "Cooperative Sensing With Imperfect Reporting Channels: Hard Decisions or Soft Decisions?," *IEEE Transactions on Signal Processing*, vol. 60, no. 1, pp. 18–28, Jan. 2012.

[71] L. Rabiner and R. Schafer, "Introduction to Digital Speech Processing," *Foundations and Trends in Signal Processing*, vol. 1, nos. 1–2, pp. 1–194, 2007.

[72] A. Noll, "Cepstrum Pitch Determination," *Journal of the Acoustical Society of America*, vol. 41, no. 2, pp. 293 – 309, Feb. 1967.

[73] J. Flanagan, *Speech Analysis, Synthesis and Perception.* 2nd Ed., Springer-Verlag: Berlin, 1965, 317 pages.

[74] J. Deller, J. Hansen and J. Proakis, *Discrete-Time Processing of Speech Signals.* Wiley-IEEE Press, 2000, 936 pages.

[75] A. Oppenheim, R. Schafer and T. Stockham, "Nonlinear Filtering of Multiplied and Convolved Signals," *IEEE Transactions on Audio and Electroacoustics*, vol. AU-16, no. 3, Sep. 1968.

[76] J. Proakis and D. Manolakis, *Digital Signal Processing: Principles, Algorithms and Applications.* 4th Ed., Pearson Education, 2007, 1156 pages.

[77] P. Vary and R. Martin, *Digital Speech Transmission: Enhancement, Coding and Error Concealment.* John Wiley & Sons, 2006, 644 pages.

[78] A. Oppenheim, R. Schafer and J. Buck, *Discrete-Time Signal Processing,* 2nd Ed., Prentice-Hall, 1999, 870 pages.

[79] L. Rabiner and R. Schafer, *Theory and Applications in Digital Speech Processing.* Prentice-Hall, 2010, 1056 pages.

[80] D. Zazula and L. Gyergyek, "Complexity in Signal Processing Using Cepstral Approach," *Electrotechnical Review*, vol. 59, nos. 3–4, pp. 165–170, Dec. 1992.

[81] J. Tribolet, "A New Phase Unwrapping Algorithm," *IEEE Transactions on Acoustics, Speech and Signal Processing*, vol. ASSP-25, pp. 170–177, Apr. 1977.

[82] L. Rabiner and R. Schafer, *Digital Processing of Speech Signals.* Prentice-Hall, 1978, 512 pages.

[83] B. Liang, S. Iwnicki and Y. Zhao, "Application of Power Spectrum, Cepstrum, Higher Order Spectrum and Neural Network Analyses for Induction Motor Fault Diagnosis," *Mechanical Systems and Signal Processing*, vol. 39, pp. 342–360, Feb. 2013.

[84] M. Norton and D. Karczub, *Fundamentals of Noise and Vibration Analysis for Engineers*. 2nd Ed., Cambridge University Press, 2003, 631 pages.

[85] J. Haigh and J. Mason, "Robust Voice Activity Detection Using Cepstral Features," *Proceedings of the IEEE TENCON'93*, vol. 3, pp. 321–324, 1993.

[86] A. Oppenheim, "A Speech Analysis-Synthesis System Based on Homomorphic Filtering," *Journal of the Acoustical Society of America*, vol. 45, no. 2, pp. 293– 309, Feb. 1969.

[87] G. Zheng and W. Wang, "A New Cepstral Analysis Procedure of Recovering Excitations for Transient Components of Vibration Signals and Applications to Rotating Machinery Condition Monitoring," *Transactions of the AMSE*, vol. 123, pp. 222–229, Apr. 2001.

[88] M. Akay, *Biomedical Signal Processing*. Academic Press, 1994, 377 pages.

[89] S. Imai, "Low Bit Rate Cepstral Vocoder Using the Log Magnitude Approximation Filter," *Proceedings of the IEEE International Conference on Acoustics, Speech and Signal Processing (ICASSP '78)*, vol. 3, pp. 441 – 449, 1978.

[90] Y. Tohkura, "A Weighted Cepstral Distance Measure for Speech Recognition," *IEEE Transactions on Acoustics, Speech, and Signal Processing*, vol. 35, no. 10, pp. 1414–1422, Oct. 1987.

[91] O. Viikki and K. Laurila, "Cepstral Domain Segmental Feature Vector Normalization for Noise Robust Speech Recognition," *Speech Communication*, vol. 25, pp. 133–147, Feb. 1998.

[92] S. Ahmadi, "Cepstrum-Based Pitch Detection Using a New Statistical V/UV Classification Algorithm," *IEEE Transactions on Speech and Audio Processing*, vol. 7, no. 3, pp. 333–338, May 1999.

[93] A. Noll, "Short-Time Spectrum and "Cepstrum" Techniques for Vocal-Pitch Detection," *Journal of the Acoustical Society of America*, vol. 36, no. 2, pp. 296–302, Feb. 1964.

[94] J, Ramirez, J. Gorriz and J. Segura, "Voice Activity Detection. Fundamentals and Speech Recognition System Robustness," in *Robust Speech Recognition and Understanding*, M. Grimm and K. Kroschel, Eds., I-Tech: Vienna, Jun. 2007.

[95] D. Hatzinakos and C. Nikias, "Estimation of Multipath Channel Response in Frequency Selective Channels," *IEEE Journal on Selected Areas in Communications*, vol. 7, no. 1, pp. 12–19, 1989.

[96] A. Stephenne and B. Champagne, "Cepstral Prefiltering for Time Delay Estimation in Reverberant Environments," *Proceedings of the IEEE 1995 International Conference on Acoustics, Speech and Signal Processing (ICASSP-95)*, vol. 5, pp. 3055–3058, 1995.

[97] F. Liedtke and U. Albers, "Evaluation of Features for the Automatic Recognition of OFDM Signals in Monitoring of Cognitive Receivers," *Journal of Telecommunications and Information Technology*, vol. 2, pp. 30–36, 2008.

[98] R. Al-Makhlasawy, M. Elnaby, H. El-Khobby and F. El-Samie, "Automatic Modulation Recognition in OFDM Systems Using Cepstral Analysis and a Fussy Logic Interface," *Proceedings of the 8th International Conference on INFOrmatics and Systems (INFOS2012)*, pp. 56–62, May 2012.

[99] D. Lacroix and D. Castelain, "A Study of OFDM Parameters for High Data Rate Radio LAN's," *Proceedings of the IEEE Conference on Vehicular Technology*, vol. 2, pp. 1075–1079, May 2000.

[100] N. Al-Ghazu, *A Study of the Next WLAN Standard IEEE 802.11ac Physical Layer,* M. Sc. Thesis, KTH School of Electrical Engineering, Department of Signal Processing, Jan. 2013.

[101] T. Hwang, C. Yang, G. Wu, S. Li and G. Ye Li, "OFDM and Its Wireless Applications: A Survey," *IEEE Transactions on Vehicular Technology*, vol. 58, no. 4, pp. 1673–1694, May 2009.

[102] S. Kay, *Fundamentals of Statistical Signal Processing, Volume I: Estimation Theory.* Prentice Hall: New Jersey, 1993, 625 pages.

[103] "Digital Video Broadcasting (DVB); Frame Structure, Channel Coding and Modulation for a Second Generation Terrestrial Television Broadcasting System," *European Standard (EN) 302 755 V1.3.1*, European Telecommunications Standards Institute (ETSI), Apr. 2012.

[104] "IEEE 802.11ac-2013: IEEE Standard for Information Technology–Telecommunications and Information Exchange Between Systems Local and Metropolitan Area Networks– Specific Requirements–Part 11: Wireless LAN Medium Access Control (MAC) and Physical Layer (PHY) Specifications," *IEEE Standards Association*, Dec. 2013.

[105] "IEEE 802.16e/D5-2004, Part 16: Air Licence for Fixed and Mobile Broadband Wireless Access Systems – Amendment for Physical and

Medium Access Control Layers for Combined Fixed and Mobile Operation in Licensed Bands," *IEEE Standards Association*, Nov. 2004.

[106] E. Dahlman, S. Parkvall, J. Skold and P. Beming, *3G Evolution: HSPA and LTE for Mobile Broadband*. Academic Press: London, 2007, 648 pages.

[107] "Digital Video Broadcasting (DVB); Framing Structure, Channel Coding and Modulation for Terrestrial Television," *European Standard (EN) 300 744 V1.6.1*, European Telecommunications Standards Institute (ETSI), Jan. 2009.

[108] B. Rivet, L. Girin and C. Jutten, "Log-Rayleigh Distribution: A Simple and Efficient Statistical Representation of Log-Spectral Coefficients," *IEEE Transactions on Audio, Speech, and Language Processing*, vol. 15, no. 3, pp. 796–802, Mar. 2007.

[109] M. Simon and M. Alouini, "A Simple Single Integral Representation of the Bivariate Rayleigh Distribution," *IEEE Communications Letters*, vol. 2, no. 5, pp. 128–130, May 1998.

[110] A. Joarder, "Product Moments of Bivariate Wishart Distribution," *Journal of Probability and Statistical Science*, vol. 4, no. 2, pp. 233–244, Aug. 2006.

Appendix A

Derivation of $\mathbb{V}\mathrm{ar}[X(k)]$

Using Eq. (5.16), Eq. (5.15) can be written in three parts, where $m = n$, $m = n - N_d$ and $m = n + N_d$:

$$\begin{aligned}
\mathbb{V}\mathrm{ar}[X(k)] &= \frac{1}{N_r}\sum_{n=0}^{N_r-1}\sum_{m=0}^{N_r-1}\mathbb{E}[x(n)x^*(m)]e^{-j\frac{2\pi k(n-m)}{N_r}} && \text{(A1)}\\
&= \frac{1}{N_r}\sum_{n=0}^{N_r-1}\mathbb{E}[x(n)x^*(n)] && \text{(A2)}\\
&+ \frac{1}{N_r}\sum_{n=0}^{N_r-1}\mathbb{E}[x(n)x^*(n-N_d)]e^{j\frac{2\pi kN_d}{N_r}} && \text{(A3)}\\
&+ \frac{1}{N_r}\sum_{n=0}^{N_r-1}\mathbb{E}[x(n)x^*(n+N_d)]e^{-j\frac{2\pi kN_d}{N_r}} && \text{(A4)}\\
&= \sigma_x^2 + \frac{N_c}{N_c+N_d}\sigma_s^2\big(e^{j\frac{2\pi kN_d}{N_r}} + e^{-j\frac{2\pi kN_d}{N_r}}\big) && \text{(A5)}\\
&= \sigma_x^2 + 2\frac{N_c}{N_c+N_d}\sigma_s^2\cos(\tfrac{2\pi kN_d}{N_r}) && \text{(A6)}\\
&= \sigma_x^2\big(1 + 2\rho_x\cos(\tfrac{2\pi kN_d}{N_r})\big), && \text{(A7)}
\end{aligned}$$

where $\rho_x = \frac{N_c}{N_c+N_d}\frac{\sigma_s^2}{\sigma_x^2} = \frac{N_c}{N_c+N_d}\frac{\sigma_s^2}{\sigma_w^2+\sigma_s^2}$ [23].

Appendix B

Derivation of $\mathbb{E}[X(k)X^*(l)]$

Using Eq. (5.16), $\mathbb{E}[X(k)X^*(l)]$ can be written in three parts, where $m = n$, $m = n + N_d$, and $m = n - N_d$:

$$\begin{aligned}
\mathbb{E}[X(k)X^*(l)] &= \frac{1}{N_r}\sum_{n=0}^{N_r-1}\mathbb{E}[x(n)x^*(n)]e^{-j\frac{2\pi(k-l)n}{N_r}} \\
&+ \frac{1}{N_r}\sum_{n=0}^{N_r-1}\mathbb{E}[x(n)x^*(n+N_d)]e^{-j\frac{2\pi(kn-l(n+N_d))}{N_r}} \\
&+ \frac{1}{N_r}\sum_{n=0}^{N_r-1}\mathbb{E}[x(n)x^*(n-N_d)]e^{-j\frac{2\pi(kn-l(n-N_d))}{N_r}} \\
&= \textcircled{\text{I}} + \textcircled{\text{II}} + \textcircled{\text{III}} \qquad \text{(B1)}
\end{aligned}$$

The first part of Eq. (B1) that corresponds to $n = m$ (marked as $\textcircled{\text{I}}$) is simply:

$$\frac{1}{N_r}\sum_{n=0}^{N_r-1}\mathbb{E}[x(n)x^*(n)]e^{-j\frac{2\pi(k-l)n}{N_r}} = \begin{cases} 0 & k \neq l \\ \sigma_x^2 & k = l. \end{cases} \qquad \text{(B2)}$$

The second part of Eq. (B1) for $m = n + N_d$ (marked as $\textcircled{\text{II}}$) depends on $\mathbb{E}[x(n)x^*(n+N_d)]$ which gives non zero values only when the samples included in the cyclic prefix are taken into account. Fig. 4.7 shows how $\mathbb{E}[x(n)x^*(n\pm N_d)]$

can have only binary set of possible values (0 and σ_s^2). From that we have

$$\begin{aligned}
\text{(II)} &= \frac{1}{N_r}\sum_{n=0}^{N_r-1}\mathbb{E}[x(n)x^*(n+N_d)]e^{-j\frac{2\pi((k-l)n-lN_d)}{N_r}} \\
&= \frac{1}{N_r}\sum_{n=0}^{N_r-1}\mathbb{E}[x(n)x^*(n+N_d)]e^{-j\frac{2\pi(k-l)n}{N_r}}e^{j\frac{2\pi lN_d}{N_r}} \\
&= \frac{1}{N_r}\sum_{b=0}^{B-1}\sum_{p=0}^{N_c-1}\mathbb{E}[x(p+bN_s)x^*(p+bN_s+N_d)]e^{j\frac{2\pi lN_d}{N_r}} \\
&\quad \cdot e^{-j\frac{2\pi(k-l)(p+bN_s)}{N_r}} \\
&= \frac{\sigma_s^2}{N_r}e^{j\frac{2\pi lN_d}{N_r}}\Bigg(\underbrace{\sum_{b=0}^{B-1}e^{-j\frac{2\pi(k-l)bN_s}{N_r}}}_{\text{(A)}}\Bigg)\Bigg(\underbrace{\sum_{p=0}^{N_c-1}e^{-j\frac{2\pi(k-l)p}{N_r}}}_{\text{(B)}}\Bigg).
\end{aligned} \tag{B3}$$

Here we have used change of variable $n = p + bN_s$ where N_s is number of samples in one OFDM symbol (or block), b denotes OFDM symbol (or block) index, while p denotes sample index inside an OFDM symbol. Noting that $N_r = BN_s$ for the considered scenario, part (A) of Eq. (B3) becomes

$$\text{(A)} = \sum_{b=0}^{B-1}e^{-j\frac{2\pi(k-l)bN_s}{N_r}} = \begin{cases} B, & |k-l|=0,B,2B,\ldots,(N_s-1)B \\ 0, & \text{otherwise.} \end{cases} \tag{B4}$$

For the case $k \neq l$, using $\theta_{kl} = \frac{\pi(k-l)}{N_r}$, part (B) of Eq. (B3) is:

$$\begin{aligned}
\text{(B)} &= \sum_{p=0}^{N_c-1}(e^{-j2\theta_{kl}})^p = \frac{1-e^{-j2\theta_{kl}N_c}}{1-e^{-j2\theta_{kl}}} \\
&= \frac{e^{-j\theta_{kl}N_c}}{e^{-j\theta_{kl}}}\frac{e^{j\theta_{kl}BN_s}-e^{-j\theta_{kl}N_c}}{e^{j\theta_{kl}}-e^{-j\theta_{kl}}} \\
&= e^{-j\theta_{kl}(N_c-1)}\frac{\sin(\theta_{kl}N_c)}{\sin(\theta_{kl})}
\end{aligned} \tag{B5}$$

Therefore, we have:

$$\text{(B)} = \begin{cases} N_c, & |k-l|=0, \\ e^{-j\theta_{kl}(N_c-1)}\frac{\sin(\theta_{kl}N_c)}{\sin(\theta_{kl})}, & \text{otherwise.} \end{cases} \tag{B6}$$

Using Eqs. (B4) and (B6) in Eq. (B3) we have:

$$\text{(II)} = \frac{\sigma_s^2}{N_r}e^{j\frac{2\pi lN_d}{N_r}}\Delta, \tag{B7}$$

where

$$\Delta = \begin{cases} BN_c, & |k-l|=0, \\ Be^{-j\theta_{kl}(N_c-1)}\frac{\sin(\theta_{kl}N_c)}{\sin(\theta_{kl})}, & |k-l|=B,2B,\ldots,(N_s-1)B \\ 0, & \text{otherwise.} \end{cases} \tag{B8}$$

The third part of Eq. (B1) for $m = n - N_d$ (marked as (III)) depends on $\mathbb{E}[x(n)x^*(n-N_d)]$ which gives non zero values only when the samples included in the cyclic prefix are taken into account as shown in Fig. 4.7. Similar to the second part, the third part of Eq. (B1) can be derived as

$$\text{(III)} = \frac{\sigma_s^2}{N_r} e^{-j\frac{2\pi k N_d}{N_r}} \Delta, \tag{B9}$$

Finally substituting Eqs. (B2), (B7), and (B9) in Eq. (B1) we finally get:

$$\mathbb{E}[X(k)X^*(l)] = \sigma_x^2 \delta(k-l) + \frac{\sigma_s^2 \Delta}{N_r} \Big(e^{j\frac{2\pi l N_d}{N_r}} + e^{-j\frac{2\pi k N_d}{N_r}} \Big), \tag{B10}$$

where $\delta(n)$ represents the discrete unit impulse function

$$\delta(n) = \begin{cases} 1, & n = 0 \\ 0, & n \neq 0. \end{cases} \tag{B11}$$